Published in final edited form as:

Chem Rev. 2020 June 24; 120(12): 5158–5193. doi:10.1021/acs.chemrev.9b00663.

Electron transfer in nitrogenase

Hannah L. Rutledge, **F. Akif Tezcan**

Department of Chemistry and Biochemistry, University of California, San Diego, 9500 Gilman Drive, La Jolla, California 92093-0340

Abstract

Nitrogenase is the only enzyme capable of reducing N_2 to NH_3. This challenging reaction requires the coordinated transfer of multiple electrons from the reductase, Fe-protein, to the catalytic component, MoFe-protein, in an ATP-dependent fashion. In the last two decades, there have been significant advances in our understanding of how nitrogenase orchestrates electron transfer (ET) from the Fe-protein to the catalytic site of MoFe-protein and how energy from ATP hydrolysis transduces the ET processes. In this review, we summarize these advances, with focus on the structural and thermodynamic redox properties of nitrogenase component proteins and their complexes, as well as on new insights regarding the mechanism of ET reactions during catalysis and how they are coupled to ATP hydrolysis. We also discuss recently developed chemical, photochemical and electrochemical methods for uncoupling substrate reduction from ATP hydrolysis, which may provide new avenues for studying the catalytic mechanism of nitrogenase.

Graphical Abstract

Corresponding Author: tezcan@ucsd.edu.

The authors declare no competing financial interest.

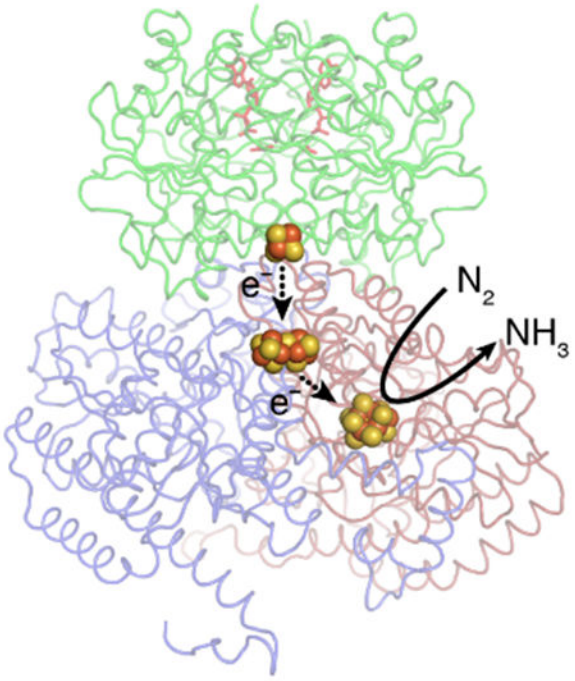

1. Introduction

Nitrogenase is a microbial enzyme that executes one of the most essential and complex biochemical reactions in the biosphere – the fixation of atmospheric dinitrogen (N_2) into ammonia (NH_3). The chemical reaction carried out by Mo-nitrogenase, the most commonly studied isoform of nitrogenase, is generally described by the equation: [1]

$$N_2 + 8e^- + 8H^+ + nATP \rightarrow 2NH_3 + H_2 + nATP + nP_i \quad \text{(Equation 1)}$$

where n is commonly believed to be 16, yielding a stoichiometry of two ATPs hydrolyzed per one electron and one proton transferred.[2–5] A consideration of this equation illustrates the several daunting tasks that nitrogenases have to carry out in concert: the activation of one of the most thermodynamically stable and kinetically inert molecular bonds (:N≡N:), which requires the sequential transfer of multiple electrons over long distances, which in turn is powered and choreographed by ATP hydrolysis. To accomplish this unique combination of tasks, evolution also has converged on a biochemical machine with unique components. There are three known classes of nitrogenases, Mo-, V- and Fe-only nitrogenases (named after the metal content of their catalytic clusters),[6] with the Mo-containing isoform being the primary subject of this review. V- and Fe-only nitrogenases are less efficient than their Mo-counterpart in that they require more ATP and evolve more H_2 per N_2 reduced.[7–10] The catalytic component of Mo-nitrogenase is termed the MoFe-protein (MoFeP), which houses two FeS superclusters: the FeMo-cofactor (FeMoco) with a composition of [Mo-7Fe-9S-C-homocitrate] functioning as the site of N_2 reduction[11–13] and the P-cluster with a composition of [8Fe-7S] acting as the electron-relay site to FeMoco (Figure 1).[14–16] The reductase component of nitrogenase is called Fe-protein (FeP). FeP is an ATPase that

contains a [4Fe-4S] cluster[17] and is the only known biological electron donor to MoFeP to enable catalysis (Figure 1).

Much of the nitrogenase research has revolved around three distinct, but interrelated questions that underlie the uniqueness of this enzyme:

1. Catalytic mechanism: What is the mechanism for the catalytic reduction of N_2 and other substrates by the catalytic cluster of nitrogenase? Why does it require such a complex cluster?
2. Biosynthesis: How are MoFeP and its metal clusters assembled?
3. Energy transduction and electron transfer: How are the electron transfer (ET) and catalytic processes coupled to ATP hydrolysis? Why is ATP hydrolysis necessary for N_2 reduction?

As reviewed in this journal by Burgess & Lowe[18] and Rees & Howard[19] in 1996, the general outlines of nitrogenase composition, structure, catalytic activity, biosynthesis and genetics were established through extensive biochemical and biophysical studies spanning several decades leading up to the 90's. These early efforts culminated in the determination of the first X-ray crystal structures of MoFeP[20] and FeP[17] from *Azotobacter vinelandii (Av).* The initial crystal structures not only helped rationalize earlier findings, but also provided a much-needed platform to start addressing the three questions above. Indeed, the last two decades have witnessed much progress on all fronts, fueled in particular by technical advances in crystallography, spectroscopy and electronic structure calculations as well as in the molecular biology and biochemistry of nitrogenase. For example, on the structural front, high-resolution crystal structures and X-ray absorption/emission spectroscopy studies of MoFeP have identified the previously undetected carbon atom in the center of FeMoco, thus elucidating its true composition.[11–13] The structures of both FeMoco and FeVco have been captured in the presence of extrinsic ligands/inhibitors for the first time, showing the compositional lability of the cofactor and identifying possible substrate binding modes.[21–23] The structures of the FeP-MoFeP complexes in different nucleotide states have provided insights into the mechanism of ATP-dependent energy transduction and longdistance ET.[24–28] Finally, the structures of the scaffolding protein NifEN[29] and apo-MoFeP[30] have shed light on MoFeP maturation. These structures have been paralleled by an impressive array of biochemical and spectroscopic studies (particularly magnetic resonance) that started offering detailed views into the mechanism of substrate activation by FeMoco[31–36] as well as into the elaborate biosynthetic pathway of MoFeP.[37–49] In addition, it was discovered that nitrogenases are also capable of reducing CO and carrying out C-C coupling reactions,[50–55] and that they can be activated for catalysis through chemical,[56,57] electrochemical[58–60] and photochemical[61–63] means without requiring ATP. Clearly, the studies over the last two decades drastically advanced our understanding of the mechanism of nitrogenase catalysis, energy transduction and biosynthesis. In doing so, they have also provided many surprises and spawned new questions, meaning that there is still much left to be discovered about this enzyme.

This is certainly true regarding the issue of why ATP is necessary for nitrogenase activity and how its binding and hydrolysis are used to control the structural dynamics of nitrogenase

and the attendant electron and proton transfer events. Importantly, elucidating ATP-dependent ET processes also are central to a detailed understanding of the catalytic N_2 reduction mechanism and to the exciting prospect of uncoupling catalysis from ATP hydrolysis, thus being able to control the choreography of eight electrons and eight protons through external means. With these points in mind, our aim here is to summarize our knowledge pertaining to ET processes in nitrogenase, the proteins and redox cofactors involved in these processes, and how ET is coupled to (and can be uncoupled from) ATP binding and hydrolysis, with emphasis on advances made in the last two decades since the reviews by Burgess & Lowe[18] and Rees & Howard.[19]

2. Structural and physical determinants of electron transfer in nitrogenase

2.1 Structure and redox properties of the individual proteins and clusters

2.1.1 Fe-protein and the [4Fe-4S] cluster—FeP, encoded by the highly conserved nifH gene,[64] is the obligate biological redox partner of MoFeP. In addition to its function as a MoFeP-reductase, it also has vital roles in MoFeP cluster maturation, as reviewed recently.[65] FeP is a C_2 symmetric γ_2 homodimer (Figure 2),[17] with each γ-subunit containing an α/β domain consisting of an eight-stranded β-sheet surrounded by nine α-helices.[17] The two subunits are bridged by a [4Fe-4S] cluster which lies on the C_2 symmetry axis and is coordinated by two cysteine residues from each monomer (Figure 2).[17]

FeP's distinctive architecture underlies its unique ability to transfer electrons to FeMoco for N_2 reduction. FeP is considerably larger (MW ~60 kDa) than typical ET proteins such as flavodoxins, ferredoxins, and cytochromes (MW < 20 kDa) which possess single-domain structures. The dimeric construction is critical for FeP's ability to specifically interact with MoFeP in an ATP-dependent fashion and couple its reduction to ATP hydrolysis.[66–70] Each FeP subunit binds one molecule of ATP and contains canonical nucleotide binding motifs: the Walker A motif (also known as the P-loop, residues γ9 – 16) and Walker B motif (residues γ125 – 128).[19,71,72] In addition, FeP contains two regions homologous to the switch regions in G-proteins [Switch I (Av γ39 – 69) and Switch II (Av γ125 - 132)], which interact with the γ-phosphate of ATP and undergo conformational changes upon ATP hydrolysis (Figure 2).[73,74] Although there is no crystal structure of ATP-bound wild-type FeP, these nucleotide-dependent conformational changes have been characterized using solution-based methods. Small-angle X-ray scattering (SAXS) experiments show a 2.0 Å decrease in the radius of gyration upon MgATP binding, interpreted as a contraction of FeP in a hinged movement between the two subunits.[75] Further evidence of distinct MgATP-FeP and MgADP-FeP conformations in solution has been demonstrated by variations in proteolysis and cross-linking patterns,[76] changes from a rhombic electron paramagnetic resonance (EPR) signal for nucleotide-free FeP to an axial signal upon MgATP binding,[77] and differences in circular dichroism (CD) spectra.[73,78,79]

A unique structural feature of FeP is the location of its [4Fe-4S] cluster. Most [4Fe-4S] ferredoxins contain somewhat buried clusters, but the [4Fe-4S] cluster in FeP is highly solvent exposed.[17] The extent of solvent accessibility appears to be further modulated by nucleotide-induced conformational changes in FeP. Fe-chelation experiments using 2,2'-bipyridine and bathophenanthroline disulfonate indicate that MgATP-FeP has the most

solvent-exposed [4Fe-4S] cluster as evidenced by fast Fe-removal kinetics in the case of MgATP-FeP (>80% Fe removed within one hour), compared to slow chelation in nucleotide-free FeP and MgADP-FeP (<1% Fe removed within one hour).[80–85] Of course, the possibility cannot be discounted that MgATP binding may cause labilization of the [4Fe-4S] through a conformational strain mediated by the P-loop and Switch II (Figure 2) or through electrostatic induction.[86]

Proteins containing canonical, Cys-ligated [4Fe-4S] clusters are classified either as low-potential ferredoxins or as high-potential iron-sulfur proteins (HiPIPs) depending on which redox couple is accessed by the cluster under physiological conditions, either $[4Fe\text{-}4S]^{2+}$/$[4Fe\text{-}4S]^{1+}$ or $[4Fe\text{-}4S]^{3+}$/$[4Fe\text{-}4S]^{2+}$, respectively.[87] Potentials of these clusters are modulated by the protein environment, with low-potential ferredoxins ranging from −150 mV to −700 mV and HiPIPs from +100 mV to +400 mV vs. normal hydrogen electrode (NHE).[88] Importantly, [4Fe-4S]-ferredoxins can access only one of these two redox couples during their physiological operation.[87,88] The [4Fe-4S] cluster in FeP possesses unique redox properties in that 1) it can attain an all-ferrous state, $[4Fe\text{-}4S]^{0}$, which is more reduced than canonical [4Fe-4S] clusters[89–93] and has only been reported in rare cases in biological systems[94,95] and model complexes,[96,97] and 2) it is able to reversibly access two redox couples ($[4Fe\text{-}4S]^{2+}$/$[4Fe\text{-}4S]^{1+}$ and $[4Fe\text{-}4S]^{1+}$/$[4Fe\text{-}4S]^{0}$) within the biological redox range (approximately −1 V to +1 V) (Table 1). This observation naturally raises the question as to whether FeP can operate as a two-electron donor to MoFeP (see section 3.3 for more on this topic).

Great strides have been made in combining spectroscopic and theoretical techniques to provide detailed insights into the oxidation state assignments, redox thermodynamics, and structure of FeP's [4Fe-4S] cluster. These characterization methods include ^{57}Fe nuclear resonance vibrational spectroscopy (NRVS),[98] Fe-edge extended X-ray absorption fine structure spectroscopy (EXAFS),[78,91,98–100] density functional theory (DFT) calculations[98,101] and spatially resolved anomalous dispersion (SpReAD) refinement, combining X-ray crystallography with X-ray absorption spectroscopy.[102] Many of the initial EXAFS experiments were carried out in the presence of a glassing agent, such as glycerol, which has been shown to affect FeP's properties.[98,99,103,104] Recently, both EXAFS and NRVS data were collected on nucleotide-free FeP in the absence of glycerol with the [4Fe-4S] cluster in each of the three accessible oxidation states, providing insights into the cluster structure.[98] These data, in combination with DFT calculations, have revealed that the oxidized $[4Fe\text{-}4S]^{2+}$ cluster has Fe-Fe distances that are all nearly identical (2.720 Å ± 0.067 Å), and one-electron reduction to $[4Fe\text{-}4S]^{1+}$ reduces the cluster's symmetry (2.721 Å ± 0.083 Å).[98] In the all-ferrous state, $[4Fe\text{-}4S]^{0}$, the structure of the cluster becomes distorted such that the Fe-Fe distances are split into short and long distances (2.562 Å and 2.748 Å).[98] The oxidation state assignments of the iron centers in the [4Fe-4S] cluster have been determined using SpReAD refinement of FeP in four states: 1) $[4Fe\text{-}4S]^{1+}$, ADP-bound FeP, 2) $[4Fe\text{-}4S]^{1+}$, nucleotide-free FeP, 3) $[4Fe\text{-}4S]^{2+}$, ADP-bound FeP, and 4) $[4Fe\text{-}4S]^{0}$, nucleotide-free FeP.[102] In both of the $[4Fe\text{-}4S]^{1+}$ structures, the two more solvent-exposed iron centers are delocalized $Fe^{2.5+}$, and the other two iron centers are Fe^{2+}.[102] In the $[4Fe\text{-}4S]^{2+}$ state, all four iron centers were assigned as $Fe^{2.5+}$.[102]

The redox potential of the 2+/1+ couple of *Av* FeP (universally agreed upon as being physiologically relevant) has been determined via controlled potential microcoulometry, spectroelectrochemistry, and EPR potentiometric titrations to be *ca.* −300 mV in the absence of nucleotides (Table 1).[89,105,106] Watt and colleagues carried out controlled potential microcoulometry experiments to report a potential of −460 mV for the 1+/0 couple of *Av* FeP. [87,107] The highly analogous FeP from *Clostridium pasteurianum (Cp)* displays nearly identical potentials of *ca.* −270 mV and −410 mV for the 2+/1+ and 1+/0 couples, respectively (Table 1).[80,106,108] However, the potential of the 1+/0 couple remains to be concretely established: Burgess et al. reported that singly reduced methyl vio-logen could not reduce *Av* FeP [4Fe-4S] beyond the 1+ oxidation state in contrast to Watt's earlier findings; they conducted controlled-potential electrolysis experiments to arrive at a value of −790 mV for the 1+/0 couple (Table 1), calling into question whether the all-ferrous state can be attained *in vivo*.[109] In general, the literature remains divided on whether the midpoint potential of the 1+/0 redox couple and the spin state of the all-ferrous FeP are E° = −790 mV and $S = 4$,[109–112] or E° = −460 mV and (likely) $S = 0$.[89,107] Theoretical values of E° were calculated for FeP in all three possible FeP geometries (with MgATP, with MgADP, and without nucleotides bound) and in both the $S = 4$ and $S = 0$ states.[101] Interestingly, differences in the geometry and spin state parameters used in the calculations led to calculated reduction potentials ranging from −347 mV to −765 mV suggesting that FeP may be able to accommodate both of the previously reported potentials, just under varying conditions.[101] Clearly, direct electrochemical or spectroe-lectrochemical measurements on FeP under different conditions (e.g., different pHs) would shed much-needed light on the redox thermodynamics of FeP and the possibility of attaining the all-ferrous state *in vivo.*

The redox potential of the *Av* [4Fe-4S] cluster is significantly influenced by nucleotide binding.[82,105,106,113] Complexation with either MgATP or MgADP renders the cluster more reducing, with 2+/1+ midpoint potentials shifting to *ca.* −430 mV and −490 mV, respectively (Table 1).[105,113] Given that the [4Fe-4S] cluster coordination environment stays invariant in the crystal structures of FeP under a variety of conditions (in the presence/absence of MgADP and in 2+, 1+ and neutral oxidation states) (Figure 3),[93,102] changes in the secondary-sphere hydrogen bonding network (Figure 3) and/or solvent accessibility are likely to account for the changes in the potentials, a phenomenon commonly observed in other FeS clusters.[114–116] The hydrogen bonding network between the residues in FeP and the sulfides in the [4Fe-4S] cluster and thiols in the Cys ligands are dependent on the nucleotides bound, but not on the oxidation state of the cluster (Figure 3).[102] Interestingly, the all-ferrous form of ADP-bound FeP could not be obtained, suggesting that the ADP-FeP conformation preferentially stabilizes more oxidized (1+ and 2+) states of the [4Fe-4S] cluster.[102] In addition, computational continuum electrostatic analyses suggested that the negative charge of the ADP and ATP could be responsible for the observed downshift.[86] The potential of the 2+/1+ couple of the [4Fe-4S] cluster was found to be further reduced to −620 mV upon complexation of FeP with MoFeP,[117] making it an even more potent reductant. This downshift has been attributed to desolvation of the cluster,[86] consistent with the crystallographically observed expulsion of water molecules from the [4Fe-4S] secondary sphere upon the formation of ET-activated FeP-MoFeP complexes (see Section 2.2.1)[24–26,28]

Finally, another feature of FeP that distinguishes it from canonical ferredoxins is the fact that its [4Fe-4S] cluster is symmetrically positioned within an uncommon helix-cluster-helix structural motif. Each γ-subunit of FeP provides one of the γ100s helices (spanning residues γ97-112), which radiates from the cluster with the N-terminal ends proximal to the cluster. Interestingly, this arrangement places the [4Fe-4S] cluster at the positive ends of the helix dipoles, which may yet provide another means to tune the [4Fe-4S] redox properties and facilitate the attainment of its reduced states. Such a motif is found in only a handful of other ATPases, and the geometry has been compared to an archer's bowstring, hence the term "archerases" for this class of [4Fe-4S] proteins.[118,119] A member of this class, the activator of 2-hydroxyacyl-CoA dehydratase (HAD), possesses several similar features to FeP including its large size (MW ~55 kDa homodimer), a highly solvent-exposed [4Fe-4S] cluster situated between two subunits, and its ability to access both the 2+/1+ and 1+/0 redox couples.[94] Coincidentally, ET from the activator to its redox partner, HAD, is also dependent on ATP hydrolysis.[120] The similarities between the structural and electrochemical properties of the HAD activator and FeP may provide insights into their unusual redox properties and ATP-dependent ET reactions.

2.1.2 MoFe-protein, the P-cluster and FeMoco—The catalytic component of nitrogenase, MoFeP, is a ~240-kDa, heterotetrameric protein with an $\alpha_2\beta_2$ composition (Figure 4). Both the α- and β-subunits are similar in size and structure, each consisting of ~500 amino acids arranged in three α/β-type domains with the two αβ dimers roughly related by a C_2 rotation-axis.[20] Each αβ-dimer contains two superclusters unique to nitrogenase: the intermediary electron-relay center known as the P-cluster (an [8Fe-7S] cluster) that bridges the α- and β-subunits, and the catalytically active site cofactor FeMoco (a [Mo-7Fe-9S-C-homocitrate] cluster) buried within the α-subunit.[11–13,15,20] Metalloclusters are generally thought to be static in nature, but recently there has been evidence that the function of many clusters,[22,23,121–123] including the P-cluster and FeMoco,[15,21,124] may depend on them being structurally and compositionally dynamic.

The P-cluster orchestrates interprotein ET from the FeP [4Fe-4S] cluster to FeMoco.[125] Structurally, the P-cluster resembles two [4Fe-4S] cubanes joined by a shared, μ^6 sulfide. In the as-isolated, dithionite (DT)-reduced state (P^N), all iron centers in the P-cluster are in the 2+ state.[126–128] Unlike canonical [4Fe-4S] clusters coordinated only by terminal Cys residues, the P-cluster is ligated by two bridging and four terminal Cys residues,[15] thus reducing the overall negative charge of the cluster. This structural feature likely contributes to the stabilization of the highly-reduced, all-ferrous state. Upon oxidation, the P-cluster undergoes sizeable structural changes (Figure 5).[15,129] Peters et al. reported the crystal structure of a one-electron oxidized P-cluster (P^{1+}) obtained by poising *Av* MoFeP crystals at a controlled potential in an electrochemical cell. This structure indicated that one-electron oxidation of the P-cluster results in Fe6 moving out of bonding distance from the central sulfide (S1), subsequently coordinating to a Ser side chain Ŝer188) (Figure 5b).[129] A more recent DFT analysis and quantum refinement of this crystal structure suggested that the P-cluster might actually be a mixture of the P^{1+} and two-electron oxidized (P^{2+}) states.[130] Crystal structures of the P^{2+} state can be obtained in quantitative yield by using chemical oxidants like indigo disulfonate (IDS)[131] or by prolonged incubation in solutions that lack

reductants.[15] Two-electron oxidation results in additional changes in coordination whereby Fe5 dissociates from S1 and ligates the backbone amide nitrogen from a bridging Cys residue Ĉys88) (Figure 5c).[15] The unusual coordination of Fe to the hard, negatively charged serinate and amidate ligands are believed to stabilize the oxidized P-cluster in a redox switchable fashion, as discussed further in Section 3.2.4. The P-cluster can be further oxidized to the P^{3+} state at redox potentials greater than 100 mV upon treatment with solid thionine,[132,133] but there is no evidence that this redox state can be populated during catalysis.[132,133128,129] The midpoint potentials for the P^N to P^{1+} and P^{1+} to P^{2+} couples are virtually indistinguishable at −310 mV at pH 7.5 − 8.0 (Table 1).[117,132,134,135] Association of MoFeP with FeP was reported to lower the P^N/P^{2+} P-cluster potential to −390 mV (obtained by EPR potentiometric titrations),[117] thus increasing the driving force for reduction of FeMoco. A midpoint potential of −42 mV was observed for the oxidation of FeMoco in as isolated, dithionite reduced MoFeP (termed M^N) in the course of equilibrium potentiometric titrations with redox-active dyes in which the disappearance of the S=3/2 EPR signal of M^N was monitored (Table 1).[132,136] Whether this redox transition is mechanistically relevant is open to question, as oxidation beyond the M^N state has not been observed during catalysis. The reduction of FeMoco (termed M^{RED}) beyond M^N, which is more catalytically relevant, has been probed with controlled potential microcoulometry and EPR potentiometric titrations. Potentials ranging from −320 mV to −490 mV have been reported, although assignment of the redox couples could not be made (Table 1) .[134,137–139] As in the case of FeP, the unambiguous determination of the redox potentials of the MoFeP FeS clusters by direct electrochemical methods under physiologically relevant conditions remains an important challenge.

Recent advances in electronic structure calculations have provided new insights into the redox and structural properties of MoFeP superclusters. The density matrix renormalization group (DMRG) method has permitted ab initio calculations of the ground-and excited-state energy levels of clusters as large as [4Fe-4S], which have revealed that the number of electronic states is much larger than initially hypothesized.[140] These methods have been further developed[141] and subsequently used to examine the electronic landscape of the P-cluster. [142]Not surprisingly, the P-cluster exhibits many accessible, low-energy electronic states which may contribute to the finely-tuned structural control of redox dynamics of the cluster. Furthermore, the geometry of the P-cluster and protonation states of the βSer188 and amide of oCys88 ligands have been explored using DFT calculations. The results show that deprotonation of the Ser must occur in both the P^{1+} and P^{2+} states, whereas the backbone amide of the Cys residue is only deprotonated upon oxidation from P^{1+} to P^{2+}.[130]

The unique structural, electronic and catalytic properties of FeMoco have prompted extensive spectroscopic investigations by NRVS,[143] Mo- and Fe-edge EXAFS,[144,145] and Kβ X-ray emission spectroscopy (XES),[13] as recently reviewed.[146] Initially, the structure of FeMoco was predicted using Mo- and Fe-edge EXAFS analyses. Although the preliminary structure predictions were incorrect, they did provide accurate Fe-S and Fe-Fe distances. [144,145] A 1.16-A resolution crystal structure of MoFeP revealed that FeMoco contained a light atom in the center, but the identity of the atom could not be determined at that time by single-crystal X-ray diffraction[11] or by EXAFS.[147] It was not until a higher resolution structure (1.0 Å) was solved and complemented by ^{13}C electron spin echo envelope

modulation (ESEEM) that the central atom could be unambiguously identified as carbon.[12] This finding was corroborated by XES measurements.[13] Initial oxidization state assignment of the Mo center in FeMoco was made using bond distances determined by Mo-EXAFS data that could be fitted to either Mo^{3+} or Mo^{4+}.[144,145] Recently, high-energy resolution fluorescence detected X-ray absorption spectroscopy (HERFD-XAS) was used to unambiguously settle on Mo^{3+}.[148] The large number of iron atoms in MoFeP (15–16 irons per αβ-dimer[149]) complicates oxidation state assignments of the iron centers. Fe-edge EXAFS reveals a shift in the rising edge position from ~7119 eV to ~7126 eV for the iron centers in FeMoco relative to the P-cluster, suggesting that FeMoco is more oxidized, although oxidation state assignments could not be made from these data alone.[41] More recently, the SpReAD method was used to site-specifically assign the relative oxidation states in resting state FeMoco, revealing three ferrous irons, and the remaining four iron centers were in a more oxidized state.[150]

Additionally, recent DFT studies have probed structural changes of FeMoco at different intermediate steps corroborating that FeMoco may undergo turnover-dependent structural changes in which an Fe-S bond is broken upon accumulation of four reducing equivalents.[33,151]

2.1.3 Flavodoxin and ferredoxin—Reduction of FeP requires low-potential electrons provided by small biological electron donors, specifically flavodoxins and ferredoxins.[152–160] The nature of the reductase of FeP varies greatly between aerobic, anaerobic, and phototrophic diazotrophs.[161] Additionally, *Av* has demonstrated redundancy in its electron donors by its ability to grow under diazotrophic growth conditions even when one or more of the reductases are deleted from its genome.[156,157] Analysis of the genomes of diazotrophs has identified five different flavodoxins.[161] Of these, the only flavodoxin that is capable of ET to nitrogenase *in vitro* is NifF (commonly referred to as flavodoxin II).[162–167] NifF, found in many group I diazotrophs,[161,168] is a long-chain flavodoxin with a core composed of a five-stranded parallel β-sheet flanked by five α-helices (Figure 6a).[169–171] It contains a non-covalently bound flavin mononucleotide (FMN) cofactor capable of accessing both the E_1 (semiquinone/hydroquinone) and E_2 (oxidized/semiquinone) redox couples (Figure 6a).[153,155,162,171–174] Specificity of the NifF-FeP interaction has been proposed to be mediated by an eight amino acid loop in NifF (residues 64-71),[170,175] and the midpoint potentials of the FMN are modulated by residues 56-60 in NifF.[176] The midpoint potentials for NifF are $E_1 \approx -480$ mV and $E_2 \approx -200$ mV vs NHE, with E1 being one of the lowest reported potentials in the flavodoxin family (Table 1).[153,155,162,171–174]

Similar to the flavodoxins identified in the genomes of diazotrophs, the identity of ferredoxins differs based on the nitrogenase group in which they are found,[161,168] with redundancy of the ferredoxins in some cases.[177,178] 47 ferredoxins were identified in genomes of diazotrophs,[161] many of which have demonstrated a role in ET to nitrogenase.[154,156,159,162,167,177–179] The structural properties of the ferredoxins are very diverse in both type and number of their FeS clusters. Ferredoxin I (FdI), a 106-residue protein with a pair of two-stranded anti-parallel β-sheets, is a well-characterized reductase produced by many diazotrophs that contains a [4Fe-4S] and a [3Fe-4S] cluster (Figure 6B).[180–187] FdI has been shown to act as an electron donor to nitrogenase both *in vivo*[156] and *in vitro*.[156,162,179,188]

The midpoint potentials of the [4Fe-4S] and [3Fe-4S] are *ca.* −630 mV and −420 mV, respectively (Table 1).[183,189–191] A double *Av* FdI and NifF knockout strain maintained its ability for diazotrophic growth indicating there are additional reductants capable of ET to nitrogenase in Av, although they have yet to be identified and characterized.[156]

2.2 Structures and models of nitrogenase complexes

2.2.1 Nucleotide-dependent Fe-protein-MoFe-protein complexes—Based on the observations that a) FeP is the exclusive biological electron donor to MoFeP and requires ATP hydrolysis to mediate ET to the latter, and b) ATP hydrolysis by FeP only occurs in the presence of MoFeP, it was long known that FeP must form specific interactions with MoFeP.[18,19] The first picture of such interactions was provided by Rees and colleagues, who reported the crystal structure of the isolable FeP-MoFeP complex from *Av* stabilized by ADP.A1F_4^-,[24] an analog thought to represent an intermediate state for ATP hydrolysis (Figure 1).[192,193] In this complex (hereafter referred to as *alf*), FeP is located centrally on the MoFeP surface shared by α- and β-subunits, whereby the two-fold symmetry axis of the former is aligned with the pseudo-two-fold symmetry axis of the latter. This docking geometry places the [4Fe-4S] cluster of FeP as close to the MoFeP surface and the P-cluster as physically possible, wherein the [4Fe-4S] cluster makes several direct hydrogen-bonding contacts with the MoFeP backbone. Simultaneously, FeP assumes a considerably more compact structure relative to uncomplexed FeP whereby the γ-γ subunit interface tightens and brings the side chains of γLys10 and γAsp129 into contact with the nucleotides bound in the opposing subunit to enable hydrolysis. These findings established for the first time the structural basis of how ATP binding/hydrolysis was coupled to the complex formation and ET between FeP and MoFeP.

In order to gain further structural insights into ATP-mediated energy transduction and ET, Rees et al. developed cocrystallization protocols using near-physiological MoFeP and FeP concentrations and ionic strength (150-200 mM) to capture complexes that may represent those populated during turnover.[26] They were able to crystallographically characterize FeP-MoFeP complexes in three different states: in the absence of nucleotides, in the presence of AMPPCP (a non-hydrolyzable ATP analog), and in the presence of ADP (Figure 7).[26] These structures revealed that FeP can occupy three distinct docking geometries (DGs) on the MoFeP surface in a nucleotide-dependent fashion. These are referred to as DG1 (in the nucleotide-free or *nf* state), DG2 (in the AMPPCP-bound or *pcp* state), and DG3 (in the ADP-bound or *adp* state).

In DG1, FeP is situated primarily over the β-subunit (Figure 7a).[26] Extensive hydrogen-bonding and electrostatic interactions are observed between a negative patch on FeP (γGlu68, γAsp69, γGlu111, γGlu112) and a positively charged patch on the MoFeP surface (βAsn399, βLys400, βArg401). The interaction between γGlu112 and βLys400 is particularly noteworthy, as these two residues were observed to form a specific isopeptide crosslink upon treatment of a mixture of FeP and MoFeP with *N*-[3-(dimethylamino)propyl]-*N*′-ethylcarbodiimide (EDC), both in the absence or presence of nucleotides.[25,194,195] In DG2, FeP resides in the same central location as that observed in the *alf* complex and possesses a γ_2 arrangement that is considerably more compact relative to

uncomplexed FeP, but not to the same extent as in the *alf* form (Figure 7b).[26] In the final docking geometry, DG3, FeP is found in four different conformational states, all located atop the α-subunit surface of MoFeP (Figure 7c).[26] In all three docking geometries, the FeP-MoFeP interactions bury extensive surfaces (1600-3700 $Å^2$), indicating that they are likely not crystal packing artifacts and represent structures that may be populated in solution (Table 2).

A comparison of the three complexes reveals that FeP exhibits large, nucleotide-dependent conformational changes, which can be described as a rotational motion of the γ-subunits about a hinge point located near the [4Fe-4S] cluster.[26] This motion is best visualized by the relative orientations of the γ100s helices that radiate from the [4Fe-4S] cluster and provide the primary contacts with MoFeP in different complexes (Figure 8a, top).[26] The rotational motion of the γ-subunits is further accompanied by a substantial sliding motion along the γ-γ subunit interface (Figure 8a, bottom). The angle, ϕ, between γ100s helices defines the flatness of the FeP interaction surface with MoFeP and ranges from 12° in the *alf* complex to >30° in the *nf* and *adp* complexes (0° defined as the helices being coplanar) (Table 2).[26] An important consequence of variable FeP conformations is that they are able to sterically accommodate different features on the MoFeP surface to specifically adopt different nucleotide-dependent docking geometries.[26] A second important consequence is that the same structural changes in FeP (i.e., the ϕ angle) simultaneously result in the formation and relaxation of the active site for ATP hydrolysis across the γ-γ subunit interface (Figure 8b), thus enabling a direct structural connection between the nucleotide-hydrolysis state and MoFeP docking geometry.[24,26] Interestingly, in contrast to the large structural changes observed in FeP, MoFeP remains structurally invariant in all of the complex structures (Figure 9). Thus, if there are any conformational changes in MoFeP during catalytic turnover as proposed by a conformational gating model (see Section 3.2.3), they must be associated with a transient docking geometry or a short-lived redox state (e.g., oxidized P-cluster and reduced [4Fe-4S] cluster) that is challenging to capture crystallographically.

Perhaps the most significant consequence of the different docking geometries is that the ET distance between the FeP [4Fe-4S] cluster and the MoFeP P-cluster is modulated in a nucleotide-dependent manner (Figure 10): 23 Å for DG1 and DG3 and ~18 Å for DG2. Based on the exponential decay of electron tunneling rates with a constant of β~1.1 $Å^{-1}$ [196] interprotein ET in DG2 can be estimated to be *ca.* three orders of magnitude faster than those in DG1 and DG3, rendering the former to be “ET-active” and the latter to be “ET-inactive” If these three docking geometries are populated in a temporal sequence during turnover, as implied by the ATP-hydrolysis reaction coordinate (nucleotide-free ➔ ATP-bound ➔ ADP-bound), the possibility arises that FeP may move unidirectionally on MoFeP, from the β-subunit surface toward the α-subunit surface, in close analogy to the nucleotide-fueled movement of motor proteins on their tracks.[197–199] Given that FeP itself is perfectly symmetric, such a unidirectional motion would be guided by the asymmetric nature of the MoFeP surface.

Additional evidence for such asymmetric induction is provided by the crystal structure of a recently reported FeP-MoFeP complex obtained in the presence of equimolar AMPPCP and ADP (Figure 11).[28] In this complex *(pcp/adp*), which also adopts a DG2 conformation, the

two nucleotide binding sites of FeP are asymmetrically occupied by AMPPCP and ADP, with the g-subunit positioned on the γ-subunit of MoFePcontaining a full-occupancy ADP molecule and the γ-subunit positioned atop the β-subunit containing a full-occupancy AMPPCP molecule. Free FeP has been estimated to have a considerably higher affinity (>100-fold) for ADP than AMPPCP.[200] Thus, there appears to be a thermodynamic preference for the asymmetric, site-selective binding of AMPPCP and ADP to FeP, which in turn suggests that the asymmetry of the MoFeP surface induce the stepwise-rather than synchronous-hydrolysis of two ATP molecules by FeP (see Section 3.2.5 for further discussion), reminiscent of ATP-driven motor proteins such as the Fl-ATPase or AAA+ ATPases.[201–203]

2.2.2 Flavodoxin-Fe-protein and ferredoxin-Fe-protein interactions—Alongside the nucleotide-dependent interactions between FeP and MoFeP, the interactions of FeP with biological electron donors such as flavodoxins and ferredoxins are also salient to the mechanism of nitrogen fixation (particularly *in vivo)* and have garnered considerable interest.[76,107,155,165–167,171,204] It has been shown that flavodoxin II (NifF) and FeP [isolated from both *Klebsiella pneumoniae (Kp)* and *Rhodobacter capsulatus (Rc)*] can form a complex in solution with reduction rates exceeding 10^6 $M^{-1}s^{-1}$.[165,167] Indeed, several studies have indicated that the ATP/e^- efficiency of nitrogenase and the specific catalytic activity of MoFeP increase when NifF is used as the reductant of FeP rather than dithionite (See section 3.3).[92,163,166,205,206] Based on kinetics studies, the location of FeP's [4Fe-4S] cluster, and the FeP-MoFeP docking interactions (Figure 7), it has been proposed that FeP cannot simultaneously interact with both MoFeP and its biological reductant NifF.[163,204]. On the other hand, Haaker et al. reported that experimental kinetics data for the reduction of FeP by NifF can be fit by a model in which reduction takes place prior to FeP-MoFeP complex dissociation.[207] Seefeldt et al. demonstrated reduction of an FeP mutant (ΔγLeu127 FeP) while in complex with MoFeP by NifF, although reduction of FeP by DT while in complex was not possible.[117] In the absence of direct structural information on the functionally relevant complex between NifF and FeP, investigations have largely centered on docking simulations.[76,171,204] According to a recent study by Peters and coworkers, docking interactions between NifF and MgATP-FeP place the FMN and [4Fe-4S] cofactors >9 Å apart, while docking of NifF with MgADP-FeP provides a shorter, more favorable distance of only ~6 Å (Figure 12a).[76] In a slight deviation, Rees and coworkers obtained a distance of ~5 Å between the cofactors using the same docking algorithm (ClusPro 2.0) (Figure 12b).[171] Both studies indicate that NifF shares the same interaction region on the FeP as MoFeP and that FeP-NifF interactions are guided by electrostatic interactions between the positively charged patch surrounding the [4Fe-4S] cluster and the negatively charged amino acid residues surrounding FMN.[76,171] Chemical crosslinking studies of FeP and NifF in the presence of nucleotides suggest that the MgADP-bound FeP complexes with NifF more effectively than MgATP-bound FeP, in support of the former *in silico* results.[76] The proposed NifF-FeP interface was further confirmed with time-resolved limited proteolysis experiments.[204] Mechanistically, this finding has been proposed as being favorable for the efficiency of the nitrogenase ET cycle in that MgADP-bound FeP would be more rapidly reduced by NifF whereas MgATP-bound FeP would be free to associate with MoFeP.[76] Additional docking simulations with FeP have indicated that ferredoxin I most likely shares

the same binding surface as MoFeP (Figure 12c).[171] Thus, there is consensus that ET reactions between FeP and its biological redox partners are mutually exclusive and that FeP must fully dissociate from MoFeP after each cycle of ET to accept an electron from flavo- and ferredoxins. Given that FeP and NifF can form at least a metastable complex in solution, it seems feasible that this complex can eventually be crystallographically characterized in order to validate the docking studies.

2.2.3. Interactions of Shethna protein II with nitrogenase components—FeP and MoFeP are both highly oxygen-sensitive, yet many diazotrophs are obligate aerobes and have developed mechanisms to fix nitrogen in oxygenic environments. The [4Fe-4S] cluster of FeP is especially vulnerable to oxidative damage, which is mitigated through the formation of a complex with MoFeP.[82,208] Further protection of nitrogenase from oxygen can occur through multiple mechanisms. For example, *Av* produces many highly active oxidases which maintain a very low concentration of oxygen in the cytoplasm, in a process known as respiratory protection of nitrogenase.[209] In addition to respiratory protection, *Av* employs conformational protection in which nitrogenase is temporarily protected from oxygen in an inactive state by formation of a complex with Shethna Protein II (also referred to as FeSII), a homodimeric ferredoxin containing two [2Fe-2S] clusters with E_m = −262 mV (Table 1) that undergoes large, redox-dependent conformational changes (Figure 13).[210–216] In the reduced state, Shethna Protein II is in a compact conformation in which the hinge-region of the protein folds the N-loop onto the core of the protein (Figure 13a).[213] Upon oxidation, the N-loop is open at a right angle from the protein core and is more ordered than in the reduced state, exposing the interface hypothesized to bind to nitrogenase (Figure 13b).[213] The Shethna-nitrogenase complex has a stoichiometry of 1FeP:1MoFeP:1Shethna as demonstrated by size exclusion chromatography,[211,213] and the structure of the complex has been predicted using the HADDOCK docking server (Figure 13c).[213] In this model, one FeP dimer is bound to MoFeP in DG1 and the oxidized, open-state Shethna Protein II clamps the FeP-MoFeP cleft,[213] thereby sterically occluding the [4Fe-4S] of FeP and protecting it from damage under oxidizing conditions (Figure 13c).

3. Mechanism of electron transfer in nitrogenase

3.1 The Fe-protein cycle of the Thorneley-Lowe model

Detailed investigations into the catalytic mechanism of nitrogenase by Thorneley and Lowe began in the 1970s, well before the structures of the proteins had been solved. Their analyses resulted in the development of the Thorneley-Lowe (TL) kinetic model of the nitrogenase catalytic cycle.[67,68,165,217–226] The TL model has impressively withstood the test of time; while specific details have been added to the model, no major revisions have been necessary.[227] The flow of electrons during biological nitrogen fixation proceeds from the electron donors (ferredoxins and flavodoxins) to FeP, then from FeP to MoFeP, and subsequently to the substrate. The catalytic cycle can be broken down into the FeP cycle (Figure 14a) and the MoFeP cycle.

In the TL FeP cycle, FeP binds two molecules of MgATP prior to complex formation with MoFeP.[83,219,224] Upon binding MoFeP, multiple events occur, including ATP hydrolysis, ET

from FeP to MoFeP, and release of phosphates, although the order of these events was unclear at the time of the proposed TL catalytic scheme.[67,224,225,228,229] Dissociation of MgADP-bound FeP from MoFeP is followed by the reduction of FeP and exchange of the two MgADPs for MgATPs, returning FeP to the beginning of the cycle (Figure 14a).[165,217,224,226] In the MoFeP cycle, the reduction of one molecule of N_2 and concomitant reduction of protons require a minimum of eight electrons to accumulate at the catalytic site, necessitating many FeP cycles to occur before ammonia (or other reduced products) can form.[66,222–224,230] Thus, MoFeP traverses an ensemble of states in which FeMoco is reduced by FeP up to eight times to effect product formation.

In their 1996 review, Rees and Howard proposed a more structurally-detailed scheme of the nitrogenase turnover and FeP cycle.[19] According to this scheme, MgATP-FeP forms an encounter complex with MoFeP that must then undergo conformational changes in order to reach the transduction complex state (Figure 14b).[19] In this model, the transient transduction state is competent for ET from the P-cluster to FeMoco, which is then followed by ATP hydrolysis to provide the driving force for the reduction of MoFeP by FeP (Figure 14b).[19] It was hypothesized that the conformational changes induced by FeP must open a ‘gate’ within MoFeP, allowing ET to occur. As discussed in Section 2.2.1, many aspects of this scheme were validated by the crystal structures of the FeP-MoFeP complexes.

Yet, questions regarding the essential mechanistic details concerning energy transduction and ET in nitrogenase remain unanswered, including:

1. What drives the formation of the initial complex and what is the mechanistic role of this complex?
2. How is ATP hydrolysis coupled to ET in nitrogenase? What is the nature of the transduction complex? What conformational changes occur in this complex to make inter- and intraprotein ET reactions proceed?
3. What is the order of ATP hydrolysis, ET, and P* release?
4. How many electrons are transferred per FeP cycle under physiological conditions?

In the following sections, we will summarize recent insights that have been obtained toward answering these questions.

3.2. Fe-protein-MoFe-protein interactions

3.2.1 Functional relevance of multiple Fe-protein-MoFe-protein docking modes and a revised Fe-protein cycle—

Of the three FeP-MoFeP docking geometries (Figure 7), only DG2 has clear mechanistic relevance based on crystallographic information. It is best suited for ET from FeP to MoFeP, as evidenced by the closest distance physically possible between the [4Fe-4S] and P-clusters, and it enables the population of compact FeP conformational sub-states (bound to AMPPCP, ADP.AlF_4^- and AMPPCP/ADP) that likely represent those that lie on the reaction coordinate for ATP hydrolysis.[24,26,28] Indeed, a structural overlay of the three complexes obtained in the DG2 state reveals that FeP undergoes considerable conformational changes in regions away from the MoFeP docking

surface, particularly around the nucleotide binding sites, whereas the position of the [4Fe-4S] cluster remains in the “ET-active“ state during the ATP hydrolysis/phosphate release process, enabled by the extensive, highly complementary interaction surface (>3500 $Å^2$) between the two proteins (Figure 7). Such an interface is more characteristic of high-affinity protein-protein interactions than short-lived protein complexes with smaller (<1000 $Å^2$), poorly packed interfaces typically involved in interprotein ET.[231] A long-lived ET-active conformation may be requirement for allowing conformational gating events to occur within MoFeP during ATP hydrolysis (see Section 3.2.3).

Given that ATP-energy transduction and interprotein ET likely take place within DG2, the question arises as to whether the other two conformations, DG1 and DG3, are mechanistically important or even populated in solution. In particular, the DG1 complex is obtained in a nucleotide-free state, which is unlikely to be physiologically relevant in light of the nucleotide binding affinities of FeP[232] and high cellular ATP/ADP concentrations.[233] On the other hand, as mentioned in Section 2.2.1, the DG1 complex features a very large interface (>2800 $Å^2$) between FeP and MoFeP, which includes highly specific interactions between gGlu112 and bLys400 that were observed to form an EDC-mediated crosslink in the absence and the presence of ATP (Figure 15a).[25,194,195]

To investigate the functional relevance of DG1, three MoFeP mutants (βAsn399Glu, βLys400Glu and βArg401Glu) were prepared, aimed at destabilizing the electrostatic and hydrogen-bonding interactions between the oppositely charged patches on FeP and MoFeP.[234] None of these mutants were found to be capable of forming the EDC-mediated crosslink to FeP in the presence or absence of ADP and ATP. The fact that crosslinking is eliminated not only in the case of bLys400Glu but also the other two variants strongly suggests that the crystallographically observed interactions between FeP and MoFeP in the DG1 state are also populated in solution. Notably, all mutants also had diminished C_2H_2 and H^+ reduction activities compared to wild-type MoFeP, with the βLys400Glu variant displaying the greatest decrease in activity (by ~30%) (Figure 15b).[234] The catalytic activity of this variant was also found to be significantly more sensitive to inhibition by increased salt concentrations than the wild-type enzyme,[234] consistent with the importance of electrostatic interactions between FeP and MoFeP during turnover (Figure 15c). Accordingly, the βLys400Glu mutant was also less efficient in sterically protecting the [4Fe-4S] cluster of FeP from chelating agents(Figure 15d).[234] To quantitatively assess FeP-MoFeP association kinetics, the researchers then carried out “dilution experiments” (originally reported by Thorneley and coworkers)[223,235] in which nitrogenase catalytic activity was measured at progressively lower FeP and MoFeP concentrations at which protein-protein association becomes the rate-limiting step of catalysis. An analysis of the results within the TL kinetics framework revealed that the βLys400Glu mutation caused a 5-fold decrease in the FeP-MoFeP association rate ($0.5 \chi 10^7$ $M^{-1}s^{-1}$ vs 2.5×10^7 $M^{-1}s^{-1}$ for wild-type-MoFeP). Interestingly, the βLys400Glu variant displayed a wild-type-like ratio of 2.1±0.4 ATP molecules hydrolyzed for every electron transferred to substrates.[234] Therefore, it was concluded that the FeP-MoFeP interactions in DG1 conformation must be involved in a step that precedes ATP/e^- coupling, such as the formation of an FeP-MoFeP encounter complex[234] as originally proposed by Rees and Howard.[19] Collectively, these findings suggest that interactions in the crystallographically observed DG1 complex are functionally

important for nitrogenase catalysis and populated along a productive reaction pathway toward the formation of the activated DG2 complex (i.e., the transduction state).

A similar mutational analysis of the ADP-bound DG3 state has not yet been conducted and consequently there is no evidence that the crystallographically observed DG3 conformation(s) are populated in solution during turnover. This is partly because ADP-bound FeP is observed in four conformations in the crystal lattice, engaging different, but partially overlapping patches on the MoFeP surface. Nevertheless, it is probably safe to suggest that these conformations are physiologically relevant, given their large FeP-MoFeP buried surface areas (1600–2000 $Å^2$) and the distinct preference of ADP-bound FeP to engage the a-subunit surface of MoFeP. The conformational fluxionality of the DG3 state (as implied by four conformations) is also consistent with the dissociative nature of the ADP-bound complex.

Based on the available crystallographic and biochemical data, an updated scheme for nucleotide-dependent FeP-MoFeP interactions was proposed (Figure 16).[236] In this model, FeP and MoFeP initially form a fluxional ensemble of electrostatically driven encounter complexes centered around the β399–401 patch on the MoFeP β-subunit. This ensemble is then steered to form a metastable, but specific DG1 complex (in which the crosslinking of γGlu112 and βLys400 is possible), followed by a rapid transition to the activated DG2 conformation via a 2D conformational sampling of the MoFeP surface. In this conformation, the complex is committed to interprotein ET and ATP hydrolysis, which likely proceeds in a stepwise fashion involving different conformations of FeP.[24,26,28] The lifetimes of these intermediates could serve as a timing mechanism for orchestrating underlying reactions within the complex, e.g., conformational changes of the P-cluster (see Section 3.2.4), ET between P-cluster and FeMoco (see Section 3.2.3), the rearrangement and reactions at FeMoco (or the alternative FeVco active site).[21–23,124] Following ET and phosphate release, FeP then dissociates from the DG2 state to initiate the next ATP hydrolysis/ET cycle, likely through the intermediacy of the DG3 state.

3.2.2. Solute effects on the dynamics of interprotein electron transfer—To further investigate the dynamics of interactions between FeP and MoFeP, Hoffman, Seefeldt, Dean and colleagues examined how solution viscosity (η) and osmotic pressure affected ET between the two proteins.[237] If interprotein ET were governed or limited by a dynamical conformational transformation, its rate would be expected to decrease with increasing viscosity, with $k(\eta) \propto 1/\eta$.[238] Changes in osmotic pressure, on the other hand, would affect the energetics of ET if this process involved a release or uptake of water molecules according to the equation, $k(m) \propto \exp[-(\Delta n/55.6)m]$, where m is the molality of the added solute and Δn is the number of absorbed water molecules.[239] Interprotein ET kinetics were measured by monitoring the oxidation of reduced FeP by the resting-state MoFeP upon addition of MgATP; these experiments were conducted in the presence of various solutes at different concentrations (Figure 17).[237] The results showed that ET kinetics were independent of viscosity but decreased exponentially with solute molality (i.e., osmotic pressure); in the case of sucrose as a solute, k_{ET} was reduced by as much as 10-fold upon an increase in molality from 0 to 2.[237] These findings indicated that ET from FeP to MoFeP was not limited by a dynamical process such as protein diffusion, but by an energy-requiring

conformational gating event. This event was interpreted in terms of a model in which the rate-limiting step for ET is preceded by a rapid pre-equilibrium between the ATP-bound form of the FeP-MoFeP complex and a higher-energy transduction complex that is activated for ET:[237]

$$(\mathrm{FeP_{red}{:}MoFeP}) \rightleftharpoons (\mathrm{FeP_{red}{:}MoFeP})^{*} \rightarrow (\mathrm{FeP_{ox}{:}MoFeP_{red}})$$

An analysis of the osmotic-pressure dependence experiments suggested that the conformational transition controlling the interprotein ET involved the uptake of more than 80 water molecules, corresponding to an increase of ≥800 Å^2 of exposed protein surface area.[237] Originally, this transition was attributed to the shift of the activated FeP-MoFeP complex from the DG2 state (>3600 Å^2 buried surface, Table 2) to the ADP-bound DG3 state (1600–2000 Å^2 buried surface), exposing nearly 2000 Å^2 of protein surface area in the process.[237] In hindsight, the estimated value of 800 Å^2 accords much better with a transition from the pre-activated DG1 complex (2800 Å^2 buried surface) to the DG3 state through the intermediacy of the DG2 state. The model shown above would also be congruent with the revised FeP cycle (Figure 16), in which the pre-activated DG1 complex is steered towards the activated DG2 conformation in rapid pre-equilibrium. Within DG2, the nitrogenase then undergoes a “compound” conformational gating and ET process powered by ATP hydrolysis,[237] leading eventually to the DG3 state and complex dissociation.

$$(\mathrm{FeP_{red}{:}MoFeP})^{\mathrm{DGI}} \rightleftharpoons [(\mathrm{FeP_{red}{:}MoFeP}) \rightarrow (\mathrm{FeP_{ox}{:}MoFeP_{red}})]^{\mathrm{DG2}} \rightarrow (\mathrm{FeP_{ox}{:}MoFeP_{red}})^{\mathrm{DG3}}$$

3.2.3 Conformational gating of electron transfer in the Fe-protein-MoFe-protein complex and the deficit spending model—From all structural and biochemical data discussed thus far, it is clear that a dominant role of ATP hydrolysis is to control the association/dissociation dynamics of the FeP-MoFeP complex and position the two proteins within an activated DG2 complex to enable coupling between ATP hydrolysis and ET from the FeP [4Fe-4S] cluster to the P-cluster. The role of the P-cluster as the obligatory electron relay center between the [4Fe-4S] cluster and FeMoco is evident not only from the structures of nitrogenase complexes in the DG2 state, but has also been corroborated by the observation that P-cluster undergoes oxidation-state changes during enzymatic turnover.[16] Yet, in the DT-reduced resting-state of MoFeP, the P-cluster is in an all-ferrous form (P^N). Because there is no precedent (yet) for an Fe center in a biological FeS cluster to be reduced beyond the ferrous oxidation state, it was concluded that interprotein ET in nitrogenase must be conformationally gated or energized in an ATP-dependent fashion.[19] Indirect evidence for gating was provided by a study on the temperature-dependence of ET from MgATP-bound FeP to MoFeP, which found that the derived Marcus parameters were well outside the theoretical range that would be expected for a process limited by electron tunneling kinetics.[240] So, how does the ET gate in the nitrogenase complex operate? In the first scenario, a conformational change (of unknown nature) within the activated FeP-MoFeP complex would enable an initial ET event between

the P-cluster and FeMoco and subsequently, the oxidized P-cluster would be reduced by the FeP [4Fe-4S] cluster. This scenario, depicted in Figure 14, was originally articulated by Rees and Howard,[19,241] and later termed the “deficit spending model” by Hoffman, Seefeldt and Dean.[70] The second scenario would entail a hopping mechanism in which the P-cluster is transiently enabled (also in an unknown fashion) to accept an electron from FeP, followed by ET from the P-cluster to FeMoco. Unfortunately, none of the nitrogenase complex structures obtained in nucleotide-bound states (Figure 7) offer any obvious insights into the structural basis of conformational gating. In all complexes, the structure of MoFeP is essentially invariant including the positions of internal water molecules. For reference, a structural alignment of MoFePs from the nitrogenase complexes shows RMS deviations of less than 0.5 Å (Figure 9), which is in stark contrast to the FeP component that displays deviations up to 4.1 Å (Figure 8).

Notwithstanding the lack of a clear structural explanation for gating, recent experimental findings using a P-cluster variant of MoFeP support the deficit spending model.[16,70] The βSer188Cys mutation, which replaces the βSer188 ligand to the oxidized P-cluster (P^{2+} and P^{1+}) with a Cys residue, was found to shift the P-cluster redox equilibrium such that 65% of the clusters are in the P^{1+} state (which displays an $S = ½$ EPR signal) in the presence of DT and the remaining 35% in the P^N state.[16] The availability of P^{1+} state under equilibrium conditions allowed the monitoring of both inter- and intraprotein ET reactions involving the P-cluster. ET from FeP to MoFeP in the wild-type system occurs with a rate constant $k_{obs} \approx 170\ s^{-1}$ (Figure 18a).[70] Stopped-flow measurements of pre-steady state interprotein ET with βSer188Cys MoFeP instead revealed bi-phasic kinetics: a previously unobserved burst phase with an estimated rate of $\geq 1700\ s^{-1}$ and a slow phase with a rate constant essentially the same as that observed in the wild-type system (Figure 18a).[70] Given that the burst phase accounted for 65% of the total signal amplitude and the slow phase for 35%, it was concluded that the former must correspond to the reduction of P^{1+} by the FeP [4Fe-4S] cluster and the latter to the gated ET process observed in the wild-type FeP-MoFeP complex. Additionally, reduction of P^{1+} was not dependent on ATP hydrolysis, as evidenced by the ability of AMPPCP-bound FeP to reduce βSer188Cys MoFeP, but not wild-type MoFeP (Figure 18b).[70] To confirm that the fast ET phase does not require FeMoco, the stopped-flow measurements were repeated with ΔnifB βSer188Cys MoFeP and ΔnifB wild-type MoFeP mutants which do not contain FeMoco. The fast ET phase was still observed with ΔnifB βSer188Cys MoFeP, but not with ΔnifB wild-type MoFeP (Figure 18c), again in line with the attribution of this phase to the reduction of P^{1+}.[70] These results thus indicate that, at least in the case of βSer188Cys MoFeP variant, the gated, intramolecular ET from the P-cluster to FeMoco is slower than the reduction of the oxidized P-cluster by FeP.

3.2.4 P-cluster as a dynamic electron relay site—Regardless of the exact nature of conformational ET gating in nitrogenase, the P-cluster is undoubtedly an integral part of it. The intramolecular ET from the P-cluster to FeMoco occurs only in the presence of MgATP-bound FeP, indicating that somehow a gate must be “opened” by FeP-MoFeP interactions to activate P-cluster for reducing FeMoco.[70,82] As the distance between P-cluster and FeMoco likely stays invariant during turnover, the gate could take the form of local conformational changes in the intervening region between the two clusters to increase electronic coupling or

alterations in the cluster coordination environment to alter reduction potentials, making the P-cluster a better electron donor and FeMoco a better electron acceptor.

Considering that no obvious structural changes have been observed between the P-cluster and FeMoco in tens of different MoFeP crystal structures, it appears unlikely that an “on/off” gate can be achieved through variations in electron tunneling distances between the two clusters alone. Furthermore, the P-cluster is the only part of MoFeP (aside from FeMoco[21,124]) that has been observed to undergo redox-dependent changes in coordination, [15] lending more weight to the second possibility, i.e., thermodynamically driven gating induced by changes in reduction potentials. To recap some structural details, upon two-electron oxidation to the P^{2+} state, one of the two cubane units of the P-cluster opens up, whereby Fe5 forms a bond to the backbone amide N of αCys88, Fe6 coordinates to βSer188, and both Fe5 and Fe6 dissociate from S1 (Figure 5). In the P^{1+} state, only the Fe6-βSer188 coordination is observed. Since both the αCys88 backbone amide and βSer188 hydroxyl group likely have to be in their deprotonated, anionic forms to stably coordinate Fe,[130] they would stabilize the P-cluster in an oxidized state, thereby lowering its reduction potential and rendering it capable of delivering electrons to FeMoco. Thus, any conformational change induced by FeP-MoFeP interactions that would shift the structural equilibrium of MoFeP toward βSer188 and αCys88 backbone amide coordination could act as an ET gate.

Intriguingly, βSer188, is not strictly conserved among nitrogenases, and in many cases, is replaced by an alanine, which cannot ligate an Fe center.[131,168] The lack of conservation calls into question whether the P^{2+} or even the P^{1+} state is mechanistically important. In order to examine the functional role of βSer188 coordination, MoFeP from *Gluconocetabacter diazotrophicus* (Gd)-containing an Ala residue in the β188 position according to *Av* numbering-was isolated and structurally characterized in both DT-reduced and IDS-oxidized states.[131] The reduced *Gd* MoFeP was found to be essentially identical to the *Av* counterpart (Figure 19a). In contrast, the P-cluster in the two-electron oxidized structure revealed an unforeseen coordination of βTyr98 (β99 in *Av* numbering) to Fe8, in place of the βSer188-Fe6 ligation in *Av* (Figure 19b).[131] As in the case of *Av* MoFeP, the backbone amide N of αCys104 (α88 in *Av* numbering) also coordinated to Fe5, yielding a similarly opened cubane architecture.[131] Interestingly, an inspection of 95 aligned nitrogenase sequences revealed that the amino acid positions corresponding to β187 and β98 in *Gd* MoFeP (or β188 and β99 in *Av* MoFeP) were fully covariant in 92 species (Figure 19c).[131,242] That is, if MoFeP has a Ser in the first position, it features a non-coordinating Phe in the second. If the species has a non-coordinating Ala in the first position, it has a Tyr in the second. These findings strongly suggest that the motif of two ligands (one N- and one O-based) to stabilize the oxidized P-cluster are conserved among nitrogenases and likely to be functionally important. Coordination of Ser and Tyr to an FeS cluster is very rare among biological systems,[243] which can be readily rationalized within the context of the P-cluster acting as a switchable electron relay center. The negatively charged Tyr or Ser functionalities can both serve to stabilize the decrease in the reduction potential of the P-cluster like a Cys ligand, thus rendering the P-cluster a better electron donor to FeMoco. Unlike the soft Cys thiolate, however, the hard tyrosinate and serinate ligands cannot stably coordinate ferrous

Fe centers in the reduced P-cluster, meaning that they would act as reversible redox switches.

To further investigate the role of oxygenic ligands (Ser or Tyr), *Av* MoFeP mutants were generated in which the oxygenic ligand was removed βSer188Ala) or the ligand was swapped from the native Ser to Tyr βSer188Ala/βPhe99Tyr) to mimic the *Gd* MoFeP coordination environment.[242] Surprisingly, it was observed that the two-electron oxidation of the P-cluster in the βSer188Ala mutant led to the complete loss of two Fe centers, Fe1 and Fe5, to yield a [6Fe-7S] P-cluster, yet the intact [8Fe-7S] P-cluster reformed upon re-reduction (Figure 20a). The loss of both Fe centers occurred from the central, "over-coordinated" sulfide S1, rather than the peripheral position (Fe6) that coordinates βSer188 upon oxidation to Fe^{3+}. Similarly, the IDS-oxidized cluster in the βSer188Ala/βPhe99Tyr double mutant revealed an unusual mixture of multiple conformational states (Figure 20b). βPhe99Tyr was indeed observed to ligate Fe8 as in *Gd* MoFeP, however, Fe1, Fe5, and Fe8 (all coordinated to the S1 in the P^N state) were partially occupied with a summed average of 2.0 Fe atoms, indicating that the oxidized P-cluster possessed on average one labile Fe, with an overall [7Fe-7S] stoichiometry. This is somewhat unexpected given that the P-cluster environments in the *Av* and *Gd* MoFeP are essentially identical (RMSD = 0.165 Å), including all side chain orientations within 7–8 Å of the cluster. Taken together, these results indicate that a negatively charged, oxygenic ligand is not only necessary to stabilize the oxidized states (P^{2+} or the P^{1+}) of the P-cluster, but also to maintain the cluster composition. They also suggest that the *Av* and *Gd* MoFePs must have evolved with specific preferences for Ser and Tyr ligands.

Overall, the picture that emerges is that the P-cluster possesses many energetically close-lying, oxidation-state-dependent structural and electronic states,[130,142] which are controlled not only by the immediate coordination environment of the cluster but also by structural and dynamic elements in MoFeP that extend beyond the primary and secondary coordination spheres of the P-cluster. Such a dynamic FeS cluster would indeed be well suited, or in fact, required to support a catalytic center (FeMoco) that likely must accommodate many catalytic intermediates at different redox potentials in a way that a canonical FeS cluster cannot. What remains a mystery is what those structural and dynamic elements controlling the P-cluster dynamics are, and how they are coupled to the ATP-dependent interactions between FeP and MoFeP.

3.2.5 Sequence of events for ATP hydrolysis and electron transfer—Based on our current understanding of nitrogenase, the following is well-established regarding ATP hydrolysis: two MgATPs bind per FeP, hydrolysis of ATP by FeP only occurs in the presence of MoFeP, and ATP hydrolysis is coupled to ET in nitrogenase.[66–70,244] It is likely that ATP hydrolysis and both ET events occur while the nitrogenase complex is in DG2 as discussed in section 2.2.1. Understanding how nitrogenase precisely controls ET and couples it to ATP hydrolysis requires unambiguously determining the order of events including ATP hydrolysis, Pz release, both ET events, and dissociation of the FeP-MoFeP complex. Yet despite many investigations into the sequence of events over the last 40 years, many ambiguities still remain.

On the one hand, there is evidence indicating that ATP hydrolysis is required for ET from the P-cluster to FeMoco, suggesting that the energy released by hydrolysis promotes conformational changes that make ET to FeMoco thermodynamically favorable.[66,67,70,82,225] The energy provided by ATP hydrolysis would need to be transduced through the protein matrix (likely via conformational changes to open the "gate") to MoFeP, as the nucleotide binding sites are far from either of MoFeP's metalloclusters.[19,241] On the other hand, there is also evidence supporting the conflicting hypothesis that ATP hydrolysis occurs after ET from the [4Fe-4S] cluster to the P-cluster,[245–249] which contradicts the deficit spending model.[70] If ATP hydrolysis occurs after oxidation of the [4Fe-4S], ATP binding itself, rather than hydrolysis, would promote ET from the P-cluster to FeMoco, possibly making the role of hydrolysis to drive FeP-MoFeP dissociation.[86,245–249] In support of this view, Beratan and coworkers have calculated that the free energy requirements for interprotein ET would result in the formation of a tight FeP-MoFeP complex and that ATP hydrolysis would serve to pay the energetic penalty to allow complex dissociation.[86] While thermodynamically sensible, this cannot be entirely correct because FeP bound to non-hydrolyzable ATP analogs is known to form stable complexes with MoFeP although they are not capable of interprotein ET.[26,70]

Establishing the order of ATP hydrolysis and ET in nitrogenase requires the measurment of the rate of ATP hydrolysis, which has been investigated by a variety of methods including: 1) pre-steady state rapid-quench experiments that measure Pz release using a colorimetric assay[67,69] or ATP hydrolysis using [α-^{32}P]ATP,[204,246] 2) using a pH indicator (*o*-cresosulfonaphthalein) to monitor proton release during ATP hydrolysis,[248] 3) stopped-flow calorimetry to measure heat released as a result of ATP hydrolysis,[225] and 4) using a fluorescent probe to measure Pz release.[250] The source of discrepancies reported in the sequence of ATP hydrolysis and ET may arise from the intrinsic shortcomings of the methods used. The rate of P_i release is not necessarily equal to the rate of ATP hydrolysis, and associating changes in pH or heat to a single reaction (ATP hydrolysis in this case) can be difficult.[18,250] Additionally, determining if ATP hydrolysis precedes ET is further complicated by the ability of the FeP-MoFeP complex to hydrolyze ATP without ET under certain conditions such as the absence of chemical reductants[244,251] or sub-optimal temperature or pH.[5,252,253]

In support of the former hypothesis that ATP hydrolysis precedes ET, Eady et al. determined that the initial burst in ATP hydrolysis during catalysis occurs at a rate indistinguishable from that of ET from FeP to the P-cluster in *Kp* by monitoring pre-steady state ET from FeP to MoFeP and ATP hydrolysis using stopped-flow spectrophotometry at 430 nm and quench-flow experiments measuring P_i release, respectively.[67] Both the stopped-flow and quench-flow experiments were carried out under the same reaction conditions (10 μM *Kp* MoFeP, 50 μM *Kp* FeP, 5 mM ATP, 10 mM DT, pH 7.4).[67] More recently, using the *Av* βSer188Cys MoFeP variant, ATP hydrolysis was shown to be required for the first ET event from the P-cluster to FeMoco, but not ET from the [4Fe-4S] cluster to the P-cluster.[70] In the βSer188Cys MoFeP variant, ET from the [4Fe-4S] cluster to the P-cluster can occur in the presence of MgAMPPCP (but not in the absence of nucleotides) (Figure 18b), indicating that reduction of the P-cluster by the [4Fe-4S] cluster requires binding (but not hydrolysis) of MgATP,[70] which suggests that the nitrogenase complex must be in DG2 for the second ET

event to occur. On the other hand, the first ET event (P-cluster to FeMoco) in wild-type nitrogenase does not occur with the non-hydrolyzable ATP-analog, MgAMPPCP, but rather it requires MgATP, suggesting that ATP hydrolysis is coupled to the first ET event, and that the backfilling of electrons occurs quickly after hydrolysis.[70] The requirement of MgATP for ET from the P-cluster to FeMoco suggests that the role of ATP hydrolysis may be to open the conformational gate.

In contrast, similar experiments determining the pre-steady-state rates of ET and ATP hydrolysis in *Av* nitrogenase have recently demonstrated the reverse sequence of events; ET occurs in a distinct kinetic step prior to ATP hydrolysis.[246] These experiments monitored the oxidation of FeP using stopped-flow spectrophotometry at 430 nm and the hydrolysis of ATP using quench-flow with [α-^{32}P]ATP.[246] The results indicate that ATP hydrolysis is completely uncoupled from ET, suggesting that its role may be to relax the nitrogenase complex and allow dissociation of FeP from MoFeP (Figure 19).[246] How can the difference in results of the time-course experiments of ATP hydrolysis and ET be explained? Eady and coworkers used nitrogenase proteins from a different organism than Seefeldt and colleagues (*Kp* vs *Av*), but it is unlikely that the role and timing of ATP hydrolysis differs between organisms. A more likely explanation can be found in differences in the experimental design; Eady et al. acid-quenched their reactions to precipitate out the protein, presumably releasing P_i for the ATP-hydrolysis assay, while Seefeldt et al. used EDTA to quench the reaction,[67] possibly permitting [α-^{32}P]ADP to remain associated with the still properly-folded FeP, thus preventing ADP from being accurately quantified.[246]

Understanding the requirement of ATP hydrolysis for ET in nitrogenase will require resolving the correct sequence of events. More experiments are needed with comparable reaction conditions in order to independently verify the previously determined rate constants and sequence of events, considering the large discrepancy in published results.

3.2.6 Dissociation of the Fe-protein-MoFe-protein complex and reduction of Fe-protein—

After the [4Fe-4S] cluster has been oxidized by the P-cluster, FeP releases P_i,[246,250] dissociates from MoFeP,[66,250,254] is reduced (commonly by DT *in vitro* or by flavodoxins and/or ferredoxins *in vivo*),[165,221,254] and exchanges both MgADPs for MgATPs[226] in order to return to the beginning of the FeP cycle (Figure 14a). Dissociation of $FeP_{OX}(MgADP)_2$ from MoFeP, which occurs after P_i release,[246,250] is typically monitored indirectly by measuring the rate of reduction of FeP using stopped-flow spectrometry where one syringe contains oxidized FeP, MoFeP, and nucleotides, and the other syringe contains FePRED and DT.[163,204,221,246] Based on the assumption that FePox can only be reduced when not in complex with MoFeP, reduction of FeP (by dithionite or NifF) is used as an indirect measure of complex dissociation.[163,204,221,226,246]

Reduction of free FePox by DT is a second-order reaction with respect to FeP and the reductant with rate constants of $>10^8$ $M^{-1}s^{-1}$ (nucleotide-free FeP) and 3 x 10^6 $M^{-1}s^{-1}$ (ADP-bound FeP).[221,226] Reduction of FePox with the flavodoxin NifF has a comparable rate constant of $>10^6$ $M^{-1}s^{-1}$ (ADP-bound FeP) (Table 3).[165] Recently, these rate constants were determined under pseudo-first order conditions, and similar to the previously determined rate constants, it was shown that DT reduces nucleotide-free FeP faster than

ADP-bound FeP (Table 3).[204] However, even when taking into account the concentration of DT used (10 mM), the pseudo-first order rate constants are slower than the second order constants by more than four orders of magnitude. Interestingly, the pseudo first order rate constant for reduction of FeP by NifF was much larger than the one using DT as the reductant regardless of the state of the nucleotides bound to the free FePox(Table 3).[204] The drastic difference in the rate of reduction of FePox by dithionite and by NifF prompted a reinvestigation into the rate of complex dissociation, which until recently was widely accepted to be the rate-determining step of the TL cycle.[204]

Using DT as the reductant, the dissociation of the FeP-MoFeP complex occurs with a rate constant of ~6 s^{-1} (Table 4).[163,204,221,246] However, when dissociation of the FeP-MoFeP complex was determined using NifF instead of DT, the rateconstant increased to 759 s^{-1}, indicating that P, release (16 – 22 s^{-1}) was actually the rate-limiting step (Table 5).[204] If the rate-limiting step is in fact P, release, then the specific activity will be expected to increase when the flavodoxin NifF is used instead of dithionite, suggesting that nitrogenase activity *in vivo* may be higher than what has been measured using DT *in vitro.* As predicted, nitrogenase assays under low flux conditions with NifF demonstrate higher specific activity than those with DT. (Table 5).[166,204] Additionally, the maximum specific activity of MoFeP is reached at a much lower FeP:MoFeP ratio *in vivo* (with the physiological concentrations of biological reductants) than with DT *in vitro,*[206] in agreement with the *in vitro* assays that utilized NifF.

3.3 Fe-protein as a one- vs two-electron donor

Thus far, we have discussed the mechanism of ET without regard for the number of electrons transferred per FeP cycle. In recent literature, ET is often assumed to occur in one-electron increments, although data have also been presented in support of two electrons transferred per FeP-MoFeP association.[107,205,255,256] The activity of nitrogenase was measured in solutions of varying potential (using redox mediators), and fitting a theoretical curve using the Nernst equation to the experimental data was best achieved when n=2.[255] Additionally, both the [4Fe-4S] cluster of FeP and the P-cluster are able to access two redox couples (rare amongst biological FeS clusters), suggesting that physiological ET may occur in two-electron increments.[255,257,258] Furthermore, FeP undergoes the same nucleotide-dependent conformational changes with the $[4Fe\text{-}4S]^0$ cluster as it does in the DT-reduced 1+ state, indicating that it can also form a pro ductive complex with MoFeP.[90] ET during nitrogenase catalysis is commonly monitored by spectrophotometry at 430 nm, ere the oxidation of FeP's cluster from $[4Fe\text{-}4S]^{1+}$ to $[4Fe\text{-}4S]^{2+}$ results in an increase in absorbance.[69,70,83,117,125,193,204,221,225,228,237,247,259–263] Such *in vitro* experiments typically use DT as the sacrificial reductant of FeP, which can only reduce the [4Fe-4S] cluster to the 1+ state,[89] dictating that each FeP cycle operates exclusively within the 2+/1+ redox couple of FeP, thus transferring only one electron per FeP cycle. Measurement of ATP hydrolysis using DT as the sole reductant of FeP confirms that under these experimental conditions, only one-electron can be transferred per FeP cycle, such that a lower limit of two molecules of ATP hydrolyzed per electron transferred to substrate is approached.[5,205]

In contrast, the ATP/e^- ratio has been reported to approach unity during H_2 production in an *Av* cell lysate solution when DT is added to the lysate, suggesting that a different ET mechanism may be possible in the presence of other physiological components.[256] However, there is no DT involved in *in vivo* N_2 reduction. If the flavodoxin NifF, a biological reductant of FeP, is used in place of DT, then the 1+/0 redox couple potentially becomes accessible.[107] The all-ferrous FeP can be prepared at potentials that are biologically relevant, which means that the physiological relevance of the $[4Fe\text{-}4S]^0$ state should be considered.[89] In order to measure the ATP/e^- ratio, ATP hydrolysis is monitored in parallel with substrate reduction, allowing the ratio to be determined.[204,205,256] However, establishing the minimum ATP requirement is complicated by the ability of FeP to hydrolyze ATP in the presence of MoFeP under conditions that do not support interprotein ET (e.g., lack of reductants such as DT, extreme temperatures or pH values).[225,244,253] According to Watt and coworkers, optimized *in vitro* nitrogenase assays utilizing either NifF or Ti^{III}, both of which are capable of reducing FeP to the all-ferrous state,[89] enhance the ATP/e^- ratio such that it approaches one (Table 5).[107,205] Furthermore, the specific activity of nitrogenase increases by up to ~170% when using NifF as the reductant (Table 5).[166,204] However, Seefeldt and coworkers measured an ATP/e^- ratio that approached two plain the difference in data regarding the ATP/e^- efficiency when using NifF as the reductant. It is possible that energy utilization my differ based on assay conditions: in the experiments where the ATP/e^- ratio approached unity, reactions contained 1.0 mM NifF as the sole reductant,[205] whereas the experiments yielding an ATP/e^- ratio of approximately two used a 712 μM NifF/10 mM DT mixture,[204] which may shift the population of reduced FeP to mostly the $[4Fe\text{-}4S]^{1+}$ state. In the future, similar assays should be repeated using the biological reductant NifF (without DT) to determine the physiological ATP/e^- value.

Although the collective evidence supporting a two-electron transfer mechanism is not definitive, it certainly calls for further investigations, as the benefits of transferring two electrons per FeP cycle are considerable: 1) reduction of the ATP-energy requirement by half (Equation 1), and 2) efficient access to higher reduced states of FeMoco, which are required for N_2 binding and reduction.

4. Uncoupling electron transfer from ATP hydrolysis

In previous sections, we largely focused on how ATP hydrolysis controls ET processes in nitrogenase and why ATP and FeP are specifically required for catalysis by MoFeP. Alongside these fundamental questions, the necessity for ATP hydrolysis and FeP also has practical implications in terms of studying the catalytic mechanism of N_2 reduction. Namely, all catalytic reactions performed by nitrogenase absolutely require continuous ATP hydrolysis by FeP to maintain the electron flow to MoFeP. In solution, such turnover conditions produce a large ensemble of redox states populated by MoFeP at any given time. What's more, any electrons accumulated in FeMoco are rapidly funneled to H^+ reduction even in the presence of inhibitors such as CO.[264–266] Consequently, it is challenging to populate discrete redox intermediates or substrate-/inhibitor-bound states of FeMoco in sufficient quantities for structural and spectroscopic interrogation, necessitating freeze-quench or fast crystallization techniques.[21,33–35,124,267,268] This situation stands in contrast to, for example, the oxygen-evolving complex (OEC) of photosystem II (PSII), many of

whose catalytic intermediates can be quantitively generated by successive flashes of light.[269] As summarized in this section, these practical challenges have motivated efforts to bypass the requirements for FeP and ATP hydrolysis in nitrogenase catalysis by artificial means such as photo-induced ET,[61–63] chemical[56,57] and electrochemical reduction.[59,60,270,271] Of course, these practically-minded efforts also aim to address a fundamental question: is ATP hydrolysis (as well as the specific reductase FeP) an absolute evolutionary requirement for biological nitrogen fixation or is it simply an early solution to a challenging chemical reaction that evolution has not yet found a better alternative to (akin to the industrial Haber-Bosch process)?

4.1 Light-activated nitrogenase systems

4.1.1. Ru-photosensitizer-functionalized MoFe-protein—Light energy not only provides a biochemically cheaper alternative to ATP hydrolysis, but it also allows rapid and high-yield initiation of ET processes with tunable driving forces thanks to the availability of many photosensitizers that can be interfaced with proteins.[61–63,272–287] Photo-triggering approaches have been prominently used in the study of natural light-active systems (e.g., Photosystem II,[288–290] the bacterial photosynthetic reaction center[291,292] and DNA photolyase[293]) or many ET proteins and redox enzymes modified with artificial photosensitizers such as Ru-, Re-, and Os-polypyridyl co mplexes.[277–284] As a prominent example, the use of proteins covalently modified with photo-activatable Ru-polypyridyl complexes was instrumental in the elucidation of electron tunneling dynamics in proteins.[294]

As discussed previously, a prominent role of ATP in nitrogenase function is to enable the docking of FeP and MoFeP in the DG2 geometry, wherein the [4Fe-4S] cluster is positioned in an efficient ET-distance from the P-cluster (Figure 10) and its potential is decreased from *ca.* −420 mV to −620 mV making it a more potent electron donor (Table 1).[117] While it is almost certain that an ATP-induced conformational gating process must exist within MoFeP, it appears possible-on the basis of lack of structural changes within MoFeP-that a properly positioned photosensitizer on the MoFeP surface could be used to inject electrons into MoFeP clusters and induce catalysis.

Toward this end, a MoFeP variant (αLeu158Cys) was employed. In this variant, the αCys158 side chain is located in a surface cleft between the α and β subunits, *ca.* 15 Å away from the P-cluster, precisely where the FeP [4Fe-4S] cluster is positioned in the DG2 complex (Figures 9 and 22).[61] αCys158 MoFeP was covalently labeled with a Cys-specific derivative of the photosensitizer $[Ru(bpy)_2(phen)]^{2+}$, which possesses a long-lived photoexcited state ($*Ru^{II}$) that can be quenched by sacrificial donors to generate the highly reducing Ru^{I} species ($E^0 \approx -1.28$ V) (Figure 22a).[61,62,295] For light-driven reduction of MoFeP (Figure 22c), the two-electron substrates of nitrogenase, H^+ and C_2H_2, were initially examined using DT as a reductive quencher.[61] Continuous irradiation of the solutions of Ru-labeled MoFeP with visible light produced substantial amounts of H_2 and C_2H_4 with a turnover number of 110 per active site and velocities of 16 nmol C_2H_4/min and 14 nmol H_2/min per mg MoFeP (Figure 22d). Control experiments conclusively showed that substrate reduction stems exclusively from the delivery of electrons from the Ru-photosensitizer to FeMoco.[61] Importantly, CO fully inhibited the reduction of C_2H_2 but not H^+ (Figure 22e), paralleling

the reactivity profile of the native enzyme and confirming FeMoco as the site of light-driven catalysis.[61] When the Ru-label was attached to a surface position near FeMoco (using the αHis196Cys mutant) or away from both the P-cluster and FeMoco (using the native αCys45), no substrate reduction activity was observed, indicating that the productive ET pathway must go through the P-cluster. Subsequent experiments with a related Ru-labeled variant showed that the photoredox system was also capable of catalyzing the $6e^-/6H^+$ reduction of HCN into CH_4, albeit with a low efficiency of 0.4 nmol CH_4/min per mg MoFeP.[62] Interestingly, the quantum yield (productive electrons per photon absorbed) of 7×10^{-4} for the six-electron substrate HCN was more than 1100-fold higher than the theoretical yield of $(0.0086)^3 = 6.3 \times 10^{-7}$ based on the two-electron reduction of H^+.[62] These findings indicated that the individual ET steps from the Ru-photosensitizer to FeMoco during HCN reduction were not equivalent, which may also be reflective of electron flux during the ATP-driven catalytic reaction.

Collectively, these findings on photo-induced, ATP-uncoupled catalysis contrasted the long-standing dogma that ATP-bound FeP is the only reductant that can induce substrate reduction by MoFeP. Yet, the Ru-photosensitizer-driven system displayed only *ca.* 1% of the efficiency of the ATP-driven wild-type enzyme, and it could not reduce N_2 into NH_3 in detectable quantities.[61,62] On the one hand, these results further support the role of ATP-bound FeP in activating a conformational ET gate within MoFeP that is necessary for efficient substrate reduction. On the other hand, they also show that it is possible to inject catalytically productive electrons into FeMoco, either through the generation of super-reduced states of the P-cluster or through thermally accessible but low-population structural states of MoFeP that mimic the open state of the conformational gate. If the photocatalytic quantum yield of the Ru-labeled MoFeP hybrid can be improved through alterations in MoFeP to stabilize such an open-gate state, it may be possible to populate discrete catalytic intermediates in high quantities for structural or spectroscopic characterization.

4.1.2 MoFe-protein interfaced with CdS nanocrystals—Recently another light-driven, ATP-and FeP-independent system was developed in which CdS nanocrystals were used for electron injection into MoFeP (Figure 23a).[63] Semiconductor nanocrystals are quantum-confined materials with tunable electronic structures, optical properties and surface chemistries, and they provide high area/volume ratios that can provide efficient electronic coupling to surface-associated charge acceptors.[296,297] Indeed, nanocrystals complexed with redox enzymes were shown to perform selective, multielectron redox reactions such as H^+ and CO_2 reduction.[285–287] To generate a light-driven MoFeP hybrid catalyst system, CdS nanorods were chosen due to their favorable surface electrostatics to associate with MoFeP, their dimensions (~40 Å diameter, ~170 Å length) that complemented those of the protein (~ 70 Å diameter, ~110 Å length), and their low excited-state reduction potential (0.8 V) which can be accessed with visible light irradiation.[63]

When CdS nanocrystals were illuminated with 405-nm light in the presence of MoFeP in a 100% N_2 atmosphere, evolution of large quantities of NH_3 were observed (Figure 23b).[63] This FeP/ATP-independent system was capable of producing 315 ± 55 nmol NH_3/min per mg MoFeP at a turnover frequency of 75/min, corresponding to >50% of the efficiency of the ATP-driven system.[63] The quantum yield of the system (electrons used in N_2 reduction

per absorbed photon) was estimated to be 3.3%.[63] The absence of any of the system components resulted in no catalytic activity and the inclusion of competitive substrates like C_2H_2 or inhibitors like CO suppressed N_2 reduction, leading to the conclusion that the catalytic reaction was indeed driven by CdS-based photoreduction and occurred on FeMoco.[63] Given the heterogeneous nature of CdS-MoFeP interactions, it was not possible to ascertain whether the electrons were directly injected into FeMoco or the P-cluster served as an ET intermediate.

A comparison of the two light-activated nitrogenase systems, CdS-MoFeP and Ru-labeled MoFeP, leads to the following question: How is the CdS-hybrid capable of N_2 reduction whereas the Ru-hybrid is not, despite the latter boasting a higher reducing power (by nearly 0.5 V) and providing a homogeneous system with covalently linked photosensitizers to well-defined sites near MoFeP clusters? One possibility is that CdS nanorods may enable a more rapid delivery of successive electrons to populate the higher- reduction states of FeMoco that are necessary for N_2 binding and reduction.[63] Another possibility is that association with CdS nanorods may more effectively induce conformational changes within MoFeP to allow efficient ET into FeMoco. Nevertheless, some caveats with the system exist. There is no direct evidence that CdS nanorods form a stable complex with MoFeP in contrast to other hybrid systems like CdS-hydrogenase complexes, which have been directly imaged by electron microscopy.[298] In addition, protocols for NH_3 detection, such as the colorimetric and fluorogenic methods used in the study,[299] can be prone to background interference and contamination.[300] Regardless, the nanocrystal-MoFeP hybrid system represents a promising avenue for studying the nitrogenase mechanism and expanding is functional scope, especially when coupled with more rigorous structural/biochemical analyses and analytical characterization of photocatalytic NH_3 production.

4.2. Chemically driven catalysis by MoFe-protein

4.2.1. MoFe-protein mutants capable of ATP/Fe-protein-independent substrate reduction—

Catalytic activities of many redox enzymes can be bimolecularly induced by small-molecule reductants or oxidants, provided they possess proper reduction potentials with respect to the catalytic centers.[301–305] In contrast, it has not been possible to activate catalysis by MoFeP in an ATP/FeP-independent fashion with potent reductants such as Ti^{III}-citrate ($E° \leq -800$ mV) and Cr^{III}-EDTA ($E°\sim -1$ V; EDTA = ethylenediamine tetraacetic acid)[109,306] whose potentials are considerably lower than that of FeP. Obviously, any attempt at the biomolecular reduction of MoFeP is limited not only by diffusion and the relative inaccessibility of the P-cluster, but also by the inability of small molecules to induce the conformationally-gated ET process within MoFeP. Yet, as discussed in the previous section, the ability of light-driven systems to enable catalysis raises the prospect that the open states of the conformational gate can be thermally accessed (albeit in low yields) or induced by nanocrystal association. Likewise, they also imply that it may be possible to generate MoFeP mutants that mimic the conformational changes associated with “opening” of the gate.[56,57,306]

Toward this end, three *Av* MoFeP mutants were investigated,[56,57] in which single-residue substitutions (αTyr64His, βTyr98His, and βPhe99His) were made between the P-cluster and

FeMoco – the most plausible location for a conformational gate. When coupled with strong Eu^{II}-based reductants (E°'s ranging from –0.9 V to –1.1 V),[307,308] all three variants were able to reduce N_2H_4 and N_3^- to NH_3, with activities of up to 660 nmol NH_3/mg MoFeP (with N_2H_4) and 170 nmol NH_3/mg MoFeP (with N_3^-) over a period of 20 min (Figure 24a).[56,57] Additionally, the βTyr98His mutant displayed a substantial H^+ reduction activity of 260 nmol H_2/mg MoFeP under similar conditions.[56,57] None of the variants were capable of N_2 reduction.

In order to determine if the mutated residues were mechanically coupled with the FeP binding surface of MoFeP (and thus linked to conformational gating), normal-mode analyses were carried out.[57] These analyses revealed an out-of-phase correlation between the three mutated residues and FeP motions, suggestive of dynamic coupling between FeP and the intervening region between the P-cluster and FeMoco.[57] Additionally, the crystal structure of the βTyr98His variant showed a slight movement of the His side chain compared to the wild type tyrosine residue, resulting in a 1.5 A difference in the location of a water molecule hydrogen-bonded to homocitrate (Figure 24b).[57] These results suggest that subtle changes near the clusters of MoFeP can have substantial effects on MoFeP reactivity. They also provide further support for the conformational gating hypothesis as well as the deficit spending model, which implicate a mechanical coupling between FeP and buried regions within MoFeP.

4.2.2. Substrate reduction activities of the P-cluster and P-cluster precursors

—It is almost universally agreed upon that all catalytic activity in nitrogenase is performed by FeMoco. Yet, there are recent studies that have reported substrate reduction by the P-cluster and its precursors,[307] which may be capable of diverting electrons to substrates rather than to FeMoco. Biosynthetic maturation of the P-cluster has been proposed to involve the reductive coupling of a pair of [4Fe-4S] clusters, referred to as P-cluster precursors.[95,309] Only once the P-cluster is formed can FeMoco, whose assembly and placement into MoFeP requires the assistance of the proteins NifB and NifEN,[25,46] be inserted into the same αβ-dimer.[41] Maturation of the P-clusters is an energy intensive process that involves a host of additional Nif proteins, including NifH (FeP), NifW, and NifZ, along with MgATP.[37,40,48,49,307,309,310]

In order to probe the reactivity of the P-clusters and their precursors, Ribbe and coworkers characterized two *Av* MoFeP mutants: ΔnifB MoFeP, which lacks FeMoco, and ΔnifH MoFeP, which is thought to lack both FeMoco as well as mature P-clusters.[48,307] To assess the activity of the ΔnifH MoFeP variant, substrate reduction assays were conducted using Eu^{II}-DTPA (E° =−1.1 V; DTPA = diethylenetriaminepentaacetate) as the reductant in place of MgATP-FeP and a variety of substrates including C_2H_2, C_2H_4, CO, NaCN, NaN_3, and H^+.[306,307] Their results indicated that both the mature P-cluster and the P-cluster precursors can serve as active sites for catalysis.[307] In particular, the ΔnifH MoFeP variant with P-cluster precursors was capable of reducing substrates at a faster rate and producing a greater variety of products than the ΔnifH MoFeP mutant.[307]

Dean and coworkers have recently reported that although the ΔnifH MoFeP retains ~1-2% of wild-type activity for H^+ and C_2H_2 reduction, this activity may be due to a small population

of mature MoFeP present in the sample.[48] The mature MoFeP was proposed to arise from the expression of VnfH – an alternative FeP complementary to vanadium nitrogenase– which can also catalyze the maturation of the P-clusters and thus permit FeMoco insertion by NifB.[48] Accordingly, ΔnifH/ΔnifB MoFeP and ΔnifH/ΔvnfH MoFeP were found to be incapable of substrate reduction, leading to the conclusion that all catalytic activity occurs at FeMoco.[48] In light of these opposing findings, it is still open to question whether the unusual ET clusters of nitrogenase (i.e., the P-cluster and the non-canonical [4Fe-4S] cluster of FeP)[48,51,307,311,312] are capable of redox reactions beyond simple ET.

4.3. Electrochemical reduction of MoFe-protein

There is great interest in the development of NH_3 production strategies that are less energetically demanding than the Haber-Bosch process.[58,270,313] In this regard, electrochemically driven N_2 reduction by nitrogenase represents an attractive route alongside photo-catalysis, and has been recently investigated and put into practice.[60,270] Initial electrochemical experiments of nitrogenase involved characterization of CO binding to isolated FeMoco by FTIR spectroelectrochemistry.[314] In addition, isolated FeMoco was shown to reduce H^+ at an applied potential of −320 mV (vs NHE).[315] Solution-based electrochemical catalysis with intact MoFeP has been accomplished using a setup that required FeP and an ATP regeneration system.[270,316] ATP-uncoupled, direct electrochemical measurements or electrocatalytic experiments with intact MoFeP are complicated by the difficulty of protein attachment and orientation on electrode. To circumvent this difficulty, the first example of electrocatalytic reduction of substrates by intact, immobilized MoFeP relied on the use of a strongly reducing redox mediator, cobaltocene ($E° = −963$ mV vs. NHE) (Figure 27a).[59] In this system, FeP-uncoupled reduction of H^+ to H_2,[59] N_3^- and NO_2^- to NH_3,[59] and CO_2 to $HCOO^-$ [271] was achieved with Faradaic efficiencies of 35-46%, 101%, and 9%, respectively (Figure 25a).[59] There was no observable NH_3 production,[59] which was attributed to the large amounts of H_2 produced at the electrodes at the potentials employed,[60] leading to the inhibition of N_2 reduction.

Recently, MoFeP along with multiwalled carbon nanotubes were entrapped in a pyrene-modified linear poly(ethylenimine) (LPEI-pyrene) hydrogel. Within this matrix, the pyrene functionalities adhere to the surface of a carbon electrode and the nanotubes act as a direct ET conduit between the electrode and the enzyme (Figure 25b).[60] Cyclic and square-wave voltammetry experiments were used to identify a redox feature at −270 mV (vs NHE) which was ascribed to the P-cluster. With this system, N_2 reduction to NH_3 could be achieved without the use of redox mediators (Figure 25c), with a rate of ~ 1 nmol NH_3/min per mg MoFeP over the course of eight hours.[60] When denatured MoFeP was used instead the wild-type enzyme, the activity dropped by 40%. While the rate of the immobilized MoFeP bioelectrochemical system is 500 to 1000-fold lower than that of the ATP driven nitrogenase and solution based electrocatalytic system,[270,317,318] the results suggest that it is possible to bypass the absolute dependence on FeP and ATP hydrolysis to activate MoFeP catalysis to a certain extent. The development of more efficient nitrogenase electrocatalysis systems will likely have to await a better understanding of the conformational ET gating mechanism in MoFeP, as is the case with the light-driven systems.[58,236,319] In the meantime, the newly developed electrochemical methods offer great promise in the direct interrogation of the

nitrogenase clusters and provide much needed insights into the redox thermodynamics in nitrogenase.

5. Conclusions

In this review, we have summarized recent developments in our understanding of the complex ATP-dependent ET processes in nitrogenase. Exciting advances have included high-resolution structures which provided detailed snapshots of the clusters' redox-dependent compositions[12] and dynamics.[21–23,124,131,242] Crystal structures of the nitrogenase complex in multiple states clearly revealed why FeP is the exclusive biological reductant of MoFeP.[24–26,28] These structures showed that FeP can occupy distinct, nucleotide-dependent docking geometries on the MoFeP surface that enable a direct structural coupling between ATP hydrolysis and interprotein ET.[24–26,28] Extensive kinetic and spectroscopic studies have shed new light on the ET transfer mechanism and provided updates to the FeP cycle of the Thorneley-Lowe model.[70,234,237,246] The collective evidence is most consistent with a scheme in which FeP and MoFeP first form an electrostatically guided encounter complex (DG1), which transitions into an activated docking geometry (DG2) in an ATP-dependent manner.[234] Once in DG2, the nitrogenase complex is committed to ATP hydrolysis and interprotein ET. The first ET event is most likely a conformationally-gated, ATP-coupled reduction of FeMoco by the P-cluster,[237] which is followed by backfilling of electrons from the [4Fe-4S] cluster of FeP,[70] and subsequent dissociation of MgADP-FeP from MoFeP. In addition to these insights, researchers have devised new photochemical and electrochemical strategies to drive nitrogenase catalysis under certain conditions,[56,57,59–63] thus breaking the long-standing dogma that FeP and ATP-hydrolysis are necessary for substrate reduction.

Undoubtedly, we now have a much clearer idea about the ET processes in nitrogenase and how they are coupled to ATP hydrolysis than we did two decades ago. Nevertheless, several important questions still remain. For example, the exact nature of the FeP-induced conformational gating mechanism within MoFeP remains unclear, although evidence suggests that it likely involves the redox-dependent conformational flexibility of the P-cluster. It is not still entirely unambiguous if the FeP acts exclusively as a one-electron donor or if its all-ferrous state can be engaged to facilitate two-electron steps during nitrogenase catalysis. Along these lines, there is scant information regarding whether all ET steps between the FeP and the P-cluster or between the P-cluster and FeMoco during the catalytic reaction are equivalent. Finally, despite significant progress in kinetics measurements of ET events, the exact sequence of ATP-hydrolysis and ET events within the nitrogenase complex remains open to question. As a result, we still do not fully understand at a fundamental level why ATP hydrolysis is necessary for nitrogenase catalysis. Is it the extreme stability and inertness of N_2 that necessitates input of biochemical energy for activation (i.e., is ATP hydrolysis an inherent thermodynamic requirement)? Or is the need for a precise timing mechanism for ET events such that the reduction of N_2 is favored over that of H+ *(i.e.,* is ATP hydrolysis a kinetic requirement?). Given the increased interest in nitrogenase research and the remarkable pace at which it has advanced in recent years, we are optimistic that we will have the answers before too long.

ACKNOWLEDGMENTS

We thank R. Subramanian, R. Alberstein, J. Esselborn, R. Yu, and D. Gagnon for helpful discussions and critical reading of this manuscript. This work was supported by the National Institutes of Health (Grant GM099813 to F.A.T.). H.L.R. was additionally supported by the Molecular Biophysics Training Grant (NIH Grant T32 GM008326).

Biographies

F. Akif Tezcan was born and raised in Istanbul, Turkey, He received his B.A. degree in chemistry from Macalester College, and his Ph.D. degree from Caltech, where he worked with Harry Gray and Jay Winkler on the folding and redox properties of metalloproteins. He continued his studies at Caltech as a postdoctoral fellow in Doug Rees' group, where he focused on structural investigations of nitrogenase complexes. He has been at UCSD since 2005, where he is currently Professor of Chemistry, Biochemistry and Materials Science and Leslie Orgel Faculty Scholar. Outside of nitrogenase, his research interests generally revolve around using chemical tools and principles to address biological questions and to create new biological materials.

Hannah L. Rutledge graduated in 2012 from Rice University with a B.S. in chemistry where she performed undergraduate research optimizing germanium quantum dot solar cells. Before beginning a Ph.D. program, she taught high school chemistry in Florida. Currently, she is a chemistry graduate student at UC San Diego in the lab of Dr. F. Akif Tezcan. Her research investigates electron transfer in nitrogenase with a focus on the redox-dependent dynamics of the P-cluster.

ABBREVIATIONS

ADP	adenosine diphosphate
Adp	nitrogenase complex stabilized by MgADP
Ala	alanine
alf	nitrogenase complex stabilized by MgADP.AlF4-
AMPPCP	adenylylmethylenediphosphonate disodium salt
Arg	arginine
Asn	asparagine
Asp	aspartic acid
ATP	adenosine triphosphate
Av	Azotobacter vinelandii
CD	circular dichroism
Cp	Clostridium pasteurianum

Cys	cysteine
DFT	density functional theory
DG1	docking geometry 1
DG2	docking geometry 2
DG3	docking geometry 3
DMRG	density matrix renormalization group
DT	sodium dithionite
EDC	*N*-[3-(dimethylamino)propyl]-*N*′ -ethylcarbodiimide
EPR	electron paramagnetic resonance
ESEEM	^{13}C electron spin echo envelope modulation
ET	electron transfer
EXAFS	extended X-ray crystallography
FdI	ferredoxin I
FeMoco	FeMo-cofactor
FeP	Fe-protein
FeSII	Shethna Protein II
FeVco	FeV-cofactor
FMN	flavin mononucleotide
Gd	Gluconocetabacter diazotrophicus
Glu	glutamic acid
HAD	2-hydroxyacyl-CoA dehydratase
HERFD	high-energy resolution fluorescence detected
HiPIPs	high-potential iron-sulfur proteins
His	histidine
IDS	indigo disulfonate
Kp	Klebsiella pneumonia
Leu	leucine
LPEI	linear poly(ethylenimine)
Lys	lysine

M^N	dithionite-reduced FeMoco
MoFeP	MoFe-protein
M^{oX}	FeMoco oxidized beyond M^N
M^{RED}	FeMoco reduced beyond M^N
nf	nitrogenase complex in the nucleotide-free state
NHE,	normal hydrogen electrode
NifF	flavodoxin II
NRVS	^{57}Fe nuclear resonance vibrational spectroscopy
P^{1+}	one-electron oxidized P-cluster
P^{2+}	two-electron oxidized P-cluster
P^{3+}	three-electron oxidized P-cluster
pcp	nitrogenase complex stabilized by MgAMPPCP
pcp/adp	nitrogenase complex with MgAMPPCP and MgADP
Phe	phenylalanine
$_PN$	as isolated, dithionite-reduced P-cluster
Rc	Rhodobacter capsulatus
SAXS	small-angle X-ray scattering
Ser	serine
SpReAD	spatially resolved anomalous dispersion
TL	Thorneley-Lowe
WT	wild-type
XAS	X-ray absorption spectroscopy
XES	X-ray emission spectroscopy

REFERENCES

(1). Simpson FB; Burris RH A Nitrogen Pressure of 50 Atmospheres Does Not Prevent Evolution of Hydrogen by Nitrogenase. Science 1984, 224, 1095–1097. [PubMed: 6585956]

(2). Winter HC; Burris RH Stoichiometry of the Adenosine Triphosphate Requirement for N2 Fixation and H2 Evolution by a Partially Purified Preparation of Clostridium pasteurianum. J. Biol. Chem 1968, 243, 940–944. [PubMed: 5640978]

(3). Kennedy IR; Morris JA; Mortenson LE N2 Fixation by Purified Components of the N2-Fixing System of Clostridium pasteurianum. Biochim. Biophys. Acta 1968, 153, 777–786. [PubMed: 5660383]

(4). Hadfield KL; Bulen WA Adenosine Triphosphate Requirement of Nitrogenase from Azotobacter vinelandii. Biochemistry 1969, 8, 5103–5108. [PubMed: 5365797]

(5). Watt GD; Bulen WA; Burns A; Hadfield KL Stoichiometry, ATP/2e Values, and Energy Requirements for Reactions Catalyzed by Nitrogenase from Azotobacter vinelandii. Biochemistry 1975, 14, 4266–4272. [PubMed: 1182100]

(6). Eady RR Structure-Function Relationships of Alternative Nitrogenases. Chem. Rev 1996, 96, 3013–3030. [PubMed: 11848850]

(7). Eady RR Current Status of Structure Function Relationships of Vanadium Nitrogenase. Coord. Chem. Rev 2003, 237, 23–30.

(8). Harris DF; Lukoyanov DA; Shaw S; Compton P; Tokmina-Lukaszewska M; Bothner B; Kelleher N; Dean DR; Hoffman BM; Seefeldt LC Mechanism of N_2 Reduction Catalyzed by Fe-Nitrogenase Involves Reductive Elimination of H2. Biochemistry 2018, 57, 701–710. [PubMed: 29283553]

(9). Hales BJ In Catalysts for Nitrogen Fixation: Origins, Applications, and Research Progress; Smith BE;Richards RL;Newton WE, Eds.; Springer, Dordrecht, 2004; Vol. 1.

(10). Schneider K; Müller A In Catalysts for Nitrogen Fixation: Nitrogenases, Relevant Chemical Models and Commercial Processes; Smith BE;Richards RL;Newton WE, Eds.; Springer Netherlands: Dordrecht, 2004.

(11). Einsle O; Tezcan FA; Andrade SLA; Schmid B; Yoshida M; Howard JB; Rees DC Nitrogenase MoFe-Protein at 1.16 Angstrom Resolution: A Central Ligand in the FeMo-Cofactor. Science 2002, 297, 1696–1700. [PubMed: 12215645]

(12). Spatzal T; Aksoyoglu M; Zhang LM; Andrade SLA; Schleicher E; Weber S; Rees DC; Einsle O Evidence for Interstitial Carbon in Nitrogenase FeMo Cofactor. Science 2011, 334, 940–940. [PubMed: 22096190]

(13). Lancaster KM; Roemelt M; Ettenhuber P; Hu YL; Ribbe MW; Neese F; Bergmann U; DeBeer S X-Ray Emission Spectroscopy Evidences a Central Carbon in the Nitrogenase Iron-Molybdenum Cofactor. Science 2011, 334, 974–977. [PubMed: 22096198]

(14). Surerus KK; Hendrich MP; Christie PD; Rottgardt D; Ormejohnson WH; Munck E Mossbauer and Integer-Spin EPR of the Oxidized P-Clusters of Nitrogenase - Pox Is a Non-Kramers System with a Nearly Degenerate Ground Doublet. J. Am. Chem. Soc 1992, 114, 8579–8590.

(15). Peters JW; Stowell MH; Soltis SM; Finnegan MG; Johnson MK; Rees DC Redox-Dependent Structural Changes in the Nitrogenase P-Cluster. Biochemistry 1997, 36, 1181–1187. [PubMed: 9063865]

(16). Chan JM; Christiansen J; Dean DR; Seefeldt LC Spectroscopic Evidence for Changes in the Redox State of the Nitrogenase P-Cluster During Turnover. Biochemistry 1999, 38, 5779–5785. [PubMed: 10231529]

(17). Georgiadis MM; Komiya H; Chakrabarti P; Woo D; Kornuc JJ; Rees DC Crystallographic Structure of the Nitrogenase Iron Protein from Azotobacter vinelandii. Science 1992, 257, 1653–1659. [PubMed: 1529353]

(18). Burgess BK; Lowe DJ Mechanism of Molybdenum Nitrogenase. Chem. Rev 1996, 96, 2983–3011. [PubMed: 11848849]

(19). Howard JB; Rees DC Structural Basis of Biological Nitrogen Fixation. Chem. Rev 1996, 96, 2965–2982. [PubMed: 11848848]

(20). Kim J; Rees DC Crystallographic Structure and Functional Implications of the Nitrogenase Molybdenum-Iron Protein from Azotobacter vinelandii. Nature 1992, 360, 553–560. [PubMed: 25989647]

(21). Spatzal T; Perez KA; Einsle O; Howard JB; Rees DC Ligand Binding to the FeMo-Cofactor: Structures of CO-Bound and Reac-tivated Nitrogenase. Science 2014, 345, 1620–1623. [PubMed: 25258081]

(22). Sippel D; Einsle O The Structure of Vanadium Nitrogenase Reveals an Unusual Bridging Ligand. Nat. Chem. Biol 2017, 13, 956-+. [PubMed: 28692069]

(23). Sippel D; Rohde M; Netzer J; Trncik C; Gies J; Grunau K; Djurdjevic I; Decamps L; Andrade SLA; Einsle O A Bound Reaction Intermediate Sheds Light on the Mechanism of Nitrogenase. Science 2018, 359, 1484-+. [PubMed: 29599235]

(24). Schindelin H; Kisker C; Schlessman JL; Howard JB; Rees DC Structure of ADP.AlF4--Stabilized Nitrogenase Complex and Its Implications for Signal Transduction. Nature 1997, 387, 370–376. [PubMed: 9163420]

(25). Schmid B; Einsle O; Chiu HJ; Willing A; Yoshida M; Howard JB; Rees DC Biochemical and Structural Characterization of the Cross-Linked Complex of Nitrogenase: Comparison to the ADP.AlF4--Stabilized Structure. Biochemistry 2002, 41, 15557–15565. [PubMed: 12501184]

(26). Tezcan FA; Kaiser JT; Mustafi D; Walton MY; Howard JB; Rees DC Nitrogenase Complexes: Multiple Docking Sites for a Nucleotide Switch Protein. Science 2005, 309, 1377–1380. [PubMed: 16123301]

(27). Chiu HJ; Peters JW; Lanzilotta WN; Ryle MJ; Seefeldt LC; Howard JB; Rees DC MgATP-Bound and Nucleotide-Free Structures of a Nitrogenase Protein Complex between the Leu 127 Delta-Fe-Protein and the MoFe-Protein. Biochemistry 2001, 40, 641–650. [PubMed: 11170380]

(28). Tezcan FA; Kaiser JT; Howard JB; Rees DC Structural Evidence for Asymmetrical Nucleotide Interactions in Nitrogenase. J. Am. Chem. Soc 2015, 137, 146–149. [PubMed: 25522159]

(29). Kaiser JT; Hu Y; Wiig JA; Rees DC; Ribbe MW Structure of Precursor-Bound NifEN: A Nitrogenase FeMo Cofactor Matu-rase/Insertase. Science 2011, 331, 91–94. [PubMed: 21212358]

(30). Schmid B; Ribbe MW; Einsle O; Yoshida M; Thomas LM; Dean DR; Rees DC; Burgess BK Structure of a Cofactor-Defi-cient Nitrogenase MoFe Protein. Science 2002, 296, 352–356. [PubMed: 11951047]

(31). Hoffman BM; Lukoyanov D; Yang ZY; Dean DR; Seefeldt LC Mechanism of Nitrogen Fixation by Nitrogenase: The Next Stage. Chem. Rev 2014, 114, 4041–4062. [PubMed: 24467365]

(32). Harris DF; Yang ZY; Dean DR; Seefeldt LC; Hoffman BM Kinetic Understanding of N_2 Reduction Versus H2 Evolution at the E4(4H) Janus State in the Three Nitrogenases. Biochemistry 2018, 57, 5706–5714. [PubMed: 30183278]

(33). Hoeke V; Tociu L; Case DA; Seefeldt LC; Raugei S; Hoffman BM High-Resolution Endor Spectroscopy Combined with Quantum Chemical Calculations Reveals the Structure of Nitrogenase Janus Intermediate E4(4H). J. Am. Chem. Soc 2019.

(34). Lukoyanov D; Khadka N; Yang ZY; Dean DR; Seefeldt LC; Hoffman BM Reductive Elimination of H2 Activates Nitrogenase to Reduce the N≡N Triple Bond: Characterization of the E4(4H) Janus Intermediate in Wild-Type Enzyme. J. Am. Chem. Soc 2016, 138, 10674–10683. [PubMed: 27529724]

(35). Lukoyanov D; Khadka N; Yang ZY; Dean DR; Seefeldt LC; Hoffman BM Reversible Photoinduced Reductive Elimination of H2 from the Nitrogenase Dihydride State, the E4(4H) Janus Intermediate. J.Am. Chem. Soc 2016, 138, 1320–1327. [PubMed: 26788586]

(36). Rohde M; Sippel D; Trncik C; Andrade SLA; Einsle O The Critical E4 State of Nitrogenase Catalysis. Biochemistry 2018, 57, 5497–5504. [PubMed: 29965738]

(37). Hu YL; Fay AW; Lee CC; Yoshizawa J; Ribbe MW Assembly of Nitrogenase MoFe Protein. Biochemistry 2008, 47, 3973–3981. [PubMed: 18314963]

(38). Dos Santos PC; Dean DR; Hu Y; Ribbe MW Formation and Insertion of the Nitrogenase Iron-Molybdenum Cofactor. Chem. Rev 2004, 104, 1159–1174. [PubMed: 14871152]

(39). Ribbe MW; Hu YL; Hodgson KO; Hedman B Biosynthesis of Nitrogenase Metalloclusters. Chem. Rev 2014, 114, 4063–4080. [PubMed: 24328215]

(40). Hu Y; Fay AW; Dos Santos PC; Naderi F; Ribbe MW Characterization of Azotobacter vinelandii Nifz Deletion Strains. Indication of Stepwise MoFe Protein Assembly. J. Biol. Chem 2004, 279, 54963–54971. [PubMed: 15485884]

(41). Corbett MC; Hu YL; Naderi F; Ribbe MW; Hedman B; Hodgson KO Comparison of Iron-Molybdenum Cofactor-Deficient Nitrogenase MoFe Proteins by X-Ray Absorption Spectroscopy – Implications for P-Cluster Biosynthesis. J. Biol. Chem 2004, 279, 28276–28282. [PubMed: 15102840]

(42). Cotton MS; Rupnik K; Broach RB; Hu Y; Fay AW; Ribbe MW; Hales BJ VTVH-MCD Study of the Delta Nifb Delta Nifz MoFe Protein from Azotobacter vinelandii. J. Am. Chem. Soc 2009, 131, 4558–4559. [PubMed: 19334767]

(43). Wiig JA; Hu Y; Ribbe MW NifEN-B Complex of Azotobacter vinelandii Is Fully Functional in Nitrogenase FeMo Cofactor Assembly. Proc. Natl. Acad. Sci. U. S. A 2011, 108, 8623–8627. [PubMed: 21551100]

(44). Wiig JA; Hu Y; Chung Lee C; Ribbe MW Radical Sam-Dependent Carbon Insertion into the Nitrogenase M-Cluster. Science 2012, 337, 1672–1675. [PubMed: 23019652]

(45). Guo Y; Echavarri-Erasun C; Demuez M; Jimenez-Vicente E; Bominaar EL; Rubio LM The Nitrogenase FeMo-Cofactor Precursor Formed by NifB Protein: A Diamagnetic Cluster Containing Eight Iron Atoms. Angew. Chem. Int. Ed. Engl 2016, 55, 12764–12767. [PubMed: 27611968]

(46). Tanifuji K; Lee CC; Sickerman NS; Tatsumi K; Ohki Y; Hu Y; Ribbe MW Tracing the 'Ninth Sulfur' of the Nitrogenase Cofactor Via a Semi-Synthetic Approach. Nat Chem 2018, 10, 568–572. [PubMed: 29662207]

(47). Rupnik K; Lee CC; Hu Y; Ribbe MW; Hales BJ A VTVH MCD and EPR Spectroscopic Study of the Maturation of the “Sec-ond” Nitrogenase P-Cluster. Inorg Chem 2018, 57, 4719–4725. [PubMed: 29611695]

(48). Jimenez-Vicente E; Yang Z-Y; Ray WK; Echavarri-Erasun C; Cash VL; Rubio LM; Seefeldt LC; Dean DR Sequen-tial and Differential Interaction of Assembly Factors During Nitrogenase MoFe Protein Maturation. J. Biol. Chem 2018, 293, 9812–9823. [PubMed: 29724822]

(49). Jimenez-Vicente E; Yang ZY; Martin Del Campo JS; Cash VL; Seefeldt LC; Dean DR The NifZ Accessory Protein Has an Equivalent Function in Maturation of Both Nitrogenase MoFe Protein P-Clusters. J. Biol. Chem 2019, 294, 6204–6213. [PubMed: 30846561]

(50). Hu YL; Ribbe MW Nitrogenase and Homologs. J. Biol. Inorg. Chem 2015, 20, 435–445. [PubMed: 25491285]

(51). Rebelein JG; Stiebritz MT; Lee CC; Hu Y Activation and Reduction of Carbon Dioxide by Nitrogenase Iron Proteins. Nat Chem Biol 2017, 13, 147–149. [PubMed: 27893704]

(52). Lee CC; Hu Y; Ribbe MW Tracing the Hydrogen Source of Hydrocarbons Formed by Vanadium Nitrogenase. Angew. Chem. Int. Ed. Engl 2011, 50, 5545–5547. [PubMed: 21538750]

(53). Hu Y; Lee CC; Ribbe MW Extending the Carbon Chain: Hydrocarbon Formation Catalyzed by Vanadium/Molybdenum Nitrogenases. Science 2011, 333, 753–755. [PubMed: 21817053]

(54). Lee CC; Hu Y; Ribbe MW Vanadium Nitrogenase Reduces CO. Science 2010, 329, 642. [PubMed: 20689010]

(55). Yang ZY; Dean DR; Seefeldt LC Molybdenum Nitrogenase Catalyzes the Reduction and Coupling of CO to Form Hydrocarbons. J. Biol. Chem 2011, 286, 19417–19421. [PubMed: 21454640]

(56). Danyal K; Inglet BS; Vincent KA; Barney BM; Hoffman BM; Armstrong FA; Dean DR; Seefeldt LC Uncoupling Nitrogenase: Catalytic Reduction of Hydrazine to Ammonia by a MoFe Protein in the Absence of Fe Protein-ATP. J. Am. Chem. Soc 2010, 132, 13197–13199. [PubMed: 20812745]

(57). Danyal K; Rasmussen AJ; Keable SM; Inglet BS; Shaw S; Zadvornyy OA; Duval S; Dean DR; Raugei S; Peters JWet al. Fe Protein-Independent Substrate Reduction by Nitrogenase MoFe Protein Variants. Biochemistry 2015, 54, 2456–2462. [PubMed: 25831270]

(58). Milton RD; Minteer SD Enzymatic Bioelectrosynthetic Ammonia Production: Recent Electrochemistry of Nitrogenase, Nitrate Reductase, and Nitrite Reductase. Chempluschem 2017, 82, 513–521. [PubMed: 31961593]

(59). Milton RD; Abdellaoui S; Khadka N; Dean DR; Leech D ; Seefeldt LC; Minteer SD Nitrogenase Bioelectrocatalysis: Heterogeneous Ammonia and Hydrogen Production by MoFe Protein. Energ Environ Sci 2016, 9, 2550–2554.

(60). Hickey DP; Lim K; Cai R; Patterson AR; Yuan M; Sahin S; Abdellaoui S; Minteer SD Pyrene Hydrogel for Promoting Direct Bioelectrochemistry: ATP-Independent Electroenzymatic Reduction of N2. Chem Sci 2018, 9, 5172–5177. [PubMed: 29997870]

(61). Roth LE; Nguyen JC; Tezcan FA ATP-and Iron-Protein-Independent Activation of Nitrogenase Catalysis by Light. J. Am. Chem. Soc 2010, 132, 13672–13674. [PubMed: 20843032]

(62). Roth LE; Tezcan FA ATP-Uncoupled, Six-Electron Photoreduction of Hydrogen Cyanide to Methane by the Molybdenum-Iron Protein. J. Am. Chem. Soc 2012, 134, 8416–8419. [PubMed: 22564208]

(63). Brown KA; Harris DF; Wilker MB; Rasmussen A; Khadka N; Hamby H; Keable S; Dukovic G; Peters JW; Seefeldt LB et al. Light-Driven Dinitrogen Reduction Catalyzed by a CdS:Nitrogenase MoFe Protein Biohybrid. Science 2016, 352, 448–450. [PubMed: 27102481]

(64). Raymond J; Siefert JL; Staples CR; Blankenship RE The Natural History of Nitrogen Fixation. Mol. Biol. Evol 2004, 21, 541–554. [PubMed: 14694078]

(65). Jasniewski AJ; Sickerman NS; Hu Y; Ribbe MW The Fe Protein: An Unsung Hero of Nitrogenase. Inorganics 2018, 6, 25.

(66). Hageman RV; Burris RH Nitrogenase and Nitrogenase Reductase Associate and Dissociate with Each Catalytic Cycle. Proc. Natl. Acad. Sci. U. S. A 1978, 75, 2699–2702. [PubMed: 275837]

(67). Eady RR; Lowe DJ; Thorneley RN Nitrogenase of Klebsiella pneumoniae: A Pre-Steady State Burst of ATP Hydrolysis Is Coupled to Electron Transfer between the Component Proteins. FEBS Lett 1978, 95, 211–213. [PubMed: 363454]

(68). Thorneley RN; Lowe DJ; Eday RR; Miller RW The Coupling of Electron Transfer in Nitrogenase to the Hydrolysis of Magnesium Adenosine Triphosphate. Biochem. Soc. Trans 1979, 7, 633–636. [PubMed: 383544]

(69). Hageman RV; Orme-Johnson WH; Burris RH Role of Magnesium Adenosine 5'-Triphosphate in the Hydrogen Evolution Reaction Catalyzed by Nitrogenase from Azotobacter vinelandii. Biochemistry 1980, 19, 2333–2342. [PubMed: 6930302]

(70). Danyal K; Dean DR; Hoffman BM; Seefeldt LC Electron Transfer within Nitrogenase: Evidence for a Deficit-Spending Mechanism. Biochemistry 2011, 50, 9255–9263. [PubMed: 21939270]

(71). Walker JE; Saraste M; Runswick MJ; Gay NJ Distantly Related Sequences in the Alpha- and Beta-Subunits of ATP Synthase, Myosin, Kinases and Other ATP-Requiring Enzymes and a Common Nucleotide Binding Fold. The EMBO Journal 1982, 1, 945–951. [PubMed: 6329717]

(72). Saraste M; Sibbald PR; Wittinghofer A The P-Loop — a Common Motif in ATP- and GTP-Binding Proteins. Trends Biochem. Sci 1990, 15, 430–434. [PubMed: 2126155]

(73). Ryle MJ; Seefeldt LC Elucidation of a MgATP Signal Transduction Pathway in the Nitrogenase Iron Protein: Formation of a Conformation Resembling the MgATP-Bound State by Protein Engineering. Biochemistry 1996, 35, 4766–4775. [PubMed: 8664266]

(74). Jang SB; Seefeldt LC; Peters JW Insights into Nucleotide Signal Transduction in Nitrogenase: Structure of an Iron Protein with MgADP Bound. Biochemistry 2000, 39, 14745–14752. [PubMed: 11101289]

(75). Chen L; Gavini N; Tsuruta H; Eliezer D; Burgess BK; Doniach S; Hodgson KO MgATP-Induced Conformational Changes in the Iron Protein from Azotobacter vinelandii, as Studied by Small-Angle X-Ray Scattering. J. Biol. Chem 1994, 269, 3290–3294. [PubMed: 8106367]

(76). Pence N; Tokmina-Lukaszewska M; Yang ZY; Ledbetter RN; Seefeldt LC; Bothner B; Peters JW Unraveling the Interactions of the Physiological Reductant Flavodoxin with the Different Conformations of the Fe Protein in the Nitrogenase Cycle. J. Biol. Chem 2017, 292, 15661–15669. [PubMed: 28784660]

(77). Zumft WG; Palmer G; Mortenson LE Electron Paramagnetic Resonance Studies on Nitrogenase. II. Interaction of Adenosine 5'-Triphosphate with Azoferredoxin. Biochim. Biophys. Acta 1973, 292, 413–421. [PubMed: 4349919]

(78). Ryle MJ; Lanzilotta WN; Seefeldt LC; Scarrow RC; Jensen GM Circular Dichroism and X-Ray Spectroscopies of Azotobacter vinelandii Nitrogenase Iron Protein. MgATP and MgADP Induced Protein Conformational Changes Affecting the [4Fe-4S] Cluster and Characterization of a [2Fe-2S] Form. J. Biol. Chem 1996, 271, 1551–1557. [PubMed: 8576152]

(79). Stephens PJ; McKenna CE; Smith BE; Nguyen HT; McKenna MC; Thomson AJ; Devlin F; Jones JB Circular Dichroism and Magnetic Circular Dichroism of Nitrogenase Proteins. Proc. Natl. Acad. Sci. U. S. A 1979, 76, 2585–2589. [PubMed: 379860]

(80). Walker GA; Mortenson LE An Effect of Magnesium Adenosine 5'-Triphosphate on the Structure of Azoferredoxin from Clostridium pasteurianum. Biochem. Biophys. Res. Commun 1973, 53, 904–909. [PubMed: 4731956]

(81). Walker GA; Mortenson LE Effect of Magnesium Adenosine 5'-Triphosphate on the Accessibility of the Iron of Clostridial Azoferre-doxin, a Component of Nitrogenase. Biochemistry 1974, 13, 2382–2388. [PubMed: 4364777]

(82). Lanzilotta WN; Ryle MJ; Seefeldt LC Nucleotide Hydrolysis and Protein Conformational Changes in Azotobacter vinelandii Nitrogenase Iron Protein: Defining the Function of Aspartate 129. Biochemistry 1995, 34, 10713–10723. [PubMed: 7662655]

(83). Ljones T; Burris RH Nitrogenase: The Reaction between the Fe Protein and Bathophenanthrolinedisulfonate as a Probe for Interactions with MgATP. Biochemistry 1978, 17, 1866–1872. [PubMed: 656366]

(84). Deits TL; Howard JB Kinetics of MgATP-Dependent Iron Chelation from the Fe-Protein of the Azotobacter vinelandii Nitrogenase Complex. J. Biol. Chem 1989, 264, 6619–6628. [PubMed: 2785107]

(85). Mortenson LE; Walker MN; Walker GA Proceedings of the 1st International Symposium on Nitrogen Fixation, 1975; p 117.

(86). Kurnikov IV; Charnley AK; Beratan DN From ATP to Electron Transfer: Electrostatics and Free-Energy Transduction in Nitrogenase. The Journal of Physical Chemistry B 2001, 105, 5359–5367.

(87). Holm RH; Kennepohl P; Solomon EI Structural and Functional Aspects of Metal Sites in Biology. Chem. Rev 1996, 96, 2239–2314. [PubMed: 11848828]

(88). Noodleman L; Pique ME; Roberts VA In Wiley Encyclo-pedia of Chemical Biology; Begley T, Ed., 2008.

(89). Watt GD; Reddy KRN Formation of an All Ferrous Fe4S4 Cluster in the Iron Protein Component of Azotobacter vinelandii Nitrogenase. J. Inorg. Biochem 1994, 53, 281–294.

(90). Angove HC; Yoo SJ; Burgess BK; Munck E Mossbauer and EPR Evidence for an All-Ferrous Fe4S4 Cluster with S = 4 in the Fe Protein of Nitrogenase. J. Am. Chem. Soc 1997, 119, 8730–8731.

(91). Musgrave KB; Angove HC; Burgess BK; Hedman B; Hodgson KO All-Ferrous Titanium(III) Citrate Reduced Fe Protein of Nitrogenase: An XAS Study of Electronic and Metrical Structure. J. Am. Chem. Soc 1998, 120, 5325–5326.

(92). Jacobs D; Watt GD Nucleotide-Assisted [Fe4S4] Redox State Interconversions of the Azotobacter vinelandii Fe Protein and Their Relevance to Nitrogenase Catalysis. Biochemistry 2013, 52, 4791–4799. [PubMed: 23815521]

(93). Strop P; Takahara PM; Chiu H; Angove HC; Burgess BK; Rees DC Crystal Structure of the All-Ferrous [4Fe-4S]0 Form of the Nitrogenase Iron Protein from Azotobacter vinelandii. Biochemistry 2001, 40, 651–656. [PubMed: 11170381]

(94). Hans M; Buckel W; Bill E Spectroscopic Evidence for an All-Ferrous [4Fe-4S]0 Cluster in the Superreduced Activator of 2-Hydroxyglutaryl-CoA Dehydratase from Acidaminococcus fermentans. J Biol Inorg Chem 2008, 13, 563–574. [PubMed: 18274792]

(95). Rupnik K; Lee CC; Wiig JA; Hu YL; Ribbe MW; Hales BJ Nonenzymatic Synthesis of the P-Cluster in the Nitrogenase MoFe Protein: Evidence of the Involvement of All-Ferrous [Fe4S4]0 Intermediates. Biochemistry 2014, 53, 1108–1116. [PubMed: 24520862]

(96). Scott TA; Berlinguette CP; Holm RH; Zhou HC Initial Synthesis and Structure of an All-Ferrous Analogue of the Fully Reduced [Fe4S4]0 Cluster of the Nitrogenase Iron Protein. Proc. Natl. Acad. Sci. U. S. A 2005, 102, 9741–9744. [PubMed: 15985547]

(97). Zanello P The Competition between Chemistry and Biology in Assembling Iron-Sulfur Derivatives. Molecular Structures and Electro-chemistry. Part V. {[Fe4S4](S-Cys)4} Proteins. Coord. Chem. Rev 2017, 335, 172–227.

(98). Mitra D; George SJ; Guo Y; Kamali S; Keable S; Peters JW; Pelmenschikov V; Case DA; Cramer SP Characterization of [4Fe-4S] Cluster Vibrations and Structure in Nitrogenase Fe Protein at Three Oxidation Levels Via Combined NRVS, EXAFS, and DFT Analyses. J. Am. Chem. Soc 2013, 135, 2530–2543. [PubMed: 23282058]

(99). Lindahl PA; Teo BK; Ormejohnson WH EXAFS Studies of the Nitrogenase Iron Protein from Azotobacter vinelandii. Inorg. Chem 1987, 26, 3912–3916.

(100). Blank MA; Lee CC; Hu Y; Hodgson KO; Hedman B; Ribbe MW Structural Models of the [Fe4S4] Clusters of Homologous Nitrogenase Fe Proteins. Inorg Chem 2011, 50, 7123–7128. [PubMed: 21718019]

(101). Tan ML; Perrin BS Jr.; Niu S; Huang Q; Ichiye T Protein Dynamics and the All-Ferrous [Fe4S4] Cluster in the Nitrogenase Iron Protein. Protein Sci. 2016, 25, 12–18. [PubMed: 26271353]

(102). Wenke BB; Spatzal T; Rees DC Site-Specific Oxidation State Assignments of the Iron Atoms in the [4Fe:4S]2+/1+/0 States of the Nitrogenase Fe-Protein. Angew. Chem. Int. Ed. Engl 2019, 58, 3894–3897. [PubMed: 30698901]

(103). Lindahl PA; Day EP; Kent TA; Orme-Johnson WH; Munck E Mossbauer, EPR, and Magnetization Studies of the Azotobacter vinelandii Fe Protein. Evidence for a [4Fe-4S]1+ Cluster with Spin S = 3/2. J. Biol. Chem 1985, 260, 11160–11173. [PubMed: 2993304]

(104). Lindahl PA; Gorelick NJ; Munck E; Orme-Johnson WH EPR and Mossbauer Studies of Nucleotide-Bound Nitrogenase Iron Protein from Azotobacter vinelandii. J. Biol. Chem 1987, 262, 14945–14953. [PubMed: 2822707]

(105). Watt GD; Wang Z-C; Knotts RR Redox Reactions of and Nucleotide Binding to the Iron Protein of Azotobacter vinelandii. Biochemistry 1986, 25, 8156–8162.

(106). Morgan TV; Prince RC; Mortenson LE Electrochemical Titration of the S = 3/2 and S = ½ States of the Iron Protein of Nitrogenase. FEBS Lett. 1986, 206, 4–8.

(107). Lowery TJ; Wilson PE; Zhang B; Bunker J; Harrison RG; Nyborg AC; Thiriot D; Watt GD Flavodoxin Hydroquinone Re-duces Azotobacter vinelandii Fe Protein to the All-Ferrous Redox State with a S = 0 Spin State. Proc. Natl. Acad. Sci. U. S. A 2006, 103, 17131–17136. [PubMed: 17085583]

(108). Zumft WG; Mortenson LE; Palmer G Electron-Paramagnetic-Resonance Studies on Nitrogenase. Investigation of the Oxidation-Reduction Behaviour of Azoferredoxin and Molybdoferredoxin with Potentiometric and Rapid-Freeze Techniques. Eur. J. Biochem 1974, 46, 525–535. [PubMed: 4368670]

(109). Guo M; Sulc F; Ribbe MW; Farmer PJ; Burgess BK Direct Assessment of the Reduction Potential of the [4Fe-4S]1+/0 Couple of the Fe Protein from Azotobacter vinelandii. J. Am. Chem. Soc 2002, 124, 12100–12101. [PubMed: 12371842]

(110). Chakrabarti M; Deng L; Holm RH; Munck E; Bominaar DL Mossbauer, Electron Paramagnetic Resonance, and Theoretical Studies of a Carbene-Based All-Ferrous Fe4S4 Cluster: Electronic Origin and Structural Identification of the Unique Spectroscopic Site. Inorg Chem 2009, 48, 2735–2747. [PubMed: 19326927]

(111). Chakrabarti M; Munck E; Bominaar EL Density Functional Theory Study of an All Ferrous 4Fe-4S Cluster. Inorg Chem 2011, 50, 4322–4326. [PubMed: 21476577]

(112). Yoo SJ; Angove HC; Burgess BK; Munck E; Peterson J Magnetic Circular Dichroism Study of the All-Ferrous [4Fe-4S] Cluster of the Fe-Protein of Azotobacter vinelandii Nitrogenase. J. Am. Chem. Soc 1998, 120, 9704–9705.

(113). Braaksma A; Haaker H; Grande HJ; Veeger C The Effect of the Redox Potential on the Activity of the Nitrogenase and on the Fe-Protein of Azotobacter vinelandii. Eur. J. Biochem 1982, 121, 483–491. [PubMed: 6276174]

(114). Stephens PJ; Jollie DR; Warshel A Protein Control of Redox Potentials of Iron-Sulfur Proteins. Chem. Rev 1996, 96, 2491–2514. [PubMed: 11848834]

(115). Birrell JA; Laurich C; Reijerse EJ; Ogata H; Lubitz W Importance of Hydrogen Bonding in Fine Tuning the [2Fe-2S] Cluster Redox Potential of HydC from Thermotoga maritima. Biochemistry 2016, 55, 4344–4355. [PubMed: 27396836]

(116). Xiao Z; Maher MJ; Cross M; Bond CS; Guss JM; Wedd AG Mutation of the Surface Valine Residues 8 and 44 in the Rubredoxin from Clostridium pasteurianum: Solvent Access Versus Structural Changes as Determinants of Reversible Potential. J Biol Inorg Chem 2000, 5, 75–84. [PubMed: 10766439]

(117). Lanzilotta WN; Seefeldt LC Changes in the Midpoint Potentials of the Nitrogenase Metal Centers as a Result of Iron Protein Molybdenum-Iron Protein Complex Formation. Biochemistry 1997, 36, 12976–12983. [PubMed: 9335558]

(118). Buckel W; Hetzel M; Kim J ATP-Driven Electron Transfer in Enzymatic Radical Reactions. Curr. Opin. Chem. Biol 2004, 8, 462–467. [PubMed: 15450487]

(119). Kim J; Hetzel M; Boiangiu CD; Buckel W Dehydration of (R)-2-Hydroxyacyl-CoA to Enoyl-CoA in the Fermentation of A-Amino Acids by Anaerobic Bacteria. FEMS Microbiol. Rev 2004, 28, 455–468. [PubMed: 15374661]

(120). Knauer SH; Buckel W; Dobbek H On the ATP-Dependent Activation of the Radical Enzyme (R)-2-Hydroxyisocaproyl-CoA Dehydratase. Biochemistry 2012, 51, 6609–6622. [PubMed: 22827463]

(121). Wittenborn EC; Merrouch M; Ueda C; Fradale L; Leger B ; Fourmond V; Pandelia ME; Dementin S; Drennan CL Redox-Dependent Rearrangements of the NiFeS Cluster of Carbon Monoxide Dehydrogenase. Elife 2018, 7.

(122). Fritsch J; Scheerer P; Frielingsdorf S; Kroschinsky S; Frie-drich B; Lenz O; Spahn CMT The Crystal Structure of an Oxygen-Tolerant Hydrogenase Uncovers a Novel Iron-Sulphur Centre. Nature 2011, 479, 249–253. [PubMed: 22002606]

(123). Noor NDM; Matsuura H; Nishikawa K; Tai HL; Hirota S; Kim J; Kang JY; Tateno M; Yoon KS; Ogo Set al. Redox-De-pendent Conformational Changes of a Proximal [4Fe-4S] Cluster in Hyb-Type [NiFe]-Hydrogenase to Protect the Active Site from O2. Chem. Commun 2018, 54, 12385–12388.

(124). Spatzal T; Perez KA; Howard JB; Rees DC Catalysis-Dependent Selenium Incorporation and Migration in the Nitrogenase Active Site Iron-Molybdenum Cofactor. Elife 2015, 4, e11620. [PubMed: 26673079]

(125). Peters JW; Fisher K; Newton WE; Dean DR Involvement of the P-Cluster in Intramolecular Electron Transfer within the Nitrogenase MoFe Protein. J. Biol. Chem 1995, 270, 27007–27013. [PubMed: 7592949]

(126). Smith BE; Lang G Mossbauer Spectroscopy of the Nitrogenase Proteins from Klebsiella pneumoniae. Structural Assignments and Mechanistic Conclusions. Biochem. J 1974, 137, 169–180. [PubMed: 4596139]

(127). Zimmermann R; Munck E; Brill WJ; Shah VK; Henzl MT; Rawlings J; Orme-Johnson WH Nitrogenase X: Mossbauer and EPR Studies on Reversibly Oxidized MoFe Protein from Azotobacter vinelandii Op. Nature of the Iron Centers. Biochim. Biophys. Acta 1978, 537, 185–207. [PubMed: 215215]

(128). McLean PA; Papaefthymiou V; Orme-Johnson WH; Munck E Isotopic Hybrids of Nitrogenase. Mossbauer Study of MoFe Protein with Selective 57Fe Enrichment of the P-Cluster. J. Biol. Chem 1987, 262, 12900–12903. [PubMed: 2820958]

(129). Keable SM; Zadvornyy OA; Johnson LE; Ginovska B; Rasmussen AJ; Danyal K; Eilers BJ; Prussia GA; LeVan AX; Raugei Set al. Structural Characterization of the P1+ Intermediate State of the P-Cluster of Nitrogenase. J. Biol. Chem 2018, 293, 9629–9635. [PubMed: 29720402]

(130). Cao L; Borner MC; Bergmann J; Caldararu O; Ryde U Geometry and Electronic Structure of the P-Cluster in Nitrogenase Studied by Combined Quantum Mechanical and Molecular Mechanical Calculations and Quantum Refinement. Inorg Chem 2019.

(131). Owens CP; Katz FE; Carter CH; Oswald VF; Tezcan FA Tyrosine-Coordinated P-Cluster in G. diazotrophicus Nitrogenase: Evidence for the Importance of O-Based Ligands in Conformationally Gated Electron Transfer. J. Am. Chem. Soc 2016, 138, 10124–10127. [PubMed: 27487256]

(132). Pierik AJ; Wassink H; Haaker H; Hagen WR Redox Properties and EPR Spectroscopy of the P Clusters of Azotobacter vinelandii MoFe Protein. Eur. J. Biochem 1993, 212, 51–61. [PubMed: 8383042]

(133). Siemann S; Schneider K; Drottboom M; Muller A The Fe-Only Nitrogenase and the Mo Nitrogenase from Rhodobacter capsulatus: A Comparative Study on the Redox Properties of the Metal Clusters Present in the Dinitrogenase Components. Eur. J. Biochem 2002, 269, 1650–1661. [PubMed: 11895435]

(134). Watt GD; Burns A; Lough S; Tennent DL Redox and Spectroscopic Properties of Oxidized MoFe Protein from Azotobacter vinelandii. Biochemistry 1980, 19, 4926–4932. [PubMed: 6252962]

(135). Lanzilotta WN; Christiansen J; Dean DR; Seefeldt LC Evidence for Coupled Electron and Proton Transfer in the [8Fe-7S] Cluster of Nitrogenase. Biochemistry 1998, 37, 11376–11384. [PubMed: 9698385]

(136). O'Donnell MJ; Smith BE Electron-Paramagnetic-Reso-nance Studies on the Redox Properties of the Molybdenum-Iron Protein of Nitrogenase between +50 and −450 mV. Biochem. J 1978, 173, 831–838. [PubMed: 30448]

(137). Watt GD; Bulen WA In Proceedings of the First International Symposium on Nitrogen Fixation; Newton WE;Nymans CJ, Eds.; Washington State University Press: Washington D.C, 1976; Vol. 1.

(138). Lough S; Burns A; Watt GD Redox Reactions of the Nitrogenase Complex from Azotobacter vinelandii. Biochemistry 1983, 22, 4062–4066.

(139). Morgan TV; Mortenson LE; McDonald JW; Watt GD Comparison of Redox and EPR Properties of the Molybdenum Iron Proteins of Clostridium pasteurianum and Azotobacter vinelandii Nitrogenases. J. Inorg. Biochem 1988, 33, 111–120. [PubMed: 2842451]

(140). Sharma S; Sivalingam K; Neese F; Chan GK Low-Energy Spectrum of Iron-Sulfur Clusters Directly from Many-Particle Quantum Mechanics. Nat Chem 2014, 6, 927–933. [PubMed: 25242489]

(141). Li Z; Chan GK Spin-Projected Matrix Product States: Versatile Tool for Strongly Correlated Systems. J Chem Theory Comput 2017, 13, 2681–2695. [PubMed: 28467847]

(142). Li Z; Guo S; Sun Q; Chan GK Electronic Landscape of the P-Cluster of Nitrogenase as Revealed through Many-Electron Quantum Wavefunction Simulations. Nat Chem 2019.

(143). Xiao YM; Fisher K; Smith MC; Newton WE; Case DA ; George SJ; Wang HX; Sturhahn W; Alp EE; Zhao JYet al. How Nitrogenase Shakes - Initial Information About P-Cluster and FeMo-Cofactor Normal Modes from Nuclear Resonance Vibrational Spectroscopy (NRVS). J. Am. Chem. Soc 2006, 128, 7608–7612. [PubMed: 16756317]

(144). Cramer SP; Hodgson KO; Gillum WO; Mortenson LE Molybdenum Site of Nitrogenase - Preliminary Structural Evidence from X-Ray Absorption Spectroscopy. J. Am. Chem. Soc 1978, 100, 3398–3407.

(145). Cramer SP; Gillum WO; Hodgson KO; Mortenson LE; Stiefel EI; Chisnell JR; Brill WJ; Shah VK Molybdenum Site of Nitrogenase. 2. Comparative-Study of Mo-Fe Proteins and Iron-Molybdenum Cofactor by X-Ray Absorption Spectroscopy. J. Am. Chem. Soc 1978, 100, 3814–3819.

(146). Kowalska J; DeBeer S The Role of X-Ray Spectroscopy in Understanding the Geometric and Electronic Structure of Nitrogenase. Biochim. Biophys. Acta 2015, 1853, 1406–1415.

(147). George SJ; Barney BM; Mitra D; Igarashi RY; Guo YS ; Dean DR; Cramer SP; Seefeldt LC EXAFS and NRVS Reveal a Conformational Distortion of the FeMo-Cofactor in the MoFe Nitrogenase Propargyl Alcohol Complex. J. Inorg. Biochem 2012, 112, 85–92. [PubMed: 22564272]

(148). Bjornsson R; Lima FA; Spatzal T; Weyhermuller T; Glatzel P; Bill E; Einsle O; Neese F; DeBeer S Identification of a Spin-Coupled Mo(III) in the Nitrogenase Iron-Molybdenum Cofactor. Chemical Science 2014, 5, 3096–3103.

(149). Zhang LM; Kaiser JT; Meloni G; Yang KY; Spatzal T ; Andrade SLA; Einsle O; Howard JB; Rees DC The 16th Fe in the Nitrogenase MoFe-Protein. Angew. Chem 2013, 52, 10529–10532. [PubMed: 23963815]

(150). Spatzal T; Schlesier J; Burger EM; Sippel D; Zhang L; Andrade SL; Rees DC; Einsle O Nitrogenase FeMoco Investigated by Spatially Resolved Anomalous Dispersion Refinement. Nat Commun 2016, 7, 10902. [PubMed: 26973151]

(151). Raugei S; Seefeldt LC; Hoffman BM Critical Computa-tional Analysis Illuminates the Reductive-Elimination Mechanism That Activates Nitrogenase for N_2 Reduction. Proc. Natl. Acad. Sci. U. S. A 2018, 115, E10521–E10530. [PubMed: 30355772]

(152). Saeki K In Genetics and Regulation of Nitrogen Fixation in Free-Living Bacteria; Klipp W;Masepohl B;Gallon JR;Newton WE, Eds.; Springer Netherlands: Dordrecht, 2005.

(153). Barman BG; Tollin G Flavine-Protein Interactions in Flavoenzymes. Thermodynamics and Kinetics of Reduction of Azotobacter Flavodoxin. Biochemistry 1972, 11, 4755–4759. [PubMed: 4655253]

(154). Fixen KR; Pal Chowdhury N; Martinez-Perez M; Poudel S ; Boyd ES; Harwood CS The Path of Electron Transfer to Nitrogenase in a Phototrophic Alpha-Proteobacterium. Environ Microbiol 2018, 20, 2500–2508. [PubMed: 29708646]

(155). Klugkist J; Voorberg J; Haaker H; Veeger C Characterization of Three Different Flavodoxins from Azotobacter vinelandii. Eur. J. Biochem 1986, 155, 33–40. [PubMed: 3948879]

(156). Martin AE; Burgess BK; Iismaa SE; Smartt CT; Jacobson MR; Dean DR Construction and Characterization of an Azotobacter vinelandii Strain with Mutations in the Genes Encoding Flavodoxin and Ferredoxin I. J. Bacteriol 1989, 171, 3162–3167. [PubMed: 2722744]

(157). Bennett LT; Jacobson MR; Dean DR Isolation, Sequenc-ing, and Mutagenesis of the Niff Gene Encoding Flavodoxin from Azotobacter vinelandii. J. Biol. Chem 1988, 263, 1364–1369. [PubMed: 3121629]

(158). Ledbetter RN; Garcia Costas AM; Lubner CE; Mulder BW; Tokmina-Lukaszewska M; Artz JH; Patterson A; Magnuson TS; Jay ZJ; Duan HDet al. The Electron Bifurcating Fixabcx Protein Complex from Azotobacter vinelandii: Generation of Low-Potential Reducing Equivalents for Nitrogenase Catalysis. Biochemistry 2017, 56, 4177–4190. [PubMed: 28704608]

(159). Mortenson LE Ferredoxin Requirement for Nitrogen Fixation by Extracts of Clostridium Pasteurianum. Biochim. Biophys. Acta 1964, 81, 473–478. [PubMed: 14170319]

(160). Hill S; Kavanagh EP Roles of Niff and Nifj Gene Products in Electron Transport to Nitrogenase in Klebsiella pneumoniae. J. Bacteriol 1980, 141, 470–475. [PubMed: 6988383]

(161). Poudel S; Colman DR; Fixen KR; Ledbetter RN; Zheng Y; Pence N; Seefeldt LC; Peters JW; Harwood CS; Boyd BS Electron Transfer to Nitrogenase in Different Genomic and Metabolic Backgrounds. J. Bacteriol 2018, 200.

(162). Yoch DC The Electron Transport System in Nitrogen Fixation by Azotobacter. IV. Some Oxidation-Reduction Properties of Azotoflavin. Biochem. Biophys. Res. Commun 1972, 49, 335–342. [PubMed: 4404816]

(163). Hageman RV; Burris RH Kinetic Studies on Electron Transfer and Interaction between Nitrogenase Components from Azotobacter vinelandii. Biochemistry 1978, 17, 4117–4124. [PubMed: 708696]

(164). Deistung J; Cannon FC; Cannon MC; Hill S; Thorneley RN Electron Transfer to Nitrogenase in Klebsiella pneumoniae. Niff Gene Cloned and the Gene Product, a Flavodoxin, Purified. Biochem. J 1985, 231, 743–753. [PubMed: 3907625]

(165). Thorneley RN; Deistung J Electron-Transfer Studies Involving Flavodoxin and a Natural Redox Partner, the Iron Protein of Nitrogenase. Conformational Constraints on Protein-Protein Interactions and the Kinetics of Electron Transfer within the Protein Complex. Biochem. J 1988, 253, 587–595. [PubMed: 3140782]

(166). Yates MG Electron Transport to Nitrogenase in Azotobacter chroococcum: Azotobacter Flavodoxin Hydroquinone as an Electron Donor. FEBS Lett. 1972, 27, 63–67. [PubMed: 11946808]

(167). Hallenbeck PC; Gennaro G Stopped-Flow Kinetic Studies of Low Potential Electron Carriers of the Photosynthetic Bacterium, Rhodobacter capsulatus: Ferredoxin I and NifF. Biochim. Biophys. Acta 1998, 1365, 435–442. [PubMed: 9711296]

(168). Howard JB; Kechris KJ; Rees DC; Glazer AN Multiple Amino Acid Sequence Alignment Nitrogenase Component 1: Insights into Phylogenetics and Structure-Function Relationships. PLoS One 2013, 8, e72751. [PubMed: 24019874]

(169). Drummond MH The Base Sequence of the Niff Gene of Klebsiella pneumoniae and Homology of the Predicted Amino Acid Sequence of Its Protein Product to Other Flavodoxins. Biochem. J 1985, 232, 891–896. [PubMed: 3911951]

(170). Alagaratnam S; van Pouderoyen G; Pijning T; Dijkstra BW; Cavazzini D; Rossi GL; Van Dongen WM; van Mierlo CP; van Berkel WJ; Canters GW A Crystallographic Study of Cys69Ala Flavodoxin II from Azotobacter vinelandii: Structural Determinants of Redox Potential. Protein Sci. 2005, 14, 2284–2295. [PubMed: 16131657]

(171). Segal HM; Spatzal T; Hill MG; Udit AK; Rees DC Electrochemical and Structural Characterization of Azotobacter vinelandii Flavodoxin II. Protein Sci. 2017, 26, 1984–1993. [PubMed: 28710816]

(172). Taylor MF; Boylan MH; Edmondson DE Azotobacter vinelandii Flavodoxin: Purification and Properties of the Recombinant, Dephospho Form Expressed in Escherichia coli. Biochemistry 1990, 29, 6911–6918. [PubMed: 2204423]

(173). Steensma E; Heering HA; Hagen WR; Van Mierlo CP Redox Properties of Wild-Type, Cys69Ala, and Cys69Ser Azotobacter vinelandii Flavodoxin II as Measured by Cyclic Voltammetry and EPR Spectroscopy. Eur. J. Biochem 1996, 235, 167–172. [PubMed: 8631324]

(174). Watt GD An Electrochemical Method for Measuring Redox Potentials of Low Potential Proteins by Microcoulometry at Controlled Potentials. Anal. Biochem 1979, 99, 399–407. [PubMed: 517750]

(175). Peelen S; Wijmenga S; Erbel PJ; Robson RL; Eady RR; Vervoort J Possible Role of a Short Extra Loop of the Long-Chain Flavodoxin from Azotobacter chroococcum in Electron Transfer to Nitrogenase: Complete 1H, 15N and 13C Backbone Assignments and Secondary Solution Structure of the Flavodoxin. J. Biomol. NMR 1996, 7, 315–330. [PubMed: 8765738]

(176). Ludwig ML; Pattridge KA; Metzger AL; Dixon MM; Eren M; Feng Y; Swenson RP Control of Oxidation-Reduction Potentials in Flavodoxin from Clostridium beijerinckii: The Role of Conformation Changes. Biochemistry 1997, 36, 1259–1280. [PubMed: 9063874]

(177). Masepohl B; Scholisch K; Gorlitz K; Kutzki C; Bohme H The Heterocyst-Specific Fdxh Gene Product of the Cyanobacterium Anabaena Sp. Pcc 7120 Is Important but Not Essential for Nitrogen Fixation. Mol. Gen. Genet 1997, 253, 770–776. [PubMed: 9079890]

(178). Edgren T; Nordlund S Electron Transport to Nitrogenase in Rhodospirillum rubrum: Identification of a New Fdxn Gene Encoding the Primary Electron Donor to Nitrogenase. FEMS Microbiol. Lett 2005, 245, 345–351. [PubMed: 15837392]

(179). Schrautemeier B; Cassing A; Bohme H Characterization of the Genome Region Encoding an Fdxh-Type Ferredoxin and a New 2[4Fe-4S] Ferredoxin from the Nonheterocystous, Nitrogen-Fixing Cyanobacterium Plectonema Boryanum Pcc 73110. J. Bacteriol 1994, 176, 1037–1046. [PubMed: 8106314]

(180). Martin AE; Burgess BK; Stout CD; Cash VL; Dean BR; Jensen GM; Stephens PJ Site-Directed Mutagenesis of Azotobacter vinelandii Ferredoxin I: [Fe-S] Cluster-Driven Protein Rearrangement. Proc. Natl. Acad. Sci. U. S. A 1990, 87, 598–602. [PubMed: 2153958]

(181). Shen B; Jollie DR; Diller TC; Stout CD; Stephens PJ ; Burgess BK Site-Directed Mutagenesis of Azotobacter vinelandii Ferredoxin I: Cysteine Ligation of the [4Fe-4S] Cluster with Protein Rear rangement Is Preferred over Serine Ligation. Proc. Natl. Acad. Sci. U. S. A 1995, 92, 10064–10068. [PubMed: 7479727]

(182). Schipke CG; Goodin DB; McRee DE; Stout CD Oxidized and Reduced Azotobacter vinelandii Ferredoxin I at 1.4 A Resolution: Conformational Change of Surface Residues without Significant Change in the [3Fe-4S]+/0 Cluster. Biochemistry 1999, 38, 8228–8239. [PubMed: 10387068]

(183). Chen K; Tilley GJ; Sridhar V; Prasad GS; Stout CD; Armstrong FA; Burgess BK Alteration of the Reduction Potential of the [4Fe-4S]2+/+ Cluster of Azotobacter vinelandii Ferredoxin I. J. Biol. Chem 1999, 274, 36479–36487. [PubMed: 10593945]

(184). Chen K; Hirst J; Camba R; Bonagura CA; Stout CD; Burgess BK; Armstrong FA Atomically Defined Mechanism for Proton Transfer to a Buried Redox Centre in a Protein. Nature 2000, 405, 814–817. [PubMed: 10866206]

(185). Stout CD Structure of the Iron-Sulphur Clusters in Azotobacter Ferredoxin at 4.0 Å Resolution. Nature 1979, 279, 83–84. [PubMed: 450082]

(186). Stout CD Refinement of the 7 Fe Ferredoxin from Azotobacter vinelandii at 1.9 A Resolution. J. Mol. Biol 1989, 205, 545–555. [PubMed: 2926817]

(187). Stout CD Crystal Structures of Oxidized and Reduced Azotobacter vinelandii Ferredoxin at pH 8 and 6. J. Biol. Chem 1993, 268, 25920–25927. [PubMed: 8245025]

(188). Naud I; Meyer C; David L; Breton J; Gaillard J; Jouanneau Y Identification of Residues of Rhodobacter capsulatus Ferredoxin I Important for Its Interaction with Nitrogenase. Eur. J. Biochem 1996, 237, 399–405. [PubMed: 8647078]

(189). Iismaa SE; Vazquez AE; Jensen GM; Stephens PJ; Butt JN; Armstrong FA; Burgess BK Site-Directed Mutagenesis of Azotobacter vinelandii Ferredoxin I. Changes in [4Fe-4S] Cluster Reduction Potential and Reactivity. J. Biol. Chem 1991, 266, 21563–21571. [PubMed: 1657971]

(190). Shen B; Martin LL; Butt JN; Armstrong FA; Stout CD; Jensen GM; Stephens PJ; La Mar GN; Gorst CM; Burgess BK Azotobacter vinelandii Ferredoxin I. Aspartate 15 Facilitates Proton Transfer to the Reduced [3Fe-4S] Cluster. J. Biol. Chem 1993, 268, 25928–25939. [PubMed: 8245026]

(191). Yoch DC; Arnon DI Two Biologically Active Ferredoxins from the Aerobic Nitrogen-Fixing Bacterium, Azotobacter vinelandii. J. Biol. Chem 1972, 247, 4514–4520. [PubMed: 5043852]

(192). Renner KA; Howard JB Aluminum Fluoride Inhibition of Nitrogenase: Stabilization of a Nucleotide Fe-Protein MoFe-Protein Complex. Biochemistry 1996, 35, 5353–5358. [PubMed: 8611524]

(193). Duyvis MG; Wassink H; Haaker H Formation and Characterization of a Transition State Complex of Azotobacter vinelandii Nitrogenase. FEBS Lett. 1996, 380, 233–236. [PubMed: 8601431]

(194). Willing AH; Georgiadis MM; Rees DC; Howard JB Cross-Linking of Nitrogenase Components - Structure and Activity of the Covalent Complex. J. Biol. Chem 1989, 264, 8499–8503. [PubMed: 2722786]

(195). Willing A; Howard JB Cross-Linking Site in Azotobacter vinelandii Complex. J. Biol. Chem 1990, 265, 6596–6599. [PubMed: 2324093]

(196). Gray HB; Winkler JR Electron Transfer in Proteins. Annu. Rev. Biochem 1996, 65, 537–561. [PubMed: 8811189]

(197). Rice S; Lin AW; Safer D; Hart CL; Naber N; Carragher AO; Cain SM; Pechatnikova E; Wilson-Kubalek EM; Whittaker Met al. A Structural Change in the Kinesin Motor Protein That Drives Motility. Nature 1999, 402, 778–784. [PubMed: 10617199]

(198). Vale RD; Milligan RA The Way Things Move: Looking under the Hood of Molecular Motor Proteins. Science 2000, 288, 88–95. [PubMed: 10753125]

(199). Holmes KC; Angert I; Kull FJ; Jahn W; Schroder RR Electron Cryo-Microscopy Shows How Strong Binding of Myosin to Actin Releases Nucleotide. Nature 2003, 425, 423–427. [PubMed: 14508495]

(200). Weston MF; Kotake S; Davis LC Interaction of Nitrogenase with Nucleotide Analogs of ATP and ADP and the Effect of Metal Ions on ADP Inhibition. Arch. Biochem. Biophys 1983, 225, 809–817. [PubMed: 6354096]

(201). Abrahams JP; Leslie AG; Lutter R; Walker JE Structure at 2.8 a Resolution of F1-ATPase from Bovine Heart Mitochondria. Nature 1994, 370, 621–628. [PubMed: 8065448]

(202). Boyer PD The ATP Synthase--a Splendid Molecular Machine. Annu. Rev. Biochem 1997, 66, 717–749. [PubMed: 9242922]

(203). Sauer RT; Baker TA AAA+ Proteases: ATP-Fueled Ma-chines of Protein Destruction. Annu. Rev. Biochem 2011, 80, 587–612. [PubMed: 21469952]

(204). Yang ZY; Ledbetter R; Shaw S; Pence N; Tokmina-Lukaszewska M; Eilers B; Guo Q; Pokhrel N; Cash VL; Dean DRet al. Evidence That the Pi Release Event Is the Rate-Limiting Step in the Nitrogenase Catalytic Cycle. Biochemistry 2016, 55, 3625–3635. [PubMed: 27295169]

(205). Erickson JA; Nyborg AC; Johnson JL; Truscott SM; Gunn A; Nordmeyer FR; Watt GD Enhanced Efficiency of ATP Hydrolysis During Nitrogenase Catalysis Utilizing Reductants That Form the All-Ferrous Redox State of the Fe Protein. Biochemistry 1999, 38, 14279–14285. [PubMed: 10572002]

(206). Klugkist J; Haaker H; Wassink H; Veeger C The Catalytic Activity of Nitrogenase in Intact Azotobacter vinelandii Cells. Eur. J. Biochem 1985, 146, 509–515. [PubMed: 3855749]

(207). Duyvis MG; Wassink H; Haaker H Nitrogenase of Azotobacter vinelandii: Kinetic Analysis of the Fe Protein Redox Cycle. Biochemistry 1998, 37, 17345–17354. [PubMed: 9860849]

(208). Seefeldt LC Docking of Nitrogenase Iron-and Molybdenum-Iron Proteins for Electron Transfer and MgATP Hydrolysis: The Role of Arginine 140 and Lysine 143 of the Azotobacter vinelandii Iron Protein. Protein Sci. 1994, 3, 2073–2081. [PubMed: 7703853]

(209). Poole RK; Hill S Respiratory Protection of Nitrogenase Activity in Azotobacter vinelandii - Roles of the Terminal Oxidases. Biosci. Rep 1997, 17, 303–317. [PubMed: 9337485]

(210). Scherings G; Haaker H; Veeger C Regulation of Nitrogen Fixation by Fe-S Protein II in Azotobacter vinelandii. Eur. J. Biochem 1977, 77, 21–30. [PubMed: 196854]

(211). Robson RL Characterization of an Oxygen-Stable Nitrogenase Complex Isolated from Azotobacter chroococcum. Biochem. J 1979, 181, 569–575. [PubMed: 518541]

(212). Moshiri F; Kim JW; Fu C; Maier RJ The Fesii Protein of Azotobacter vinelandii Is Not Essential for Aerobic Nitrogen Fixation, but Confers Significant Protection to Oxygen-Mediated Inactivation of Nitrogenase in vitro and in vivo. Mol. Microbiol 1994, 14, 101–114. [PubMed: 7830548]

(213). Schlesier J; Rohde M; Gerhardt S; Einsle O A Conformational Switch Triggers Nitrogenase Protection from Oxygen Damage by Shethna Protein II (Fesii). J. Am. Chem. Soc 2016, 138, 239–247. [PubMed: 26654855]

(214). Moshiri F; Crouse BR; Johnson MK; Maier RJ The “Nitrogenase-Protective” Fesii Protein of Azotobacter vinelandii: Overex-pression, Characterization, and Crystallization. Biochemistry 1995, 34, 12973–12982. [PubMed: 7548055]

(215). Milton RD; Cai R; Sahin S; Abdellaoui S; Alkotaini B; Leech D; Minteer SD The in Vivo Potential-Regulated Protective Protein of Nitrogenase in Azotobacter vinelandii Supports Aerobic Bioelectrochemical Dinitrogen Reduction in Vitro. J. Am. Chem. Soc 2017, 139, 9044–9052. [PubMed: 28595003]

(216). Ke B; Bulen WA; Shaw ER; Breeze RH Determination of Oxidation-Reduction Potentials by Spectropolarimetric Titration: Appli-cation to Several Iron-Sulfur Proteins. Arch. Biochem. Biophys 1974, 162, 301–309. [PubMed: 4831335]

(217). Yates MG; Thorneley RN; Lowe DJ Nitrogenase of Azotobacter chroococcum: Inhibition of ADP of the Reduction of Oxidised Fe Protein by Sodium Dithionite. FEBS Lett. 1975, 60, 89–93. [PubMed: 179869]

(218). Thorneley RN Nitrogenase of Klebsiella pneumoniae. A Stopped-Flow Study of Magnesium-Adenosine Triphosphate-Induce Electron Transfer between the Compeonent Proteins. Biochem. J 1975, 145, 391–396. [PubMed: 1098654]

(219). Thorneley RN; Cornish-Bowden A Kinetics of Nitrogenase of Klebsiella pneumoniae. Heterotropic Interactions between Magnesium-Adenosine 5'-Diphosphate and Magnesium-Adenosine 5’-Triphosphate. Biochem. J 1977, 165, 255–262. [PubMed: 336036]

(220). Smith BE; Lowe DJ; Chen GX; O'Donnell MJ; Hawkes TR Evidence on Intramolecular Electron Transfer in the MoFe Protein of Nitrogenase from Klebsiella pneumoniae from Rapid-Freeze Electron-Paramagnetic-Resonance Studies of Its Oxidation by Ferricyanide. The Biochemical journal 1983, 209, 207–213. [PubMed: 6303301]

(221). Thorneley RN; Lowe DJ Nitrogenase of Klebsiella pneumoniae. Kinetics of the Dissociation of Oxidized Iron Protein from Molyb-denum-Iron Protein: Identification of the Rate-Limiting Step for Substrate Reduction. Biochem. J 1983, 215, 393–403. [PubMed: 6316927]

(222). Lowe DJ; Thorneley RN The Mechanism of Klebsiella pneumoniae Nitrogenase Action. The Determination of Rate Constants Re-quired for the Simulation of the Kinetics of N_2 Reduction and H2 Evolution. Biochem. J 1984, 224, 895–901. [PubMed: 6395863]

(223). Lowe DJ; Thorneley RN The Mechanism of Klebsiella pneumoniae Nitrogenase Action. Pre-Steady-State Kinetics of H2 Formation. Biochem. J 1984, 224, 877–886. [PubMed: 6395861]

(224). Thorneley RNF; Lowe DJ In Molybdenum Enzymes; Spiro TG, Ed.; Wiley-Interscience: New York, 1985.

(225). Thorneley RN; Ashby G; Howarth JV; Millar NC; Gutfreund H A Transient-Kinetic Study of the Nitrogenase of Klebsiella pneumoniae by Stopped-Flow Calorimetry. Comparison with the Myosin ATPase. Biochem. J 1989, 264, 657–661. [PubMed: 2695063]

(226). Ashby GA; Thorneley RN Nitrogenase of Klebsiella pneumoniae. Kinetic Studies on the Fe Protein Involving Reduction by Sodium Dithionite, the Binding of MgADP and a Conformation Change That Alters the Reactivity of the 4Fe-4S Centre. Biochem. J 1987, 246, 455–465. [PubMed: 3318808]

(227). Seefeldt LC; Hoffman BM; Peters JW; Raugei S; Beratan DN; Antony E; Dean DR Energy Transduction in Nitrogenase. Acc Chem Res 2018, 51, 2179–2186. [PubMed: 30095253]

(228). Fisher K; Lowe DJ; Thorneley RN Klebsiella pneumoniae Nitrogenase. The Pre-Steady-State Kinetics of MoFe-Protein Reduction and Hydrogen Evolution under Conditions of Limiting Electron Flux Show That the Rates of Association with the Fe-Protein and Electron Transfer Are Independent of the Oxidation Level of the MoFe-Protein. Biochem. J 1991, 279 (Pt 1), 81–85. [PubMed: 1656943]

(229). Lowe DJ; Fisher K; Thorneley RN Klebsiella pneumoniae Nitrogenase: Pre-Steady-State Absorbance Changes Show That Redox Changes Occur in the MoFe Protein That Depend on Substrate and Component Protein Ratio; a Role for P-Centres in Reducing Dinitrogen? Biochem. J 1993, 292 (Pt 1), 93–98. [PubMed: 8389132]

(230). Thorneley RN; Lowe DJ The Mechanism of Klebsiella pneumoniae Nitrogenase Action. Simulation of the Dependences of H2-Evolution Rate on Component-Protein Concentration and Ratio and Sodium Dithionite Concentration. Biochem. J 1984, 224, 903–909. [PubMed: 6395864]

(231). Janin J Specific Versus Non-Specific Contacts in Protein Crys-tals. Nat. Struct. Biol 1997, 4, 973–974. [PubMed: 9406542]

(232). Cordewener J; Haaker H; Veeger C Binding of MgATP to the Nitrogenase Proteins from Azotobacter vinelandii. Eur. J. Biochem 1983, 132, 47–54. [PubMed: 6601579]

(233). Knowles CJ; Smith L Measurements of ATP Levels of Intact Azotobacter vinelandii under Different Conditions. Biochim. Biophys. Acta 1970, 197, 152–160. [PubMed: 5416106]

(234). Owens CP; Katz FE; Carter CH; Luca MA; Tezcan BA Evidence for Functionally Relevant Encounter Complexes in Nitrogenase Catalysis. J. Am. Chem. Soc 2015, 137, 12704–12712. [PubMed: 26360912]

(235). Thorneley RN; Eady RR; Yates MG Nitrogenases of Klebsiella pneumoniae and Azotobacter Chroococum. Complex Formation between the Component Proteins. Biochim. Biophys. Acta 1975, 403, 269–284. [PubMed: 1101961]

(236). Katz FEH; Owens CP; Tezcan FA Electron Transfer Reactions in Biological Nitrogen Fixation. Isr. J. Chem 2016, 56, 682–692.

(237). Danyal K; Mayweather D; Dean DR; Seefeldt LC; Hoffman BM Conformational Gating of Electron Transfer from the Nitrogenase Fe Protein to MoFe Protein. J. Am. Chem. Soc 2010, 132, 6894-+. [PubMed: 20429505]

(238). Steinfeld JI; Francisco JS; Hase WL Chemical Kinetics and Dynamics; 2nd ed; Prentice-Hall, Inc: Upper Saddle River, NJ, 1999.

(239). Parsegian VA; Rand RP; Rau DC Macromolecules and Water: Probing with Osmotic Stress. Methods Enzymol 1995, 259, 43–94. [PubMed: 8538466]

(240). Lanzilotta WN; Parker VD; Seefeldt LC Electron Transfer in Nitrogenase Analyzed by Marcus Theory: Evidence for Gating by MgATP. Biochemistry 1998, 37, 399–407. [PubMed: 9425061]

(241). Howard JB; Rees DC Nitrogenase - a Nucleotide-Dependent Molecular Switch. Annu. Rev. Biochem 1994, 63, 235–264. [PubMed: 7979238]

(242). Rutledge HL; Rittle J; Williamson LM; Xu WA; Gagnon DM; Tezcan FA Redox-Dependent Metastability of the Nitrogenase P-Cluster. J. Am. Chem. Soc 2019, 141, 10091–10098. [PubMed: 31146522]

(243). Nicolet Y; Rohac R; Martin L; Fontecilla-Camps JC X-Ray Snapshots of Possible Intermediates in the Time Course of Synthesis and Degradation of Protein-Bound Fe4S4 Clusters. Proc. Natl. Acad. Sci. U. S. A 2013, 110, 7188–7192. [PubMed: 23596207]

(244). Jeng DY; Morris JA; Mortenson LE The Effect of Reductant in Inorganic Phosphate Release from Adenosine 5'-Triphosphate by Purified Nitrogenase of Clostridium pasteurianum. J. Biol. Chem 1970, 245, 2809–2813. [PubMed: 5423376]

(245). Lanzilotta WN; Fisher K; Seefeldt LC Evidence for Electron Transfer from the Nitrogenase Iron Protein to the Molybdenum-Iron Protein without MgATP Hydrolysis: Characterization of a Tight Protein-Protein Complex. Biochemistry 1996, 35, 7188–7196. [PubMed: 8679547]

(246). Duval S; Danyal K; Shaw S; Lytle AK; Dean DR; Hoffman BM; Antony E; Seefeldt LC Electron Transfer Precedes ATP Hydrolysis During Nitrogenase Catalysis. Proc. Natl. Acad. Sci. U. S. A 2013, 110, 16414–16419. [PubMed: 24062462]

(247). Lanzilotta WN; Seefeldt LC Electron Transfer from the Nitrogenase Iron Protein to the [8Fe-(7/8)S] Clusters of the Molybdenum-Iron Protein. Biochemistry 1996, 35, 16770–16776. [PubMed: 8988014]

(248). Mensink RE; Wassink H; Haaker H A Reinvestigation of the Pre-Steady-State ATPase Activity of the Nitrogenase from Azotobacter vinelandii. Eur. J. Biochem 1992, 208, 289–294. [PubMed: 1325902]

(249). Duyvis MG; Wassink H; Haaker H Pre-Steady-State MgATP-Dependent Proton Production and Electron Transfer by Nitrogenase from Azotobacter vinelandii. Eur. J. Biochem 1994, 225, 881–890. [PubMed: 7957225]

(250). Lowe DJ; Ashby GA; Brune M; Knights H; Webb MR; Thorneley RNF In Nitrogen Fixation: Fundamentals and Applications; Tikhonovich IA;Provorov NA;Romanov VI;Newton WE, Eds.; Springer, Dordrecht: The Netherlands, 1995.

(251). Ljones T; Burris RH ATP Hydrolysis and Electron Transfer in the Nitrogenase Reaction with Different Combinations of the Iron Protein and the Molybdenum-Iron Protein. Biochim. Biophys. Acta 1972, 275, 93–101. [PubMed: 5049020]

(252). Eady RR; Postgate JR Nitrogenase. Nature 1974, 249, 805–810. [PubMed: 4134899]

(253). Imam S; Eady RR Nitrogenase of Klebsiella pneumoniae: Reductant-Independent ATP Hydrolysis and the Effect of pH on the Efficiency of Coupling of ATP Hydrolysis to Substrate Reduction. FEBS Lett. 1980, 110, 35–38. [PubMed: 6444386]

(254). Thorneley RN; Lowe DJ Molybdenum Enzymes; Wiley: New York, 1985.

(255). Hallenbeck PC Nitrogenase Reduction by Electron Carriers: Influence of Redox Potential on Activity and the ATP/2e-Ratio. Arch. Biochem. Biophys 1983, 220, 657–660. [PubMed: 6572045]

(256). Hardy RWF; Knight E Reductant-Dependent Adenosine Triphosphatase of Nitrogen-Fixing Extracts of Azotobacter vinelandii. Biochim. Biophys. Acta 1966, 122, 520-&.

(257). Angove HC; Yoo SJ; Munck E; Burgess BK An All-Ferrous State of the Fe Protein of Nitrogenase. Interaction with Nucleotides and Electron Transfer to the MoFe Protein. J. Biol. Chem 1998, 273, 26330–26337. [PubMed: 9756863]

(258). Rupnik K; Hu Y; Lee CC; Wiig JA; Ribbe MW; Hales BJ P+ State of Nitrogenase P-Cluster Exhibits Electronic Structure of a [Fe4S4]+ Cluster. J. Am. Chem. Soc 2012, 134, 13749–13754. [PubMed: 22839751]

(259). Ljones T; Burris RH Evidence for One-Electron Transfer by the Fe Protein of Nitrogenase. Biochem. Biophys. Res. Commun 1978, 80, 22–25. [PubMed: 623653]

(260). Lanzilotta WN; Fisher K; Seefeldt LC Evidence for Electron Transfer-Dependent Formation of a Nitrogenase Iron Protein-Molybdenum-Iron Protein Tight Complex. The Role of Aspartate 39. J. Biol. Chem 1997, 272, 4157–4165. [PubMed: 9020128]

(261). Chan JM; Wu W; Dean DR; Seefeldt LC Construction and Characterization of a Heterodimeric Iron Protein: Defining Roles for Adenosine Triphosphate in Nitrogenase Catalysis. Biochemistry 2000, 39, 7221–7228. [PubMed: 10852721]

(262). Christiansen J; Chan JM; Seefeldt LC; Dean DR The Role of the MoFe Protein Alpha-125Phe and Beta-125Phe Residues in Azotobacter vinelandii MoFe Protein-Fe Protein Interaction. J. Inorg. Biochem 2000, 80, 195–204. [PubMed: 11001089]

(263). Danyal K; Shaw S; Page TR; Duval S; Horitani M; Marts AR; Lukoyanov D; Dean DR; Raugei S; Hoffman BMet al. Negative Cooperativity in the Nitrogenase Fe Protein Electron Delivery Cycle. Proc. Natl. Acad. Sci. U. S. A 2016, 113, E5783–E5791. [PubMed: 27698129]

(264). Davis LC; Henzl MT; Burris RH; Orme-Johnson WH Iron-Sulfur Clusters in the Molybdenum-Iron Protein Component of Nitrogenase. Electron Paramagnetic Resonance of the Carbon Monoxide Inhib-ited State. Biochemistry 1979, 18, 4860–4869. [PubMed: 228701]

(265). Meyer J Comparison of Carbon Monoxide, Nitric Oxide, and Nitrite as Inhibitors of the Nitrogenase from Clostridium pasteurianum. Arch. Biochem. Biophys 1981, 210, 246–256. [PubMed: 6945823]

(266). Lowe DJ; Fisher K; Thorneley RN Klebsiella pneumoniae Nitrogenase. Mechanism of Acetylene Reduction and Its Inhibition by Carbon Monoxide. Biochem. J 1990, 272, 621–625. [PubMed: 2268290]

(267). Henthorn JT; Arias RJ; Koroidov S; Kroll T; Sokaras D; Bergmann U; Rees DC; DeBeer S Localized Electronic Structure of Nitrogenase FeMoco Revealed by Selenium K-Edge High Resolution X-Ray Absorption Spectroscopy. J. Am. Chem. Soc 2019, 141, 13676–13688. [PubMed: 31356071]

(268). Igarashi RY; Laryukhin M; Dos Santos PC; Lee HI; Dean DR; Seefeldt LC; Hoffman BM Trapping H-Bound to the Nitrogenase FeMo-Cofactor Active Site During H2 Evolution: Characterization by Endor Spectroscopy. J. Am. Chem. Soc 2005, 127, 6231–6241. [PubMed: 15853328]

(269). Kok B; Forbush B; McGloin M Cooperation of Charges in Photosynthetic O2 Evolution - I. A Linear Four Step Mechanism. Photochem. Photobiol. 1970, 11, 457–475.

(270). Milton RD; Cai R; Abdellaoui S; Leech D; De Lacey AL ; Pita M; Minteer SD Bioelectrochemical Haber-Bosch Process: An Ammonia-Producing H2 /N2 Fuel Cell. Angew. Chem. Int. Ed. Engl 2017, 56, 2680–2683. [PubMed: 28156040]

(271). Hu B; Harris DF; Dean DR; Liu TL; Yang ZY; Seefeldt LC Electrocatalytic CO2 Reduction Catalyzed by Nitrogenase MoFe and FeFe Proteins. Bioelectrochemistry 2018, 120, 104–109. [PubMed: 29223886]

(272). Liu X; Kang F; Hu C; Wang L; Xu Z; Zheng D; Gong W; Lu Y; Ma Y; Wang J A Genetically Encoded Photosensitizer Protein Facilitates the Rational Design of a Miniature Photocatalytic CO2-Reducing Enzyme. Nat Chem 2018, 10, 1201–1206. [PubMed: 30397317]

(273). Zadvornyy OA; Lucon JE; Gerlach R; Zorin NA; Douglas T; Elgren TE; Peters JW Photo-Induced H2 Production by [NiFe]-Hydrogenase from T. roseopersicina Covalently Linked to a Ru(II) Photosensitizer. J. Inorg. Biochem 2012, 106, 151–155. [PubMed: 22119807]

(274). Millett F; Durham B Design of Photoactive Ruthenium Complexes to Study Interprotein Electron Transfer. Biochemistry 2002, 41, 11315–11324. [PubMed: 12234172]

(275). Brown KA; Dayal S; Ai X; Rumbles G; King PW Controlled Assembly of Hydrogenase-CdTe Nanocrystal Hybrids for Solar Hydrogen Production. J. Am. Chem. Soc 2010, 132, 9672–9680. [PubMed: 20583755]

(276). Hutton GA; Reuillard B; Martindale BC; Caputo CA; Lockwood CW; Butt JN; Reisner E Carbon Dots as Versatile Photosensitizers for Solar-Driven Catalysis with Redox Enzymes. J. Am. Chem. Soc 2016, 138, 16722–16730. [PubMed: 27977174]

(277). Halavaty A; Muller JJ; Contzen J; Jung C; Hannemann D ; Bernhardt R; Galander M; Lendzian F; Heinemann U Light-In-duced Reduction of Bovine Adrenodoxin Via the Covalently Bound Ruthenium(II) Bipyridyl Complex: Intramolecular Electron Transfer and Crystal Structure. Biochemistry 2006, 45, 709–718. [PubMed: 16411746]

(278). Pan LP; Frame M; Durham B; Davis D; Millett F Photoinduced Electron-Transfer within Complexes between Plastocyanin and Ruthenium Bisbipyridine Dicarboxybipyridine Cytochrome-C Derivatives. Biochemistry 1990, 29, 3231–3236. [PubMed: 2159332]

(279). Geren L; Hahm S; Durham B; Millett F Photoinduced Electron-Transfer between Cytochrome-C Peroxidase and Yeast Cytochrome-C Labeled at Cys-102 with (4-Bromomethyl-4'-Methylbipyridine)[Bis(Bipyridine)]Ruthenium2^{+}. Biochemistry 1991, 30, 9450–9457. [PubMed: 1654098]

(280). Takashima H; Shinkai S; Hamachi I Ru(Bpy)(3)-Based Ar-tificial Receptors toward a Protein Surface: Selective Binding and Efficient Photoreduction of Cytochrome C. Chem. Commun 1999, 2345–2346.

(281). Berglund J; Pascher T; Winkler JR; Gray HB Photoinduced Oxidation of Horseradish Peroxidase. J. Am. Chem. Soc 1997, 119, 2464–2469.

(282). Ener ME; Lee YT; Winkler JR; Gray HB; Cheruzel L Photooxidation of Cytochrome P450-BM3. Proc. Natl. Acad. Sci. U. S. A 2010, 107, 18783–18786. [PubMed: 20947800]

(283). Lo KKW; Hui WK; Chung CK; Tsang KHK; Ng DCM; Zhu NY; Cheung KK Biological Labelling Reagents and Probes Derived from Luminescent Transition Metal Polypyridine Complexes. Coord. Chem. Rev 2005, 249, 1434–1450.

(284). Murtaza Z; Herman P; Lakowicz JR Synthesis and Spectral Characterization of a Long-Lifetime Osmium (II) Metal-Ligand Complex: A Conjugatable Red Dye for Applications in Biophysics. Biophys. Chem 1999, 80, 143–151. [PubMed: 10483708]

(285). Chaudhary YS; Woolerton TW; Allen CS; Warner JH; Pierce E; Ragsdale SW; Armstrong FA Visible Light-Driven CO2 Reduction by Enzyme Coupled CdS Nanocrystals. Chem. Commun 2012, 48, 58–60.

(286). Brown KA; Wilker MB; Boehm M; Dukovic G; King PW Characterization of Photochemical Processes for H2 Production by CdS Nanorod-[FeFe] Hydrogenase Complexes. J. Am. Chem. Soc 2012, 134, 5627–5636. [PubMed: 22352762]

(287). Greene BL; Joseph CA; Maroney MJ; Dyer RB Direct Evidence of Active-Site Reduction and Photodriven Catalysis in Sensitized Hydrogenase Assemblies. J. Am. Chem. Soc 2012, 134, 11108–11111. [PubMed: 22716776]

(288). Novoderezhkin VI; Romero E; Dekker JP; van Grondelle R Multiple Charge-Separation Pathways in Photosystem II: Modeling of Transient Absorption Kinetics. Chemphyschem 2011, 12, 681–688. [PubMed: 21322104]

(289). Durrant JR; Hastings G; Joseph DM; Barber J; Porter D ; Klug DR Subpicosecond Equilibration of Excitation Energy in Isolated Photosystem II Reaction Centers. Proc. Natl. Acad. Sci. U. S. A 1992, 89, 11632–11636. [PubMed: 1454856]

(290). Groot ML; van Mourik F; Eijckelhoff C; van Stokkum IHM; Dekker JP; van Grondelle R Charge Separation in the Reaction Center of Photosystem II Studied as a Function of Temperature. Proc. Natl. Acad. Sci. U. S. A 1997, 94, 4389–4394. [PubMed: 9113999]

(291). Maroti P Flash-Induced Proton-Transfer in Photosynthetic Bacteria. Photosynthesis Res. 1993, 37, 1–17.

(292). Clayton RK Primary Processes in Bacterial Photosynthesis. Annu. Rev. Biophys. Bioeng 1973, 2, 131–156. [PubMed: 4583652]

(293). Brettel K; Byrdin M Reaction Mechanisms of DNA Photoly-ase. Curr. Opin. Struct. Biol 2010, 20, 693–701. [PubMed: 20705454]

(294). Winkler JR; Gray HB Electron-Transfer in Ruthenium-Modified Proteins. Chem. Rev 1992, 92, 369–379.

(295). Gray HB; Maverick AW Solar Chemistry of Metal-Complexes. Science 1981, 214, 1201–1205. [PubMed: 17789279]

(296). Alivisatos AP Semiconductor Clusters, Nanocrystals, and Quantum Dots. Science 1996, 271, 933–937.

(297). Utterback JK; Wilker MB; Mulder DW; King PW; Eaves JD; Dukovic G Quantum Efficiency of Charge Transfer Competing against Nonexponential Processes: The Case of Electron Transfer from CdS Nanorods to Hydrogenase. J Phys Chem C 2019, 123, 886–896.

(298). Wilker MB; Shinopoulos KE; Brown KA; Mulder DW; King PW; Dukovic G Electron Transfer Kinetics in CdS Nanorod-[FeFe]-Hydrogenase Complexes and Implications for Photochemical H2 Generation. J. Am. Chem. Soc 2014, 136, 4316–4324. [PubMed: 24564271]

(299). Corbin JL Liquid Chromatographic-Fluorescence Determination of Ammonia from Nitrogenase Reactions: A 2-Min Assay. Appl. Environ. Microbiol. 1984, 47, 1027–1030.

(300). Andersen SZ; Colic V; Yang S; Schwalbe JA; Nielander AC; McEnaney JM; Enemark-Rasmussen K; Baker JG; Singh AR; Rohr BAet al. A Rigorous Electrochemical Ammonia Synthesis Protocol with Quantitative Isotope Measurements. Nature 2019, 570, 504–508. [PubMed: 31117118]

(301). Monti D; Ottolina G; Carrea G; Riva S Redox Reactions Catalyzed by Isolated Enzymes. Chem. Rev 2011, 111, 4111–4140. [PubMed: 21526768]

(302). Noth J; Krawietz D; Hemschemeier A; Happe T Pyruvate:Ferredoxin Oxidoreductase Is Coupled to Light-Independent Hydrogen Production in Chlamydomonas reinhardtii. J. Biol. Chem 2013, 288, 4368–4377. [PubMed: 23258532]

(303). Zadvorny OA; Zorin NA; Gogotov IN Transformation of Metals and Metal Ions by Hydrogenases from Phototrophic Bacteria. Arch. Microbiol 2006, 184, 279–285. [PubMed: 16283252]

(304). Prasad B; Mah DJ; Lewis AR; Plettner E Water Oxidation by a Cytochrome P450: Mechanism and Function of the Reaction. PLoS One 2013, 8, e61897. [PubMed: 23634216]

(305). Rittle J; Green MT Cytochrome P450 Compound I: Capture, Characterization, and C-H Bond Activation Kinetics. Science 2010, 330, 933–937. [PubMed: 21071661]

(306). Vincent KA; Tilley GJ; Quammie NC; Streeter I; Burgess BK; Cheesman MR; Armstrong FA Instantaneous, Stoichiometric Generation of Powerfully Reducing States of Protein Active Sites Using Eu(II) and Polyaminocarboxylate Ligands. Chem Commun (Camb) 2003, 2590–2591. [PubMed: 14594295]

(307). Lee CC; Hu Y; Ribbe MW ATP-Independent Substrate Reduction by Nitrogenase P-Cluster Variant. Proc. Natl. Acad. Sci. U. S. A 2012, 109, 6922–6926. [PubMed: 22509042]

(308). Lee CC; Hu Y; Ribbe MW ATP-Independent Formation of Hydrocarbons Catalyzed by Isolated Nitrogenase Cofactors. Angew. Chem. Int. Ed. Engl 2012, 51, 1947–1949. [PubMed: 22253035]

(309). Lee CC; Blank MA; Fay AW; Yoshizawa JM; Hu YL; Hodgson KO; Hedman B; Ribbe MW Stepwise Formation of P-Cluster in Nitrogenase MoFe Protein. Proc. Natl. Acad. Sci. U. S. A 2009, 106, 18474–18478. [PubMed: 19828444]

(310). Hu Y; Fay AW; Lee CC; Ribbe MW P-Cluster Maturation on Nitrogenase MoFe Protein. Proc. Natl. Acad. Sci. U. S. A 2007, 104, 10424–10429. [PubMed: 17563349]

(311). Stiebritz MT; Hiller CJ; Sickerman NS; Lee CC; Tanifuji K; Ohki Y; Hu Y Ambient Conversion of CO2 to Hydrocarbons by Biogenic and Synthetic [Fe4S4] Clusters. Nature Catalysis 2018, 1, 444–451.

(312). Rettberg LA; Kang W; Stiebritz MT; Hiller CJ; Lee CC ; Liedtke J; Ribbe MW; Hu Y Structural Analysis of a Nitrogenase Iron Protein from Methanosarcina acetivorans: Implications for CO2 Capture by a Surface-Exposed [Fe4S4] Cluster. Mbio 2019, 10.

(313). Allen RS; Tilbrook K; Warden AC; Campbell PC; Rolland V; Singh SP; Wood CC Expression of 16 Nitrogenase Proteins within the Plant Mitochondrial Matrix. Front Plant Sci 2017, 8, 287. [PubMed: 28316608]

(314). Ibrahim SK; Vincent K; Gormal CA; Smith BE; Best SP; Pickett CJ The Isolated Iron-Molybdenum Cofactor of Nitrogenase Binds Carbon Monoxide Upon Electrochemically Accessing Reduced States. Chem. Commun 1999, 1019–1020.

(315). Le Gall T; Ibrahim SK; Gormal CA; Smith BE; Pickett CJ The Isolated Iron-Molybdenum Cofactor of Nitrogenase Catalyses Hydrogen Evolution at High Potential. Chem. Commun 1999, 773–774.

(316). Badalyan A; Yang Z-Y; Seefeldt LC A Voltammetric Study of Nitrogenase Catalysis Using Electron Transfer Mediators. ACS Catalysis 2019, 9, 1366–1372.

(317). Pham DN; Burgess BK Nitrogenase Reactivity: Effects of pH on Substrate Reduction and CO Inhibition. Biochemistry 1993, 32, 13725–13731. [PubMed: 8257707]

(318). Wherland S; Burgess BK; Stiefel EI; Newton WE Nitrogenase Reactivity: Effects of Component Ratio on Electron Flow and Distribution During Nitrogen Fixation. Biochemistry 1981, 20, 5132–5140. [PubMed: 6945871]

(319). Roth LE; Tezcan FA Light-Driven Uncoupling of Nitrogenase Catalysis from ATP Hydrolysis. ChemCatChem 2011, 3, 1549–1555.

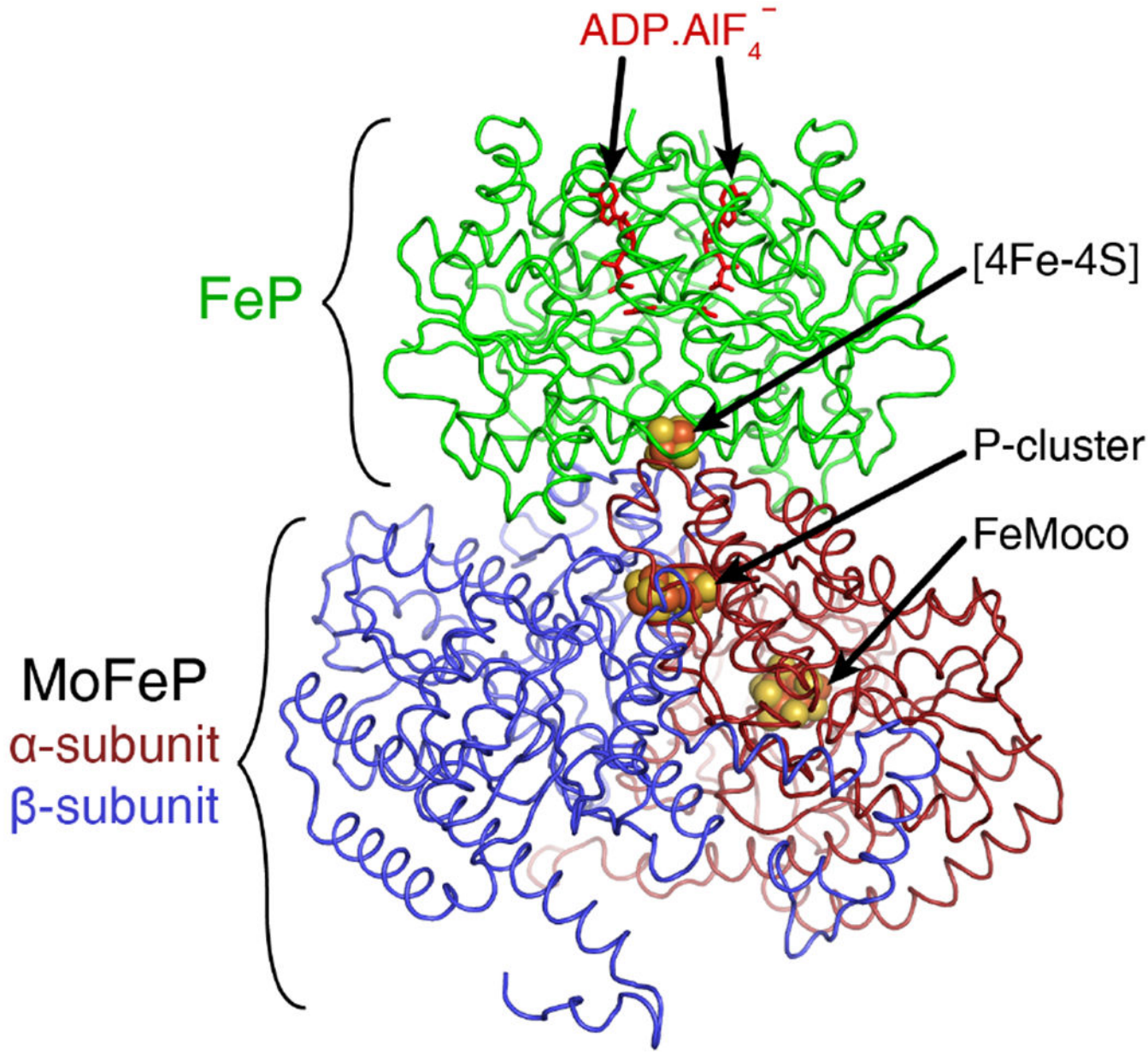

Figure 1.

One half of the ADP.AlF_4^- stabilized nitrogenase complex (PDB ID: 1M34). FeP is shown in green, and MoFeP is red (α-subunit) and blue (β-subunit). Metalloclusters are depicted as spheres, and the nucleotides are red sticks.

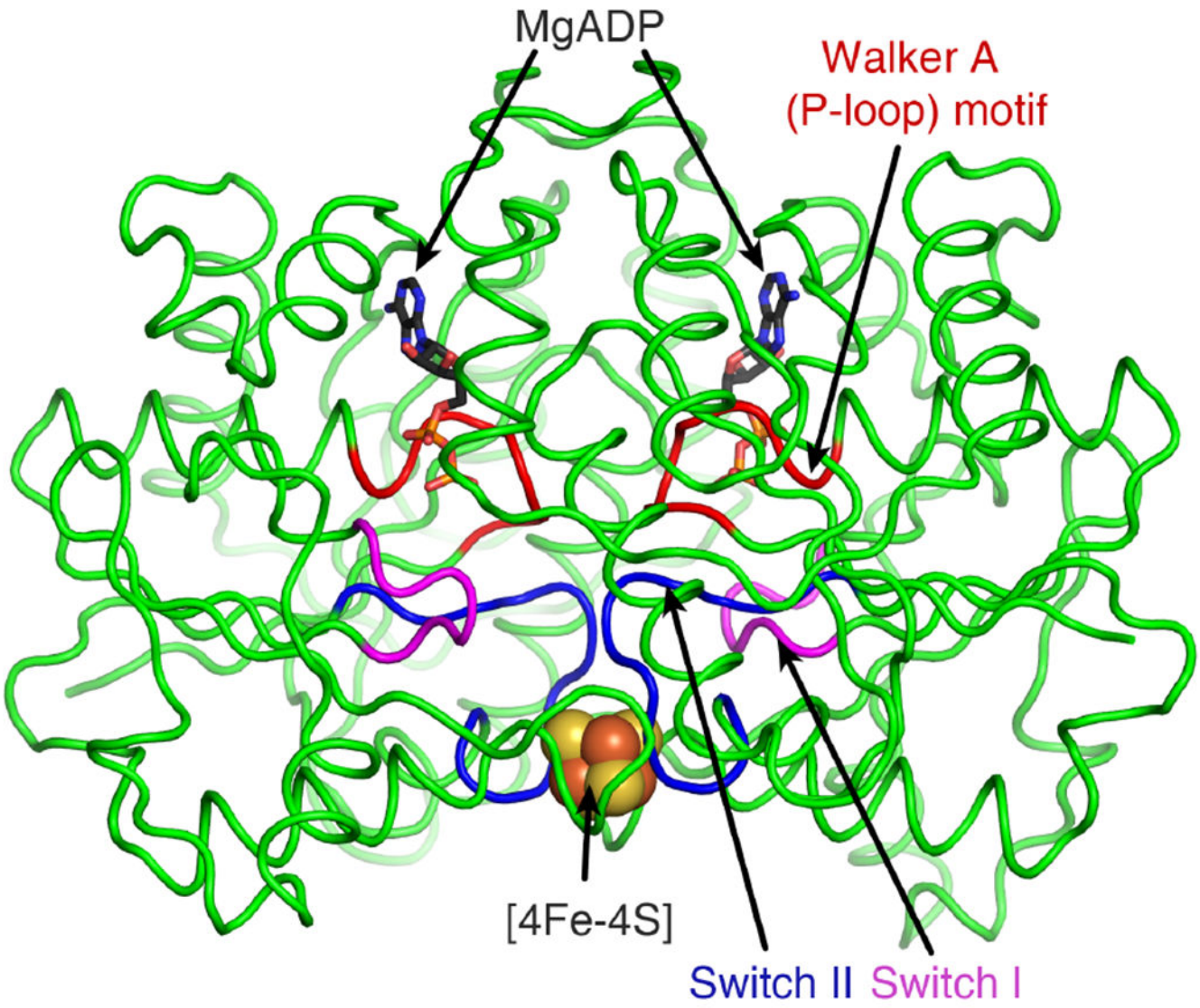

Figure 2.

MgADP bound FeP (PDB ID: 6N4L). The Walker A (P-loop) motif is shown in red (γ9 - 16), Switch I region in magenta (γ39 - 69), and Switch II region in blue (γ125 - 132). MgADP is depicted is as sticks, and the [4Fe-4S] cluster as spheres colored by element.

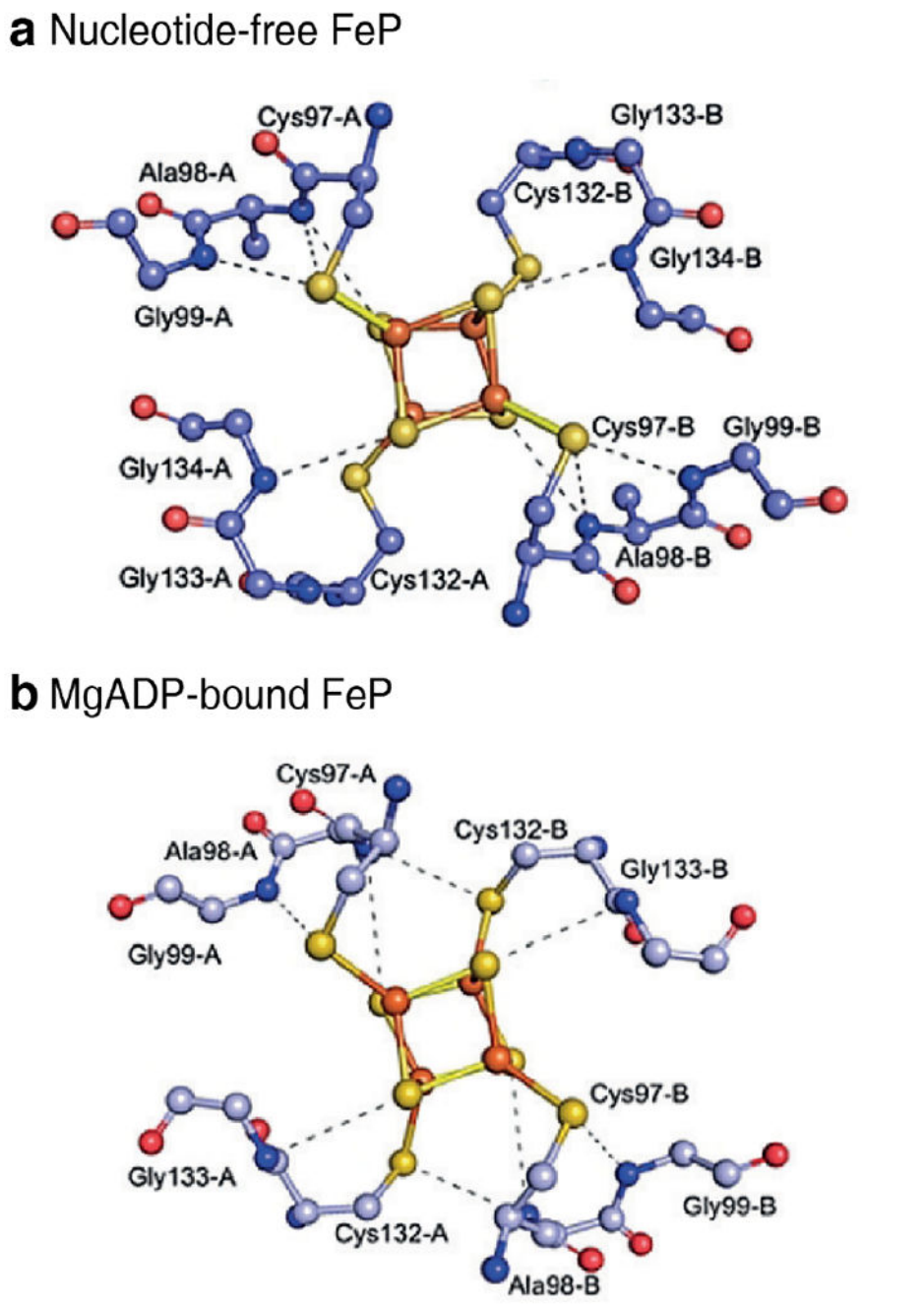

Figure 3.

Dithionite reduced $[4Fe\text{-}4S]^{1+}$ cluster of FeP. The FeS cluster is colored by element (sulfides are yellow, irons are orange), and hydrogen-bonding networks are depicted by dashed gray lines. (a) FeP in the nucleotide-free state (PDB ID: 6N4K). (b) FeP in the MgADP-bound state (PDB ID: 6N4L). Reprinted in part with permission from ref 102. Copyright 2019 John Wiley and Sons.

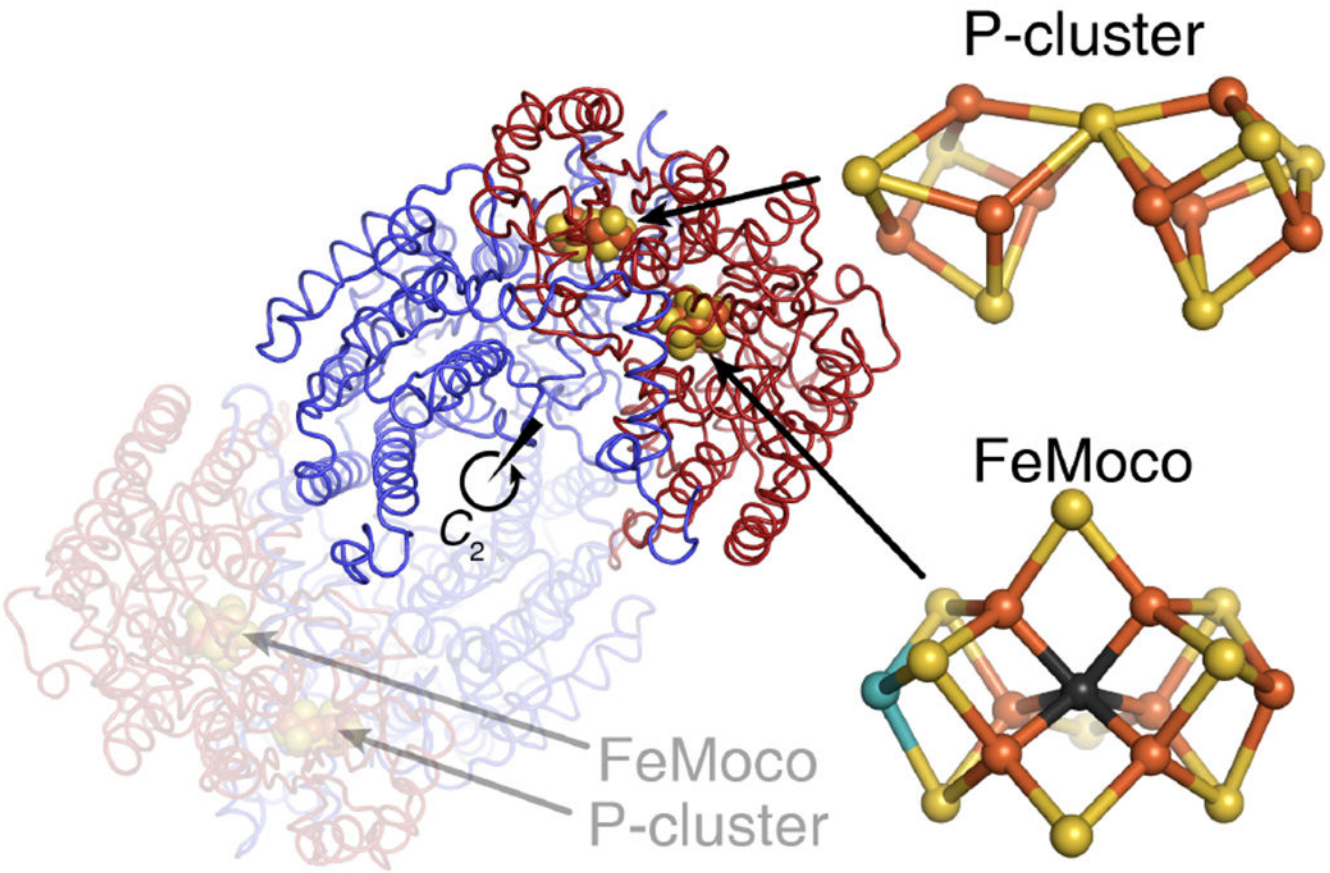

Figure 4.

MoFeP (PDB ID: 3U7Q). MoFeP is a dimer of αβ-dimers (one dimer pictured is opaque and the other is transparent). The α- and β-subunits are shown in red and blue, respectively. Each αβ-dimer contains one P-cluster and one FeMoco, represented as spheres colored by element (sulfurs are yellow, irons are orange, molybdenum is teal, and carbon is black).

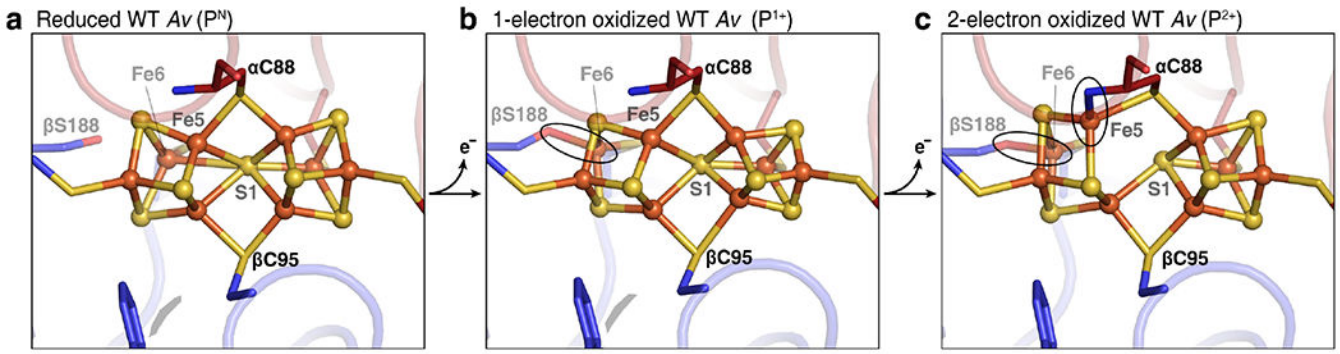

Figure 5.

Redox-dependent structural changes of the *Av* nitrogenase P-cluster. (a) The dithionite-reduced P-cluster (P^N) is ligated by six Cys residues, and the central S1 sulfide is coordinated by six Fe's (PDB ID: 3MIN). (b) Upon one-electron oxidation, the P-cluster (P^{1+}) gains a Ser ligand βSer188) to Fe6, which dissociates from the S1 sulfide (PDB ID: 6CDK). (c) The two-electron, indigo disulfonate oxidized P-cluster (P^{2+}) involves additional ligation of the backbone amide of the bridging αCys88 to Fe5, which also dissociates from S1 (PDB ID: 2MIN).

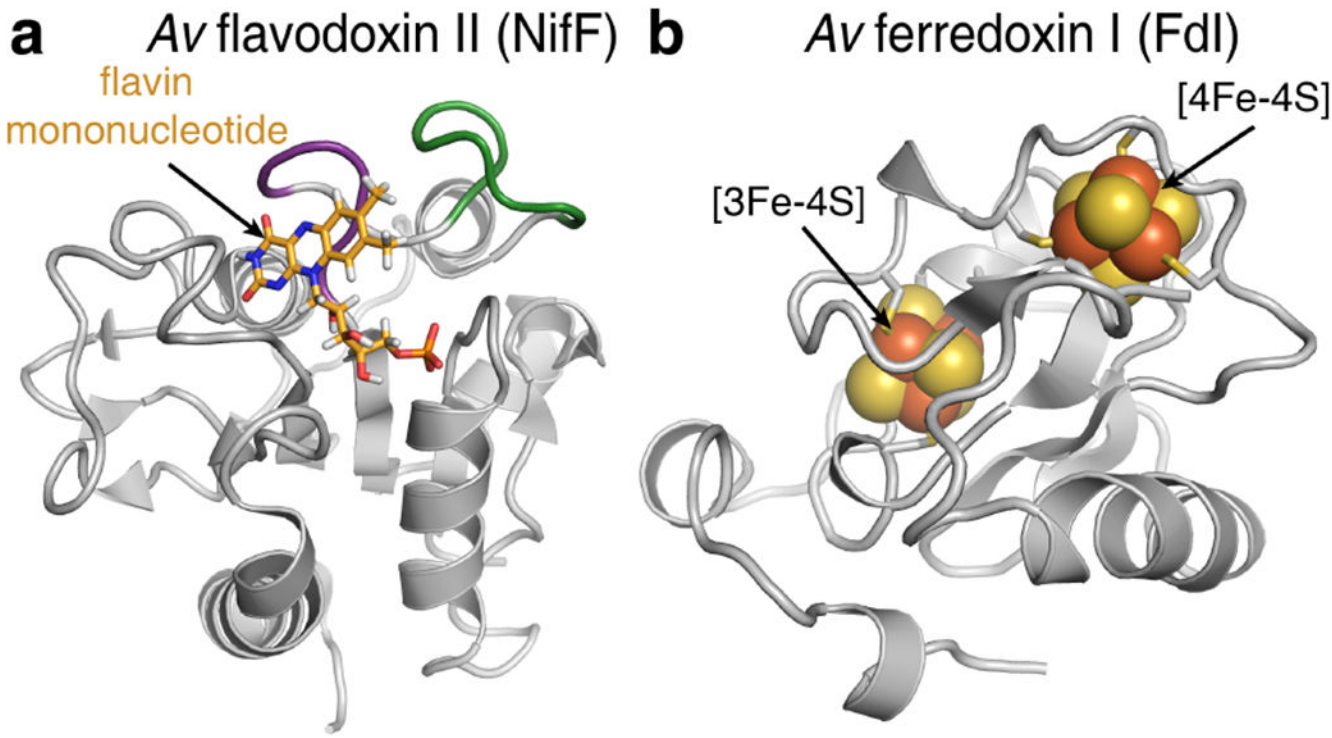

Figure 6.

Reductases of FeP in *Av*. (a) *Av* flavodoxin II (NifF) with the flavin mononucleotide (FMN) shown as orange sticks. Residues 56-60 are important in modulating the midpoint potential of FMN (purple loop), and residues 64-71 are hypothesized to be necessary for FeP binding specificity (green) (PDB ID: 5K9B). (b) *Av* ferredoxin I (FdI) contains a [3Fe-4S] and a [4Fe-4S] cluster (PDB ID: 6FDR).

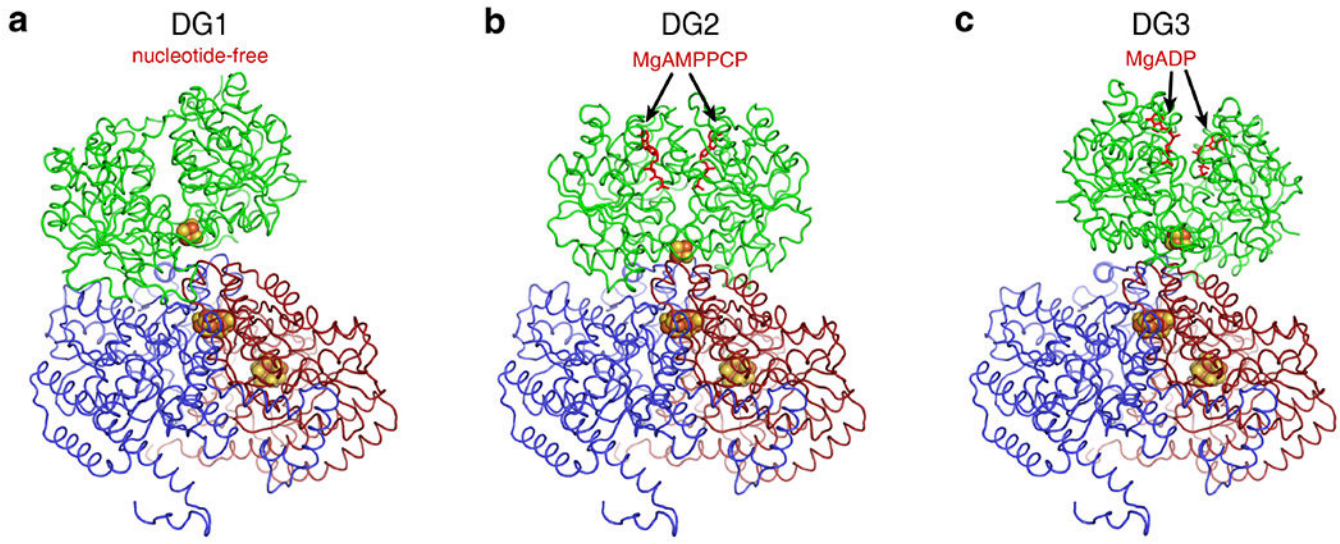

Figure 7.

Nucleotide-dependent docking geometries (DGs) of the nitrogenase complex. FeP is shown in green, and MoFeP in red (α-subunit) and blue (β-subunit). Metalloclusters are shown as spheres colored by element, and nucleotides as red sticks. (a) The nucleotide-free FeP-MoFeP structure *(nf)* is in DG1, with FeP primarily in contact with the β-subunit of MoFeP (PDB ID: 2AFH). (b) MgAMPPCP-FeP-MoFeP complex (*pcp*) structure is in DG2, with FeP situated almost equally over both subunits MoFeP (PDB ID: 4WZB). (c) MgADP-FeP-MoFeP structure *(adp)* is in DG3 with FeP mostly in contact with the α-subunit of MoFeP (PDB ID: 2AFI).

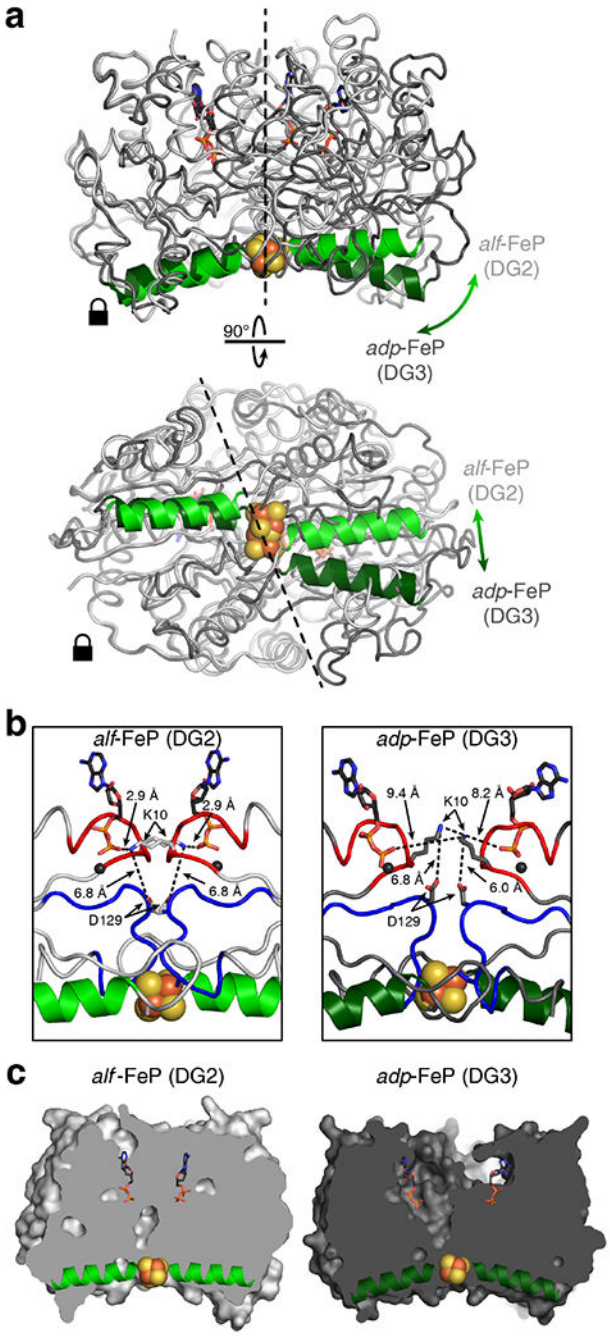

Figure 8.

Nucleotide-dependent conformational changes in FeP. FeP and the γ100s helices from the *alf* structure (DG2) are shown in light gray and light green (PDB ID: 1M34) and from the *adp* structure (DG3) in dark gray and dark green (PDB ID: 2AFI). Nucleotides and the [4Fe-4S] clusters are shown as sticks and spheres, respectively. (a) Structural alignment of the left subunit of FeP from *alf* and *adp* demonstrating (top) hinge-like movement of the right subunit about a pivot point near the [4Fe-4S] cluster resulting in af having a flatter binding surface, as seen by the γ100s helices, and (bottom) depicting sliding motion of the

subunits. (b) The flattening of the surface in *alf* poises residues γLys10 and γAsp129 across the subunit interface in a position favorable for ATP hydrolysis. (c) *alf* has a more surface-exposed [4Fe-4S] cluster than *adp*, as shown in FeP cross-sections.

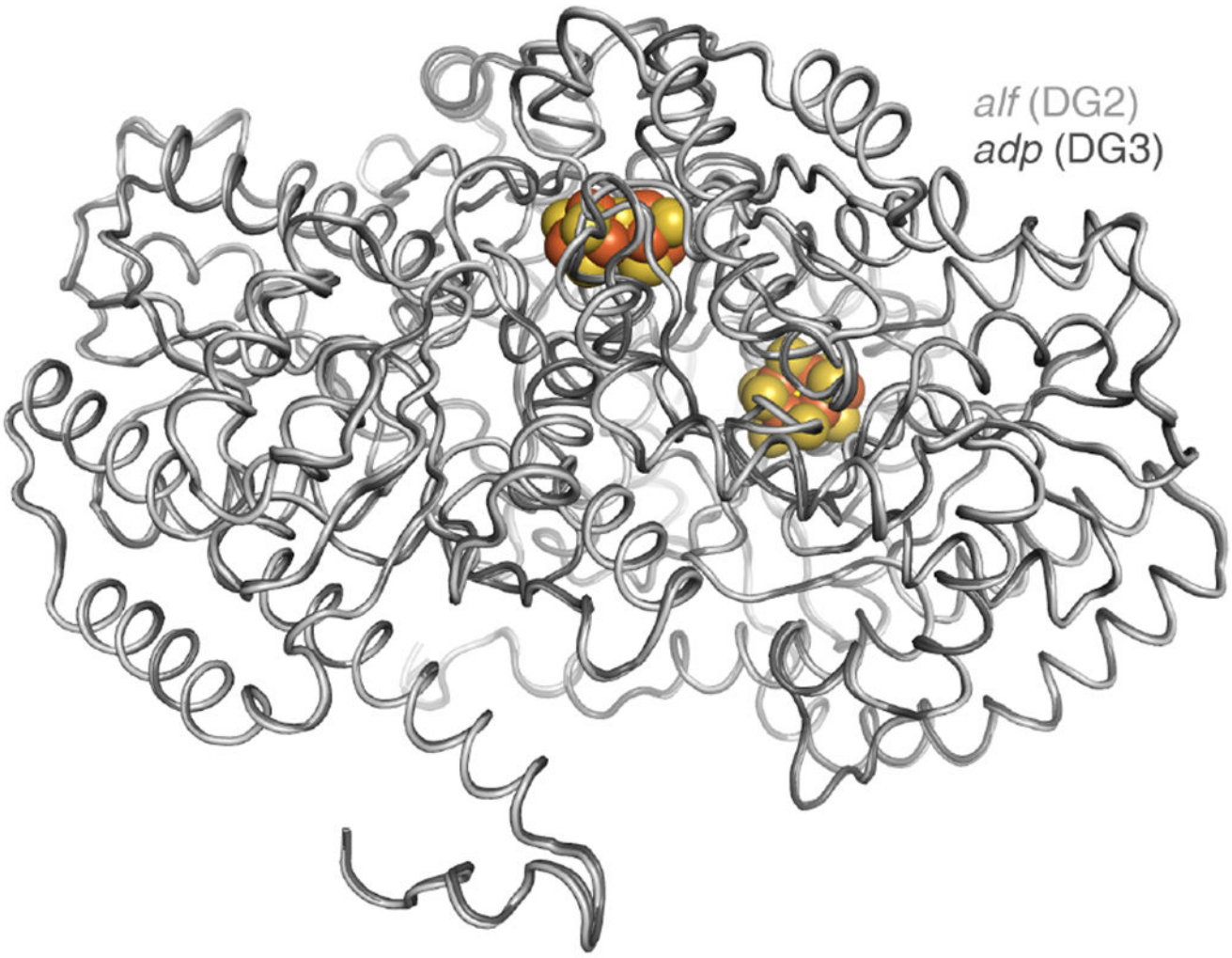

Figure 9.

Overlay of aligned MoFeP structures observed in *alf* (light gray, PDB ID: 1M34) and *adp* (dark gray, PDB ID: 2AFI) complexes (RMSD over all α-C's = 0.317 Å). The P-cluster and FeMoco are depicted as spheres.

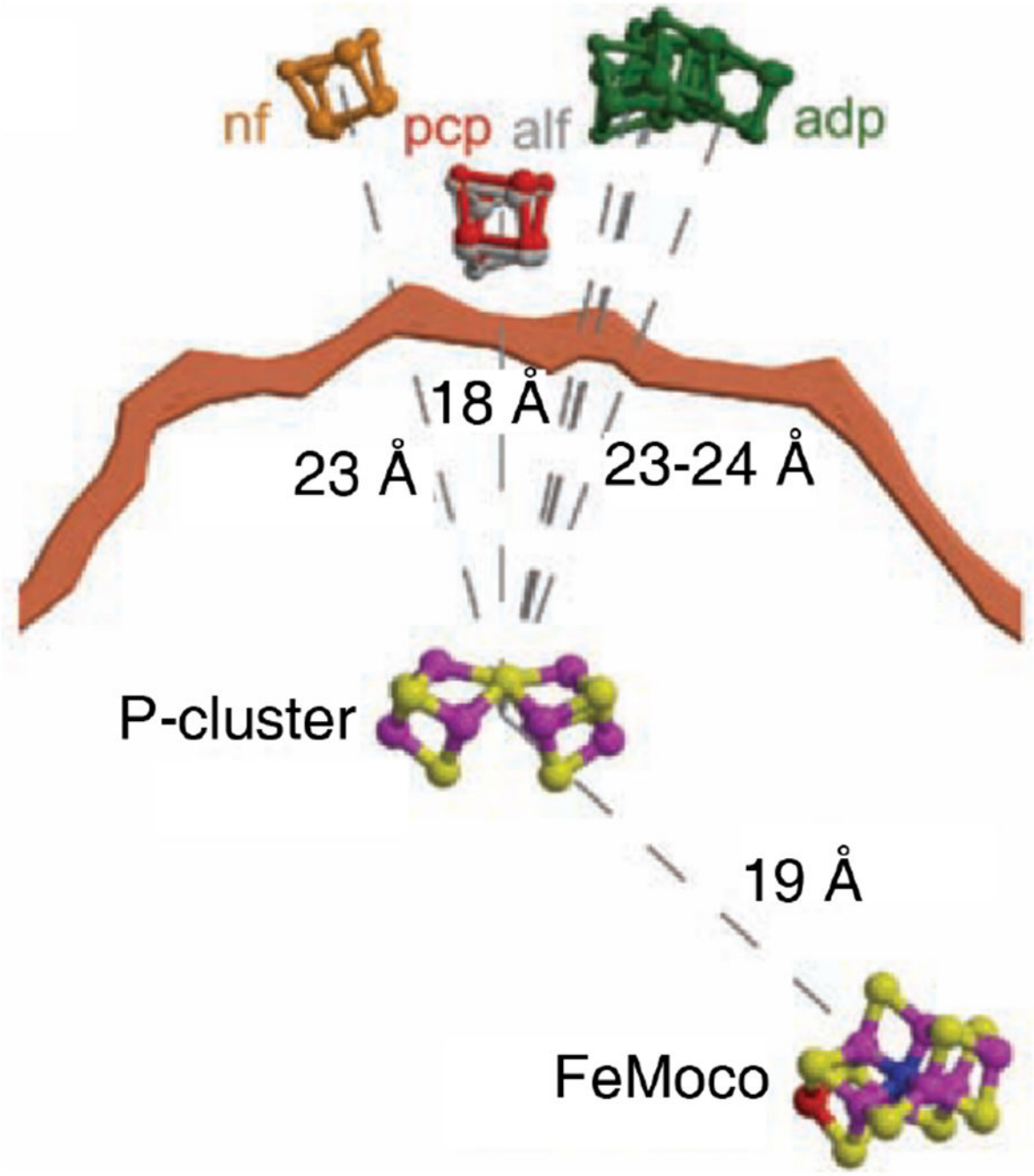

Figure 10.
Nucleotide-dependent distances (center-to-center) between the P-cluster and the FeP [4Fe-4S] cluster in the *nf pcp, alf* and *adp* nitrogenase complex structures. Reprinted in part with permission from ref 26. Copyright 2005 AAAS.

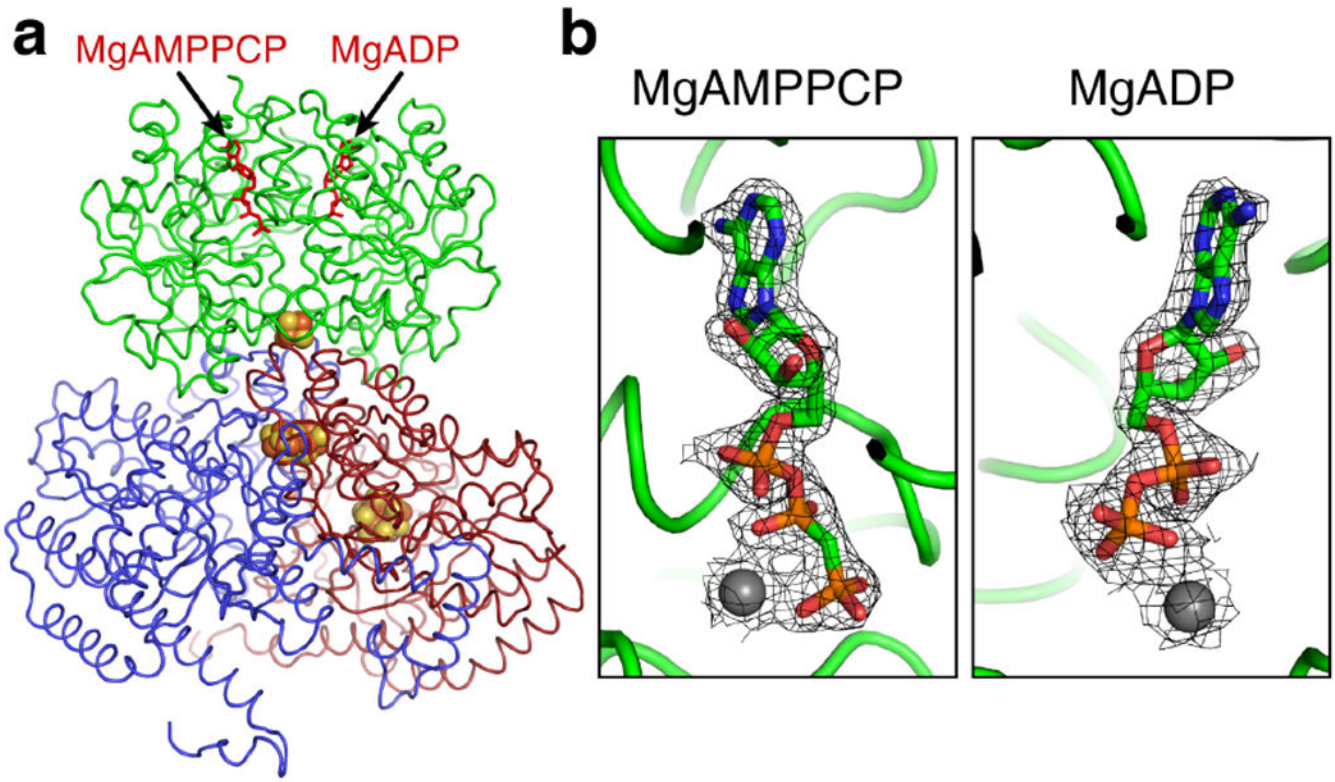

Figure 11.

Asymmetric nucleotide binding in the nitrogenase complex (*pcp/adp*) (PDB ID: 4WZA). (a) FeP is green, and MoFeP is red (α-subunit) and blue (β-subunit). MgADP is located over the α-subunit and MgAMPPCP over the β-subunit. (b) The $2F_o–F_c$ electron density map (1.0 σ) around the nucleotides is shown as a black mesh. The nucleotides are colored by element, and Mg^{2+} ions are depicted as spheres.

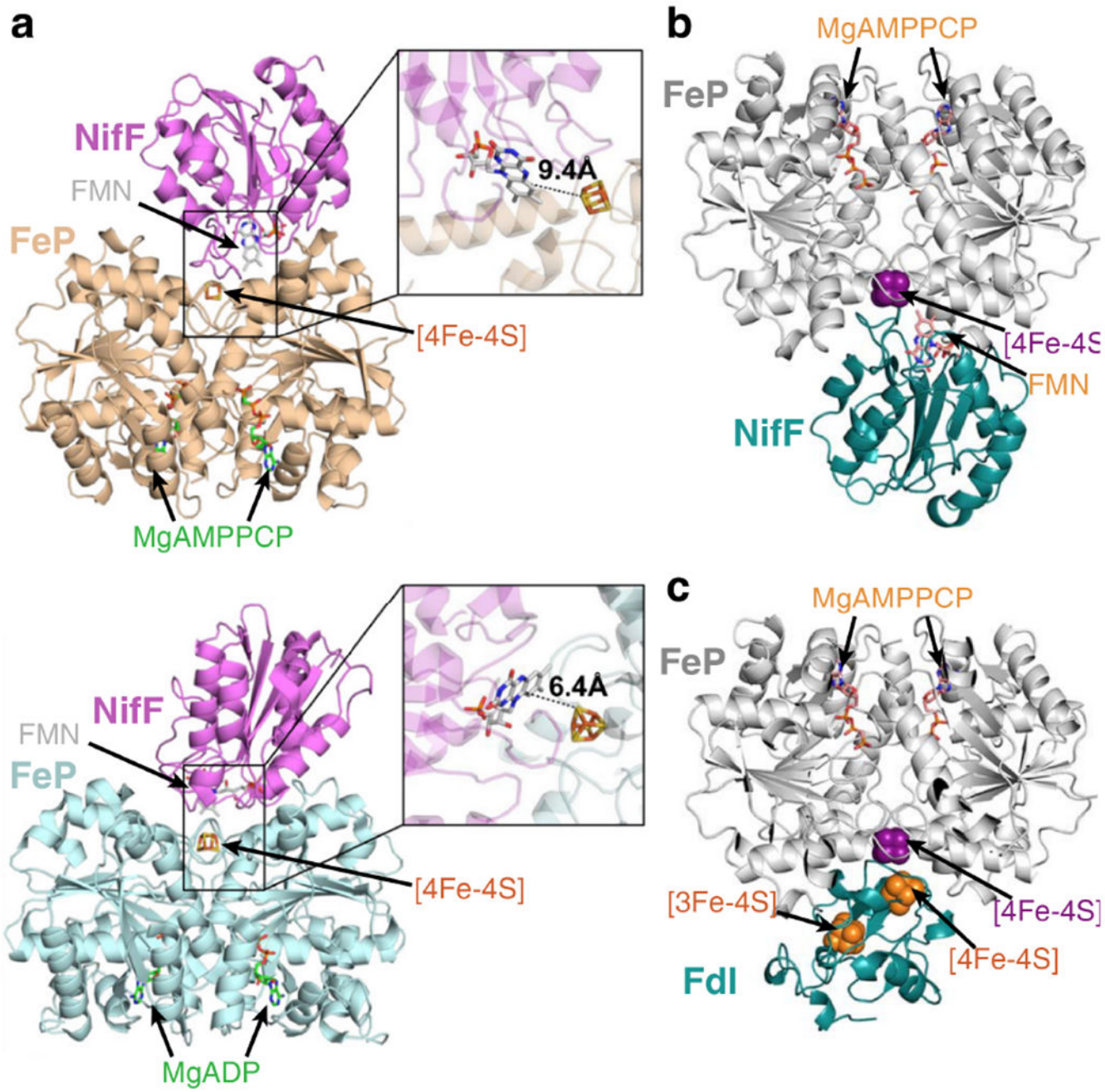

Figure 12.

Docking models of FeP reductases with FeP in different nucleotide-bound states. (a) MgAMPPCP-FeP (top, PDB ID: 4WZB) and MgADP-FeP (bottom, PDB ID: 1FP6) bound to NifF (PDB ID: 1YOB). The MgADP-FeP-NifF structure from these simulations places the redox pair in closer proximity (6.4 Å) than the MgAMPPCP-FeP-NifF model (9.4 Å). Adapted from ref 76 under the Creative Commons Attribution License (https://creativecommons.org/licenses/bync/3.0/lgalcode). Copyright 2017 ASBMB. (b) MgAMPPCP-FeP (PDB ID: 4WZB) bound to NifF (PDB ID:5K9B) and (c) FdI (PDB ID: 6FDR). Both NifF and FdxA in these models share the same binding surface on FeP. The

MgAMPPCP-FeP-NifF model (b) from these simulations places the redox pair in closer proximity (~5 Å) than the model in (a). Both (b) and (c) are adapted with permission from ref 171. Copyright 2017 John Wiley and Sons.

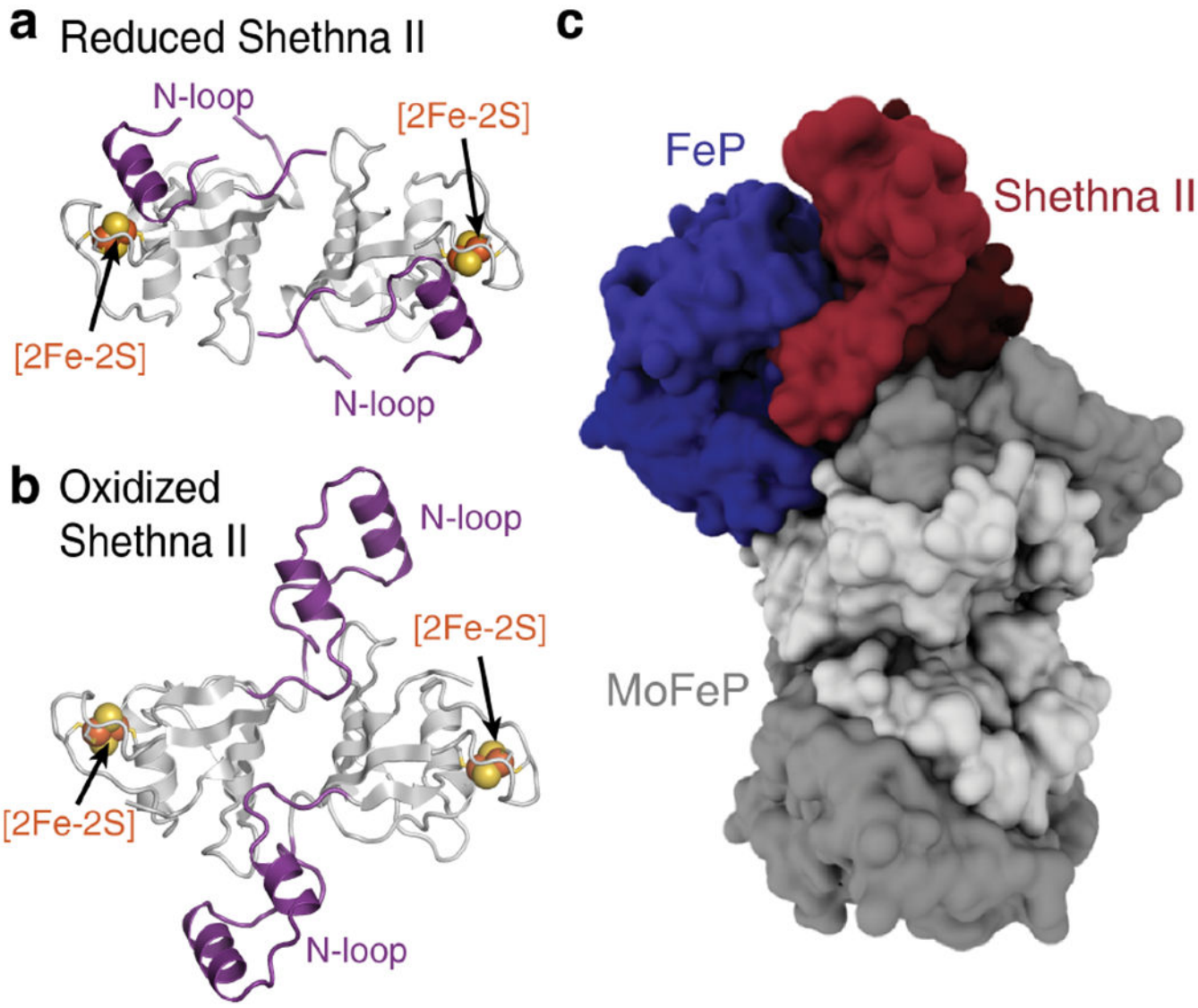

Figure 13.

Shethna II is a homodimeric [2Fe-2S] ferredoxin. (a) Reduced Shethna II dimer (PDB ID: 5FFI) is in a closed conformation that likely cannot bind the nitrogenase complex. (b) Upon oxidation, Shethna II occupies a more open conformation that is thought to form a complex with FeP and MoFeP (PDB ID: 5FFI). (b) Docking model of Shethna II forming an oxygen-protected 1:1:1 complex with FeP and MoFeP. Shethna II binds the cleft between FeP and the a-subunit of MoFeP. (c) is adapted from ref 213.

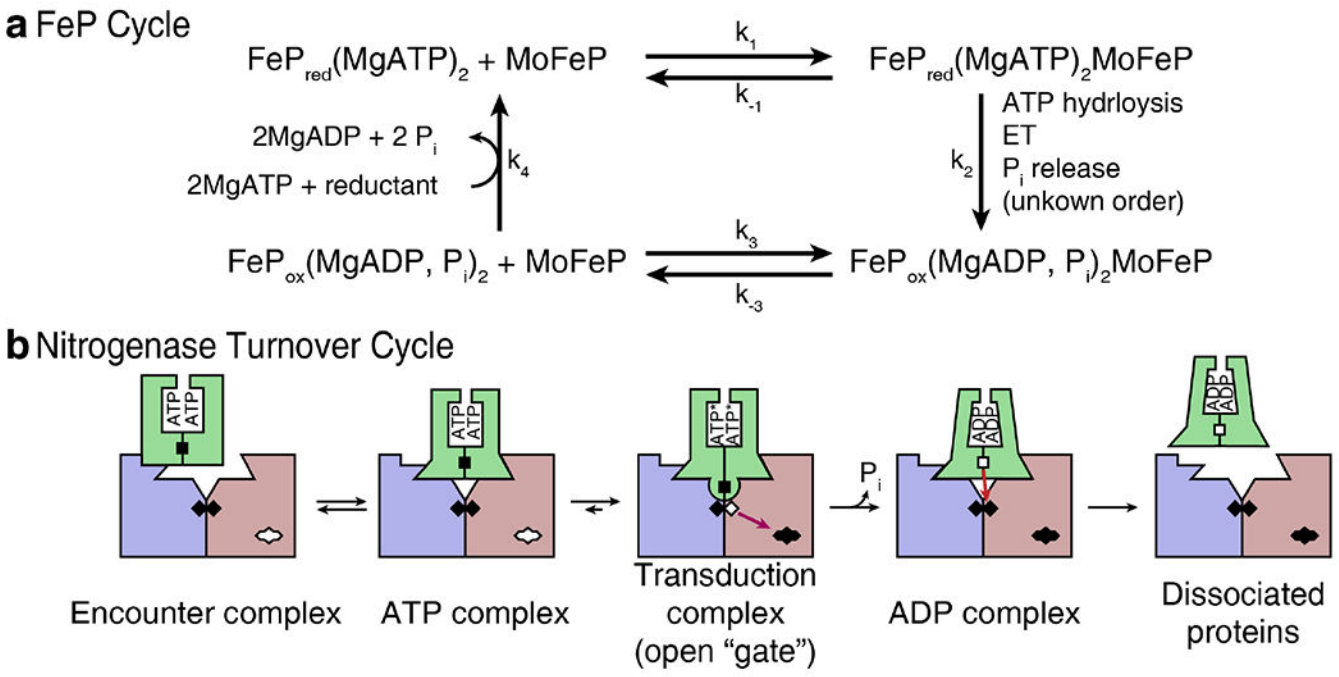

Figure 14.

Thorneley-Lowe (TL) FeP cycle. (a) The original TL FeP cycle. Adapted from ref 18. (b) Adapted TL FeP cycle with proposed order of ET events, encounter complex, and transduction complex. Adapted from ref 19.

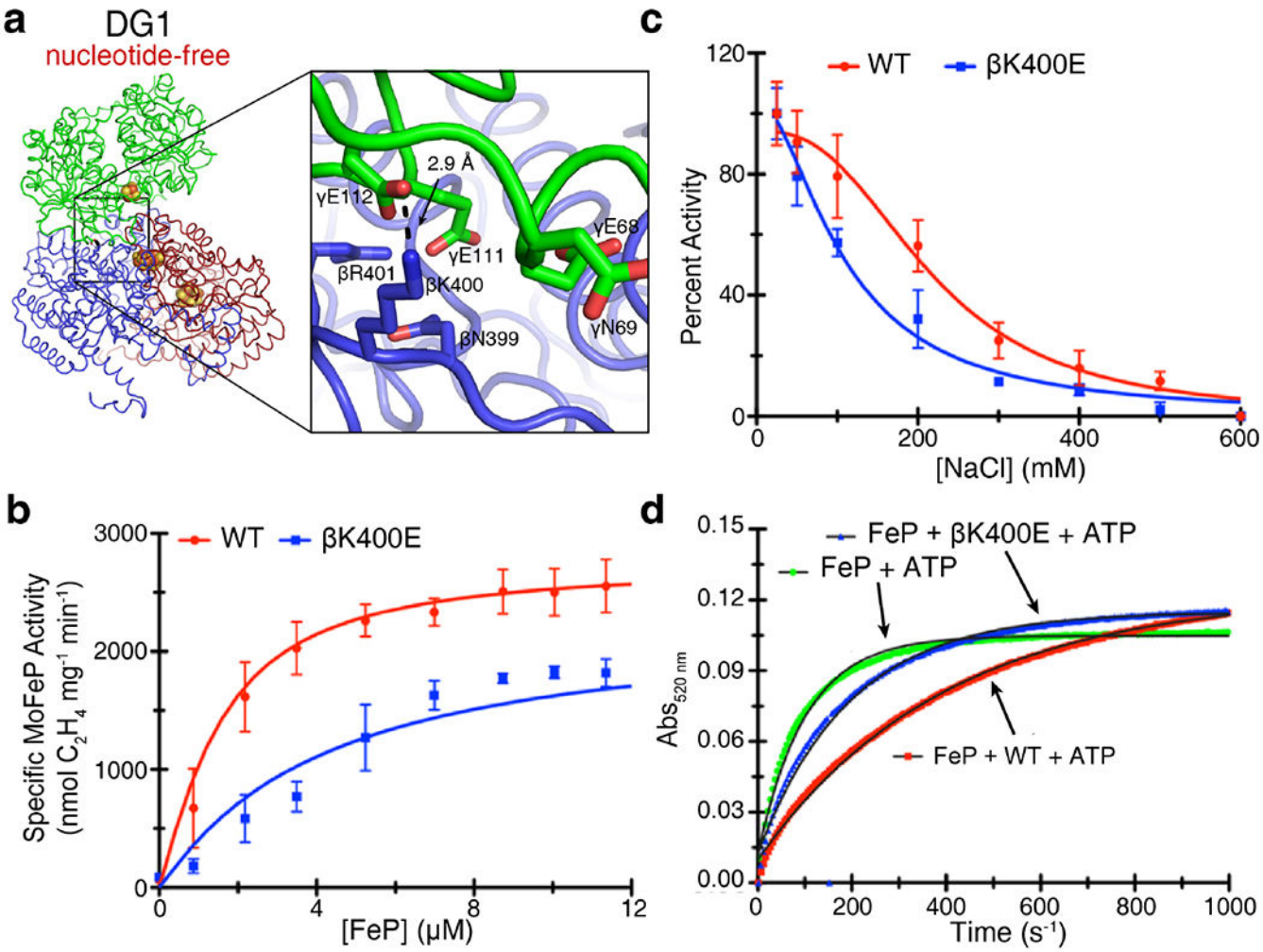

Figure 15.

Functionally relevant encounter complex mediated by electrostatic interactions. (a) In DG1 (PDB ID: 2AFH), EDC-crosslinkable residues γGlu112 and βLys400 are observed within H-binding distance (2.9 Å). (b) βLys400Glu MoFeP exhibits 28% less C_2H_2 reduction activity than wild-type MoFeP. (c) βLys400Glu MoFeP activity is more sensitive to [NaC1] than wild-type (WT) MoFeP. (b) The βLys400Glu MoFeP-FeP complex is more susceptible to iron chelation than the WT MoFeP-FeP complex. Panels (b), (c) and (d) are reprinted in part from ref 234.

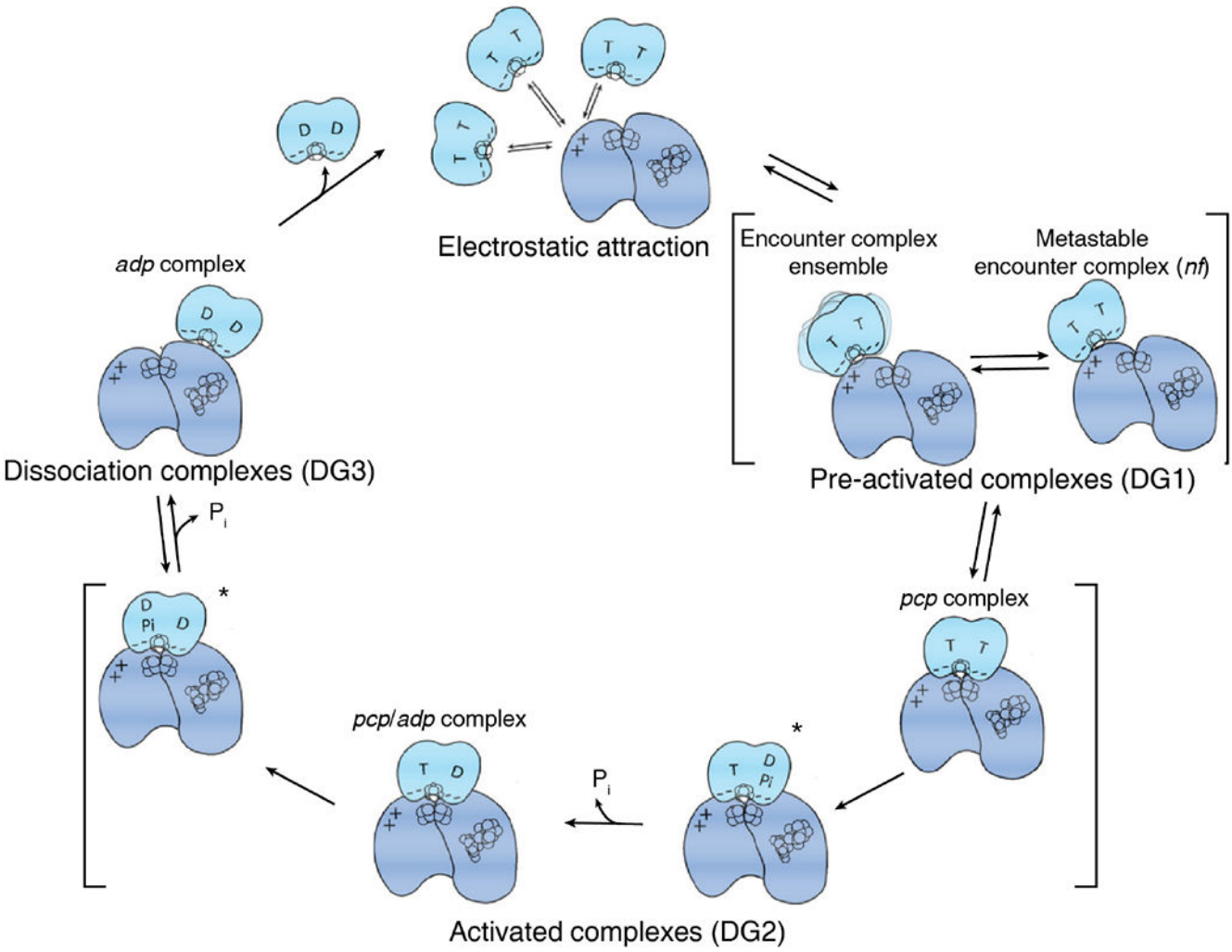

Figure 16.

The updated FeP cycle. FeP is light blue and MoFeP is dark blue. ATP and ADP are denoted by T and D, respectively. FeP forms an ensemble of transient encounter complexes with MoFeP mediated by electrostatics before reaching the metastable DG1 complex. The DG2 complexes marked with * have been proposed, but not experimentally observed. Adapted with permission from ref 236. Copyright 2016 John Wiley and Sons.

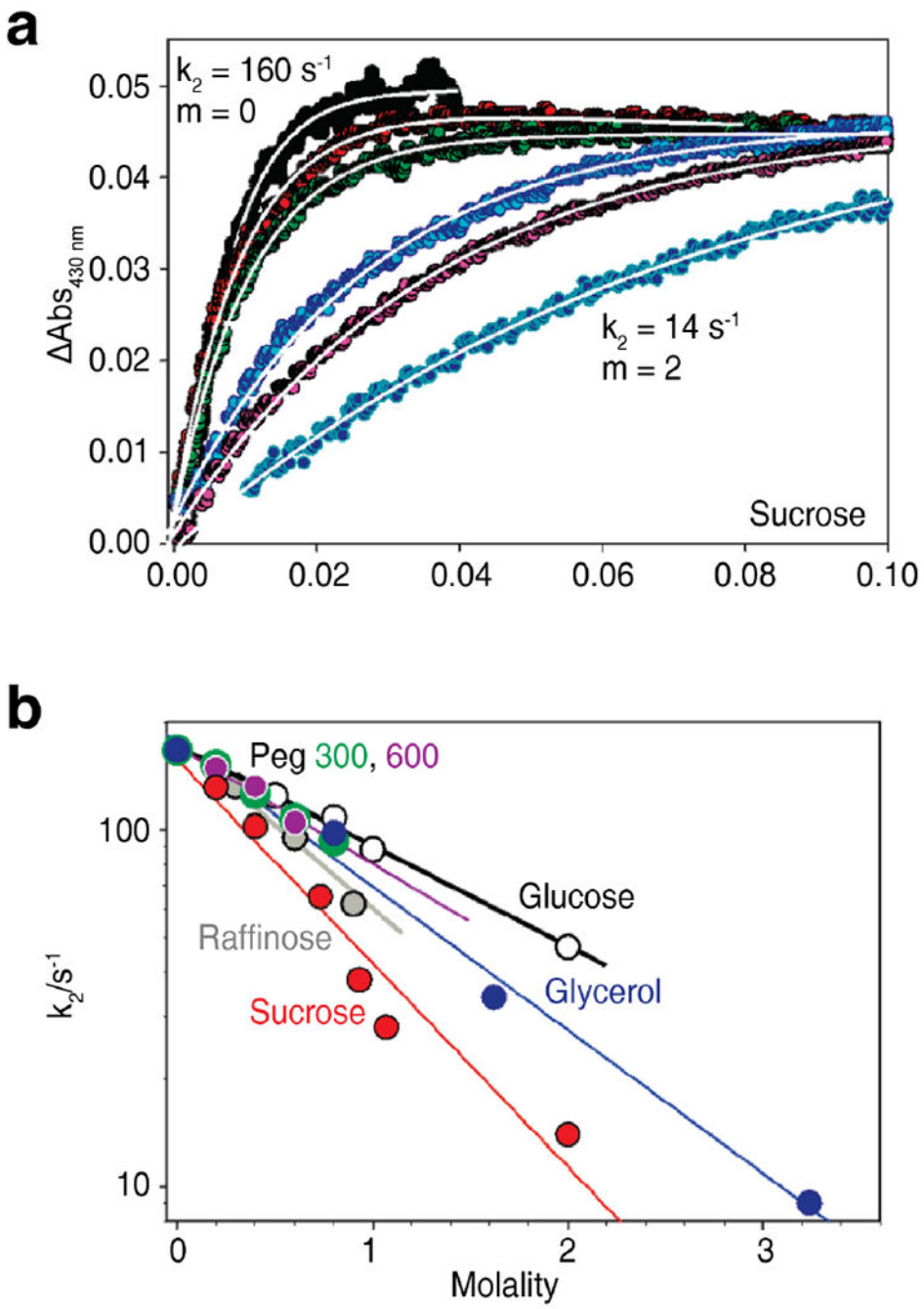

Figure 17.

Evidence for conformational gating of electron transfer. (a) Stopped-flow experiments monitoring the oxidation of FeP at 430 nm. The rate of ET decreases from 160 s^{-1} to 14 s^{-1} as sucrose molality (*m*) increases from 0 to 2. (b) Logarithmic plot of rate of ET (k_2) vs *m* of different osmolytes. (a) and (b) are reprinted from ref 237.

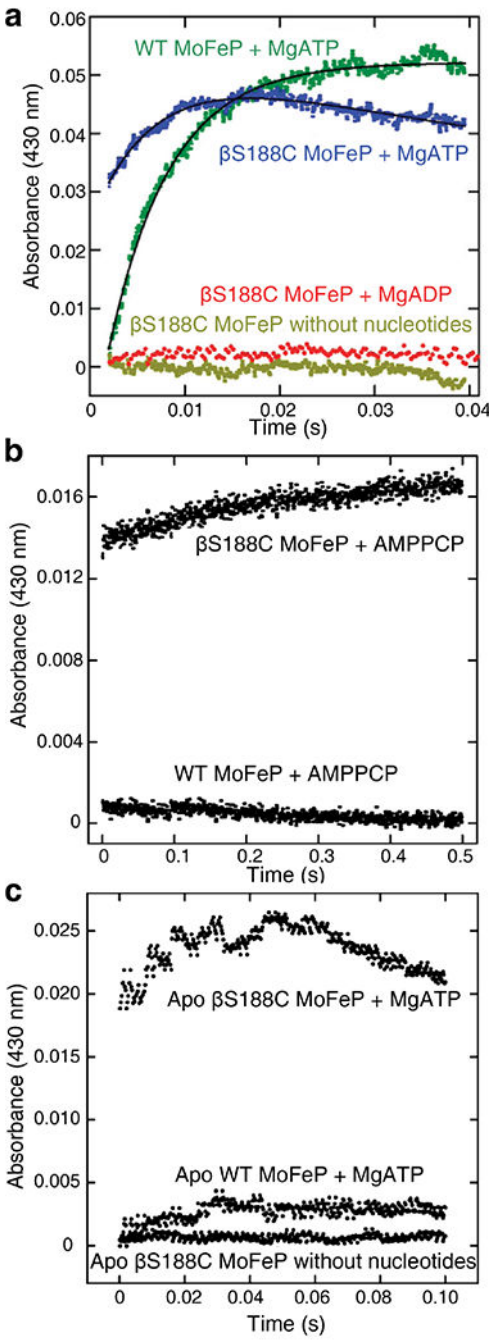

Figure 18.

Evidence for the deficit spending model: stopped-flow experiments monitoring the oxidation of FeP by MoFeP βSer188Cys and wild-type) at 430 nm. ~65% of reduced βSer188Cys MoFeP is in the P^{1+} state. (a) ATP-dependent oxidation of FeP by wild-type (WT) MoFeP (green) occurs at approximately the same rate as βSer188Cys MoFeP (blue), but unlike WT MoFeP, ~65% of FeP is oxidized by βSer188Cys MoFeP in the instrument dead time. No oxidation of FeP by βSer188Cys MoFeP occurs with MgADP (red) or without nucleotides (yellow). (b) AMPPCP enables oxidation of FeP by βSer188Cys MoFeP, unlike WT MoFeP.

(c) Oxidation of FeP by βSer188Cys MoFeP occurs without FeMoco (apo), but not for WT MoFeP. Adapted from ref 70.

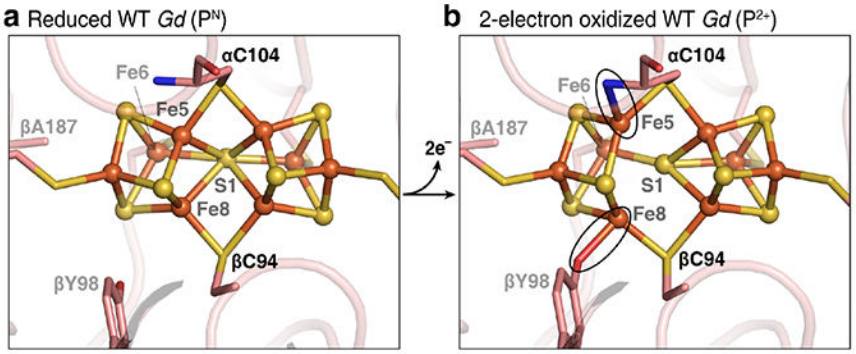

c

Organism	β185-190	β95-100
A. vinelandii	HTPSFV	CVAYFR
K. pneumoniae	HTPSFI	CVAYFR
C. pasteurianum	NTPSYV	CCSYHR
T. yellowstonii	NTPSYV	CVAYFR
B. japonicum	HTPAFV	CVAYYR
A. ferrooxidans	HTPAFV	CVAYYR
G. diazotrophicus	HTPAFV	CVAYYR
X. autotrophicus	HTPAFV	CVAYYR

Figure 19.

Covariance of Ser and Tyr ligation to the oxidized P-cluster. Residue numbers correspond to *Gluconocetabacter diazotrophicus (Gd)*. (a) The DT-reduced P-cluster of *Gd*, which contains alanine in place of serine at position β187 (β188 by Av numbering) (PDB ID: 5KOH). (b) IDS-oxidation of the P-cluster from *Gd* results in ligation of βTyr98 (residue β99 by Av numbering) to Fe8 and the backbone amide of αCys104 (residue α88 by Av numbering) to Fe6 (PDB ID: 5KOJ). (c) A sample of sequences demonstrating covariance of residues β99 and β188 (Av numbering) such that organisms have either a Tyr or a Ser in on of those positions, respectively. For a more complete list, see supplemental information of reference 242.

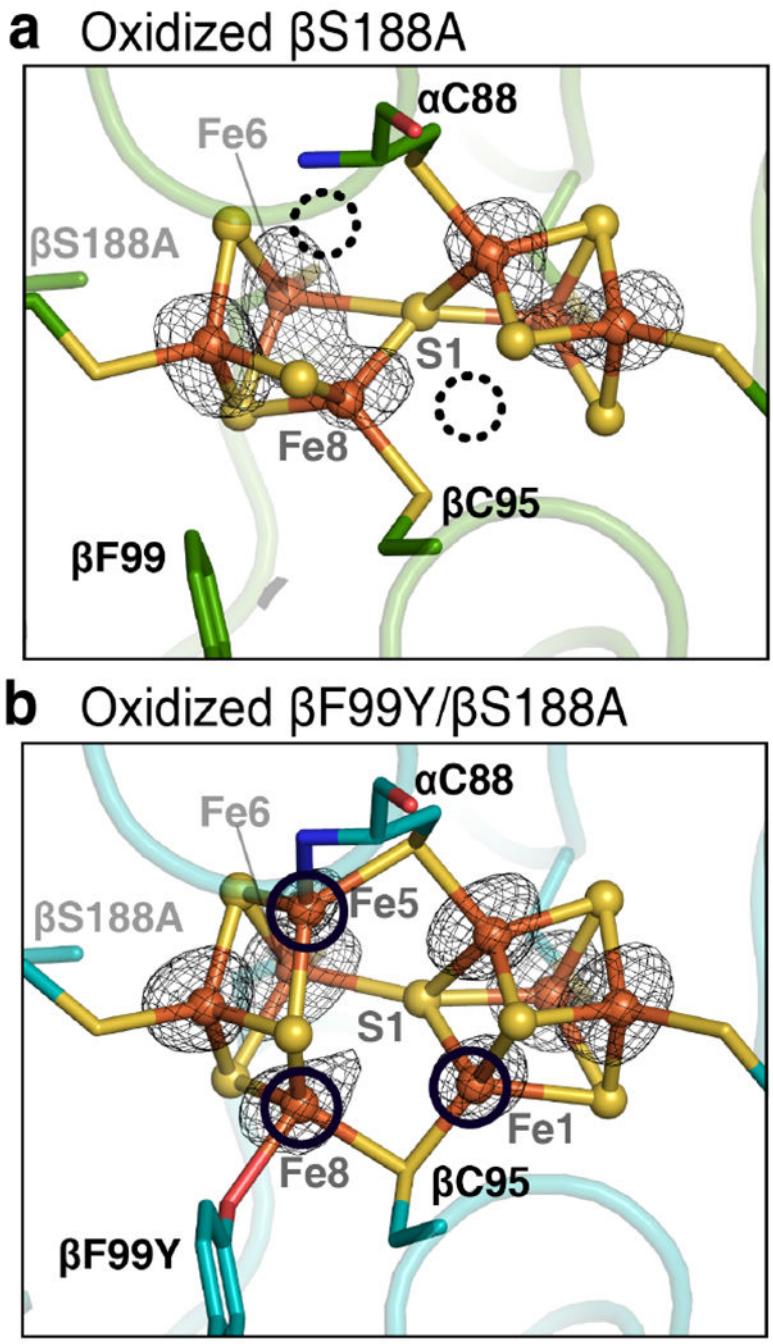

Figure 20.

Av MoFeP P-cluster primary coordination sphere mutants in the IDS-oxidized state. The anomalous electron density difference maps (near the Fe K-edge are shown in black mesh. (a) Av βSer188Ala MoFeP contains no oxygenic ligand. This mutant has two redox-labile iron centers (Fe1 and Fe5) whose positions are indicated with dashed circles. (PDB ID: 6O7S) (b) The Gd-like Av βPhe99Tyr/βSer188Ala MoFeP contains a tyrosine ligand. Upon oxidation, three irons (Fe1, Fe5 and Fe8, indicated with black circles) are partially occupied

(~67% occupied) such that there is one redox-labile iron per P-cluster on average. (PDB ID: 6O7N)

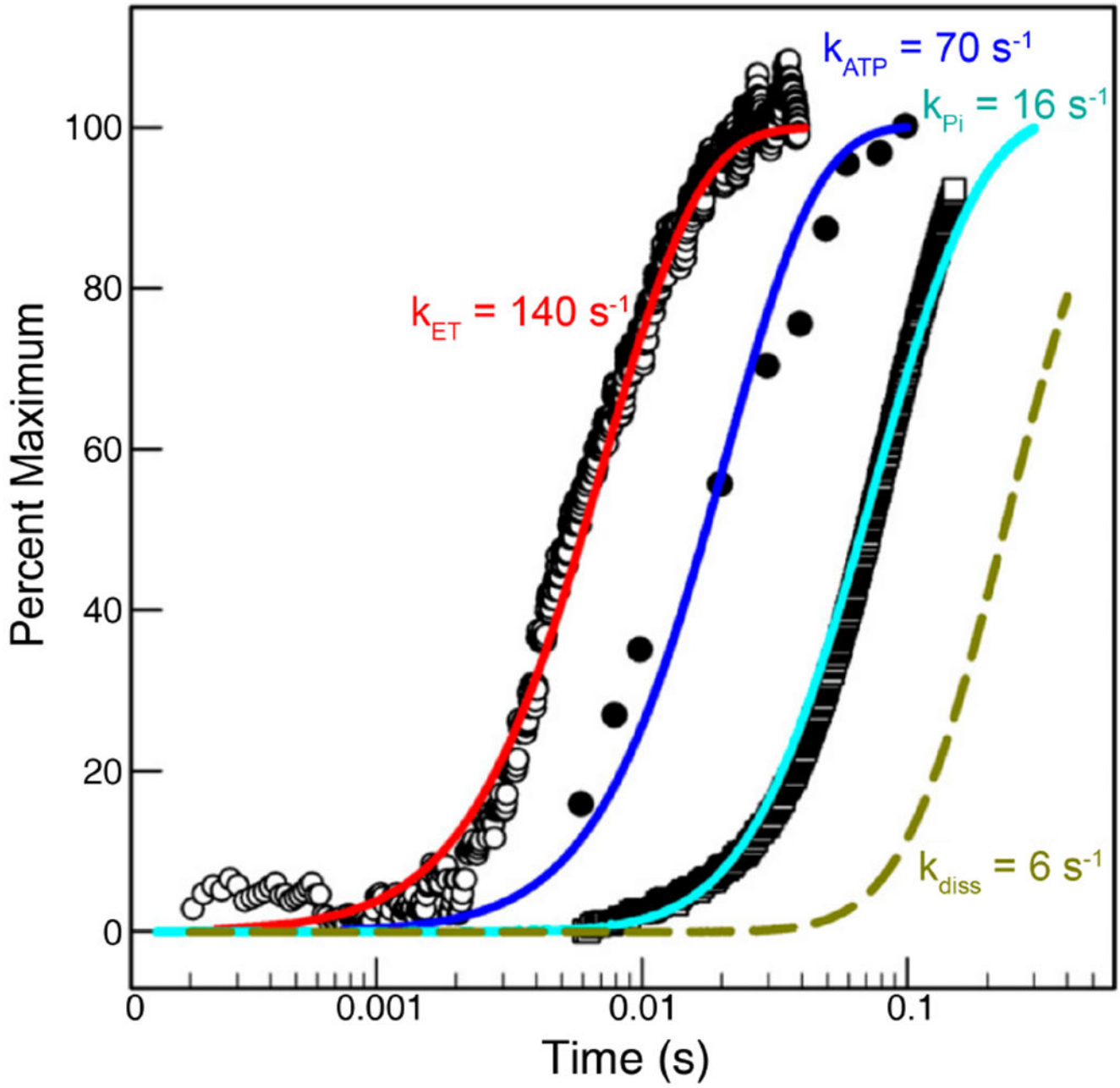

Figure 21.
Evidence for ET preceding ATP hydrolysis. The time-course of ET (red), ATP hydrolysis (blue), P_i release (cyan), and FeP-MoFeP dissociation (olive). Reprinted with permission from ref 246. Copyright 2013 NAS.

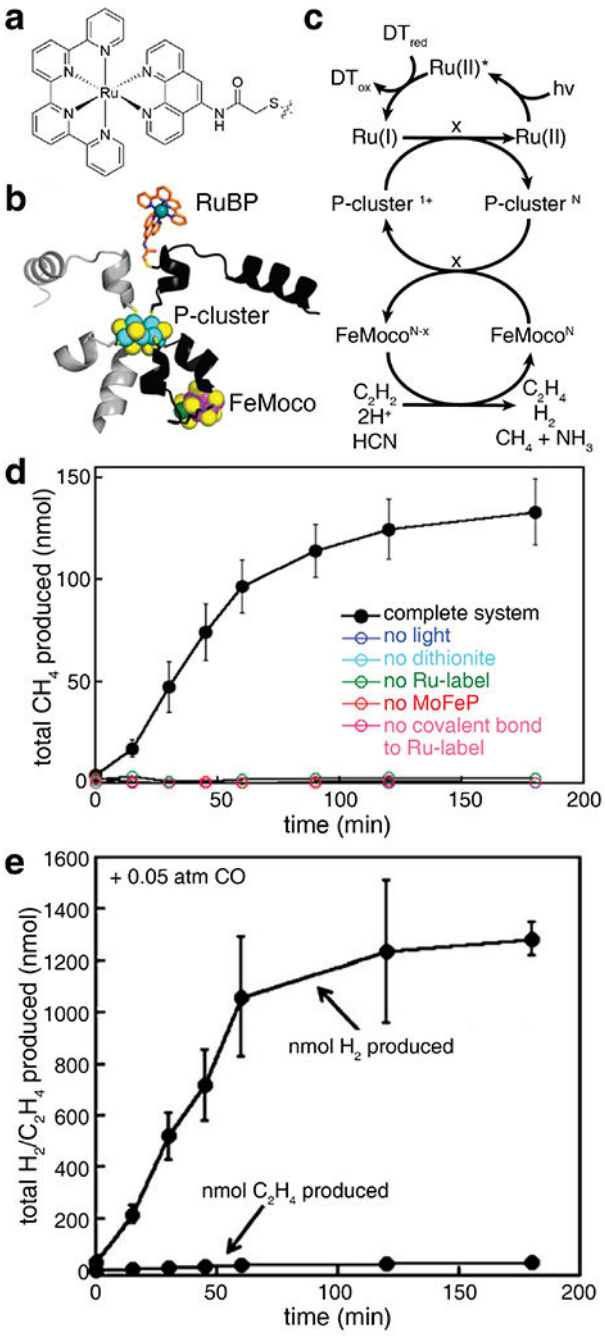

Figure 22.

Light-induced catalysis by MoFeP with a Ru-photosensitizer. (a) The chemical structure of the [Ru(bpy)2(phen)]$^{2+}$ photosensitizer. (b) Model of RuBP binding to aLeu158Cys in the cleft above the P-cluster. The α-subunit and β-subunit of MoFeP are black and gray, respectively. Reprinted from ref 62. (c) The Ru-labeled MoFeP proposed catalytic cycle. The P-cluster is depicted as cycling between P^N and P^{1+}, however it is also possible that it is cycling between P^N and a super-reduced state. FeMoco^N denotes the initial reduction state FeMoco. X indicates the number of ET events required for substrate reduction (X = 2, 2, and

6 for C2H2, H^+, and HCN reduction, respectively). Adapted from ref 62. (d) Graph of total CH4 produced after illumination using the complete photoreduction system and using negative controls in which components were omitted. Adapted from ref 62. (e) CO inhibition of C2H2 reduction but not of H+ reduction. Reprinted with permission from ref 319. Copyright 2013 John Wiley and Sons.

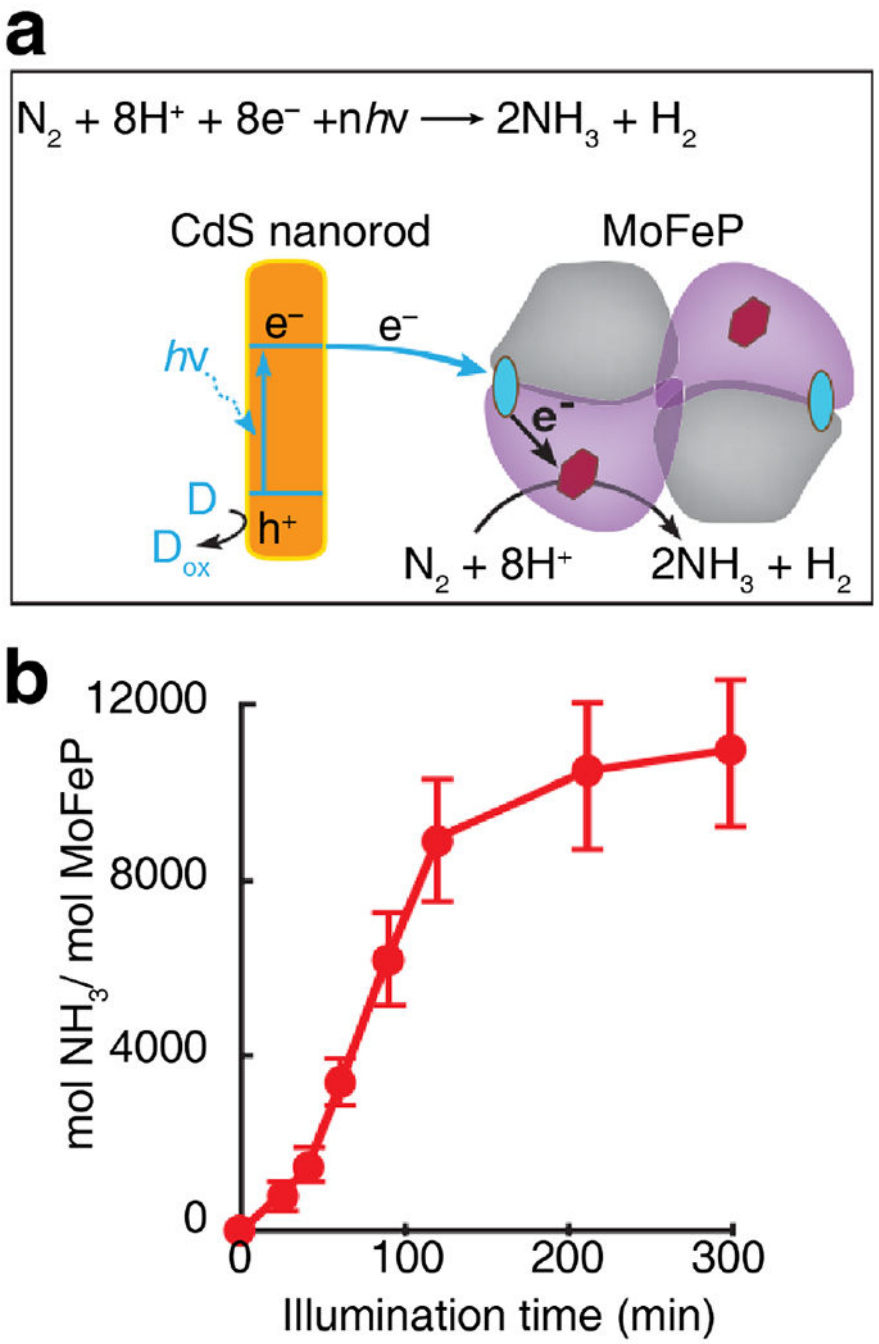

Figure 23.

Light induced catalysis by MoFeP with CdS nanorods. (a) The proposed reaction scheme for the photoreduction of N_2 to NH_3 by CdS nanorods. (b) Production of NH_3 over time. Adapted with permission from ref 63. Copyright 2016 AAAS.

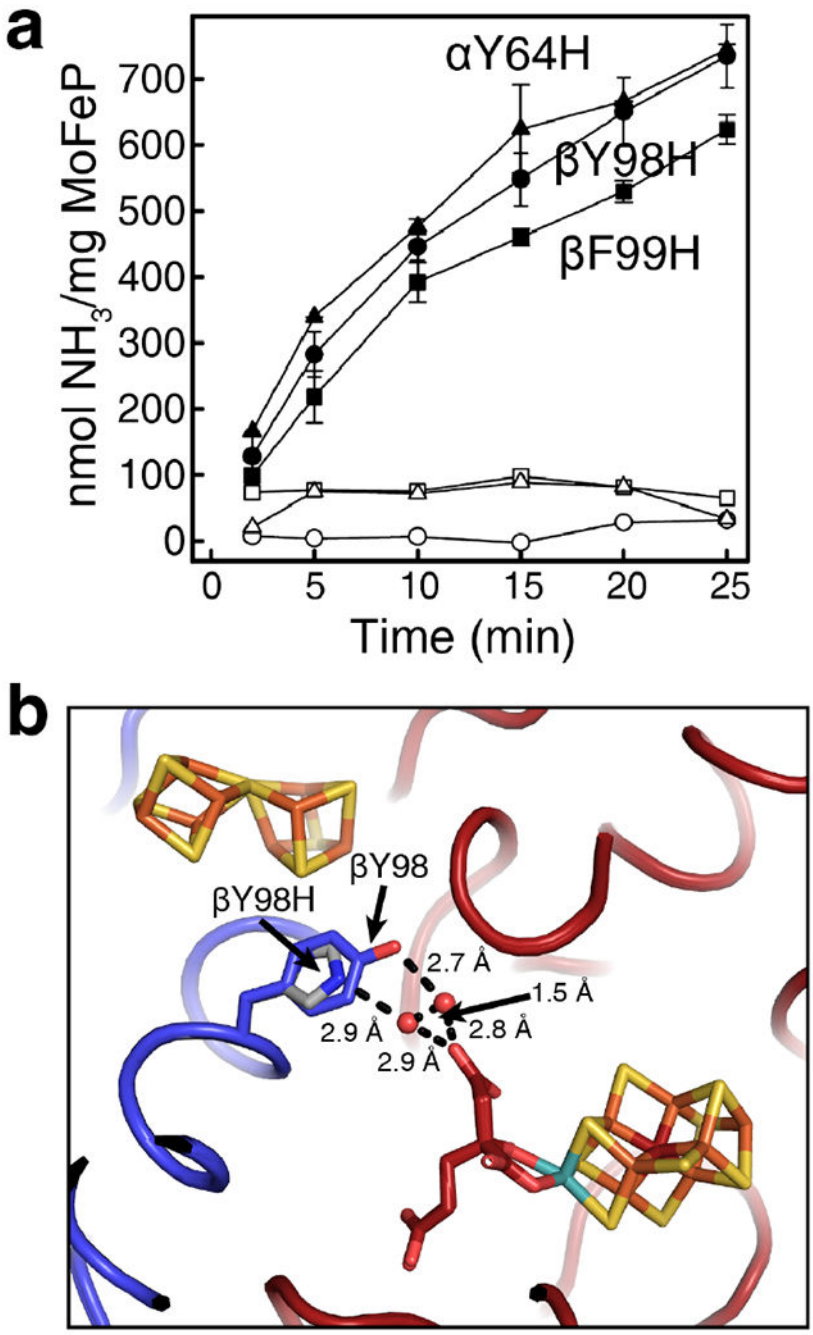

Figure 24.

Catalysis by MoFeP mutants using Eu^{II} reductants. (a) The time-course production of NH_3 from hydrazine by ATP- uncoupled catalysis. Negative controls (no protein in solution) are plotted as empty symbols. Reprinted from ref 57. (b) The crystal structure of βTyr98His demonstrates differences in the position of the solvent molecules around FeMoco that may contribute to the ability to ATP-uncoupled ET (wild-type PDB ID: 3U7Q, βTyr98His PDB: 4XPI). The native βTyr98 is depicted as blue sticks, and the mutation to His is depicted as gray sticks.

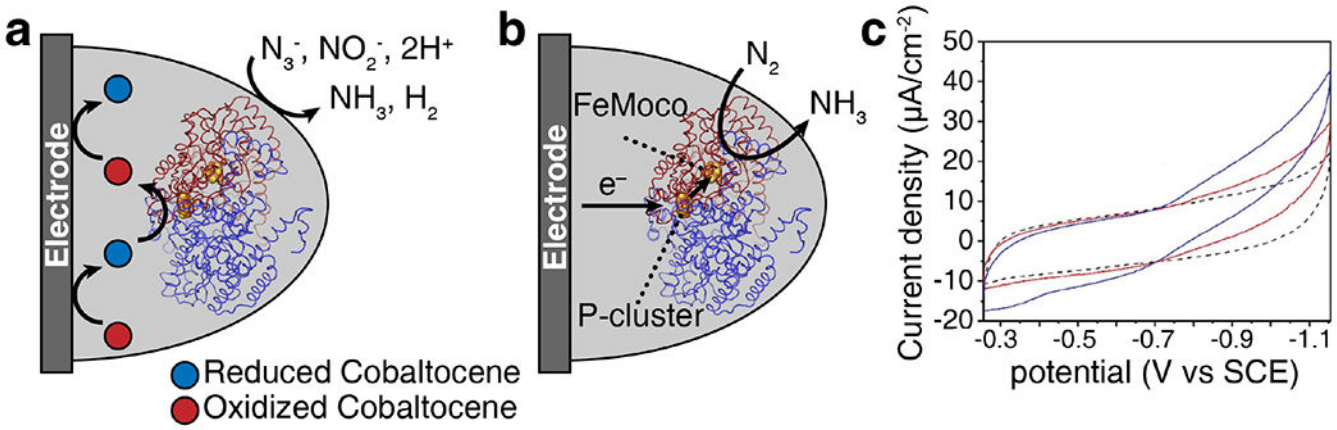

Figure 25.

Bioelectrocatalysis with MoFeP. (a) The proposed scheme of bioelectrocatalytic substrate reduction using the redox mediator cobaltocene. Adapted from ref 59 under the Creative Commons Attribution License (https://creativecommons.org/licenses/by-nc/3.0/legalcode). (b) The proposed scheme of bioelectrocatalytic substrate reduction using LPEI-pyrene hydrogels. (c) Cyclic voltammogram of MoFeP embedded in LPEI-pyrene hydrogel after 5 min (red) and 10 min (black) N_2. Ar control shown as dashed line. (b) and (c) are adapted and reptrinted, respectively, from ref 60 under the Creative Commons Attribution License (https://creativecommons.org/licenses/by-nc/3.0/legalcode).

Table 1.

Reported potentials of the redox-active centers in nitrogenase and its associated proteins. All potentials are from *Av* unless otherwise noted. Undetermined values are marked 'ND'.

Reported potentials of the [4Fe-4S] cluster of FeP					
Redox couple	**Nucleotides/Metal**	**Potential (mV) vs NHE**	**pH**	**Type of Measurement**	**Reference**
$[4Fe\text{-}4S]^{2+}/[4Fe\text{-}4S]^{1+}$	Nucleotide-free	−300	7.0 - 9.0	Controlled potential microcoulometry and spectroelectrochemistry	105
		−280	8.0	EPR potentiometric titration	106
		−310	8.0	Controlled potential microcoulometry	89
		−290	8.0	Controlled potential microcoulometry	82
$[4Fe\text{-}4S]^{2+}/[4Fe\text{-}4S]^{1+}$	$MgCl_2$	−393	7.0	EPR potentiometric titration	113
		−330	7.0 – 9.0	Controlled potential microcoulometry and spectroelectrochemistry	105
$[4Fe\text{-}4S]^{2+}/[4Fe\text{-}4S]^{1+}$ *Cp*	Nucleotide-free	−240	7.5	Spectrophotometry with redox indicator dyes	80
		−294	7.5	EPR potentiometric titration	108
		−266	8.0	EPR potentiometric titration	106
$[4Fe\text{-}4S]^{2+}/[4Fe\text{-}4S]^{1+}$	MgATP	−435	7.0	EPR potentiometric titration	113
		−430	7.0 – 9.0	Controlled potential microcoulometry and spectroelectrochemistry	105
		−430	8.0	EPR potentiometric titration	106
		−430	8.0	Controlled potential microcoulometry	82
$[4Fe\text{-}4S]^{2+}$+/$[4Fe\text{-}4S]^{1+}$ *Cp*	MgATP	−400	7.5	EPR potentiometric titration	108
		−415	8.0	EPR potentiometric titration	106
$[4Fe\text{-}4S]^{2+}/[4Fe\text{-}4S]^{1+}$	MgAMPPCP	−385	7.0 – 9.0	Controlled potential microcoulometry and spectroelectrochemistry	105
$[4Fe\text{-}4S]^{2+}/[4Fe\text{-}4S]^{1+}$	MgADP	−473	7.0	EPR potentiometric titration	113
		−490	7.0 – 9.0	Controlled potential microcoulometry and spectroelectrochemistry	105
		−440	8.0	Controlled potential microcoulometry	82
$[4Fe\text{-}4S]^{2+}/[4Fe\text{-}4S]^{1+}$ *Cp*	MgADP	−415	8.0	EPR potentiometric titration	106
$[4Fe\text{-}4S]^{2+}/[4Fe\text{-}4S]^{1+}$	ATP	−340	7.0 – 9.0	Controlled potential microcoulometry and spectroelectrochemistry	105

Reported potentials of the [4Fe-4S] cluster of FeP					
Redox couple	**Nucleotides/Metal**	**Potential (mV) vs NHE**	**pH**	**Type of Measurement**	**Reference**
$[4Fe\text{-}4S]^{1+}/[4Fe\text{-}4S]^{0}$	Nucleotide-free	−460	7.0 – 8.0	Controlled potential microcoulometry	89
		−790	8.0	Controlled potential microcoulometry	109
$[4Fe\text{-}4S]^{2+}/[4Fe\text{-}4S]^{1+}$	Nucleotide-free ΔLeu127 FeP	−420	8.0	EPR potentiometric titration	117
$[4Fe\text{-}4S]^{2+}/[4Fe\text{-}4S]^{1+}$	Nucleotide-free ΔLeu127 FeP complexed with MoFeP	−620	8.0	EPR potentiometric titration	117
Reported potentials of the P-cluster of MoFeP					
Redox couple(s)	**Potential (mV) vs NHE**	**pH**	**Type of Measurement**		**Reference**
P2+/PN	−290	8.0	EPR potentiometric titration and controlled potential microcoulometry		134
	−290	8.0	EPR potentiometric titration		139
	−307	7.5	EPR potentiometric titration		132
	−300	8.0	EPR potentiometric titration		117
	−268	7.0	Direct electrochemistry		60
	−340	8.0	EPR potentiometric titration		139
P^{2+}/P^{N} *Cp*	−224	6.0	EPR potentiometric titration		135
P^{2+}/P^{1+}	−270	7.0	EPR potentiometric titration		135
	−320	8.0	EPR potentiometric titration		135
	−348	8.5	EPR potentiometric titration		135
	−290	6.0−8.5	EPR potentiometric titration		135
$P^{1+/PN}$	+90	7.5	EPR potentiometric titration		132
$P^{3+}+/P^{2+}$	−390	8.0	EPR potentiometric titration		117
P^{2+}/P^{N} of wild-type MoFeP complexed with ΔLeu127 FeP	−290	6.5	EPR potentiometric titration		16
P^{2+}/P^{1+} of βSer188Cys MoFeP	−390	8.0	EPR potentiometric titration		16
P^{2+}/P^{DT} of βSer188Cys MoFeP[a]	−390	8.0	EPR potentiometric titration		16
	−290	6.5	EPR potentiometric titration		16
P^{DT}/P^{RED} of βSer188Cys MoFeP[b]	−550[c]	8.0	EPR potentiometric titration		16
Reported potentials of FeMoco of MoFeP					
Redox couple	**Potential (mV) vs NHE**	**Number of electrons (per MoFeP tetramer)**	**pH**	**Type of Measurement**	**Reference**

Reported potentials of the [4Fe-4S] cluster of FeP					
Redox couple	**Nucleotides/Metal**	**Potential (mV) vs NHE**	**pH**	**Type of Measurement**	**Reference**
M^{OX}/M^{N}	−42	ND	7.9	EPR potentiometric titration	136
	−42	ND	7.5	EPR potentiometric titration	132
	−52	ND	8.0	EPR potentiometric titration	117
M^{oX}/M^{N} *Cp*	−70	3.6	7.5	Spectrophotometry with redox indicator dyes	80
	−18	ND	7.5	EPR potentiometric titration	108
	0	ND	7.9	EPR potentiometric titration	136
M^{N}/M^{RED} [d]	−320, −450	~6 5.6 («=2)	8.0	Controlled potential microcoulometry	137
	−480	3 (*n*=1) 3 (*n*=1)	8.0	EPR potentiometric titration and controlled potential microcoulometry[e,f]	134
	−300[g] −465	4 (*n*=1) 12 (*n*=2)	8.0	Controlled potential microcoulometry of nitrogenase complex[e,h]	138
	−490	3	8.0	Controlled potential microcoulometry and EPR potentiometric titration[e]	138
M^{N}/M^{RED} *Cp* [d]	−580	5	8.0	Controlled potential microcoulometry and EPR potentiometric titration[e]	138
M^{oX}/M^{N} of wild-type MoFeP complexed with ΔLeu127 FeP	−52	ND	8.0	EPR potentiometric titration	117
Reported potentials of FeP reductases					
Redox couple	**Potential (mV) vs NHE**	**pH**	**Type of Measurement**		**Reference**
NifF: E_1[i]	−495	8.2	Spectroelectrochemistry		153
	−464	7.7	Spectrophotometry with redox indicator dyes		162
	−515	8.0	Controlled potential microcoulometry		174
	−500	7.0	Spectrophotometry with redox indicator dyes		155
	−458	8.0	Spectroelectrochemistry		172
	−449	6.0	Direct electrochemistry		173
	−446	6.0	EPR potentiometric titration		173
	−483	7.5	Direct electrochemistry		171
NifF: E_2[i]	+50	8.2	Spectroelectrochemistry		153
	−270	7.7	Spectrophotometry with redox indicator dyes		162

Reported potentials of the [4Fe-4S] cluster of FeP					
Redox couple	**Nucleotides/Metal**	**Potential (mV) vs NHE**	**pH**	**Type of Measurement**	**Reference**
	−245	8.0	Controlled potential microcoulometry		174
	−224	8.0	Spectroelectrochemistry		172
	−74	6.0	EPR potentiometric titration		173
	−187	7.5	Direct electrochemistry		171
FdI: $[4Fe\text{-}4S]^{2+}/[4Fe\text{-}4S]^{1+}$	−647	7.8	Direct electrochemistry		189
	−630	8.0	Direct electrochemistry		190
	−619	7.0	Direct electrochemistry		183
FdI: $[3Fe\text{-}4S]^{1+}/[3Fe\text{-}4S]^{0}$	−424	7.7	Spectrophotometry with redox indicator dyes		191
	−425	7.8	Direct electrochemistry		189
	−400	8.0	Direct electrochemistry		190
Reported potentials of the [2Fe-2S] cluster of Shethna II Protein					
Redox couple	**Potential (mV) vs NHE**	**pH**	**Type of Measurement**		**Reference**
$[2Fe\text{-}2S]^{2+}/[2Fe\text{-}2S]^{1+}$	−225	7.0 – 8.0	CD potentiometric titration		216
	−300	8.0	Controlled potential microcoulometry		174
	−262	7.0	EPR potentiometric titration		214
	−340	7.0	Spectroelectrochemistry (controlled potential microcoulometry)		215

[a] The P^{2+}/P^{DT} redox couple of pSer188Cys MoFeP likely corresponds to the P^{2+}/P^{1+} couple due to stabilization of the P'+ state by the pSer188Cys ligand.

[b] The P^{DT}/P^{RED} redox couple of pSer188Cys MoFeP likely corresponds to the P^{H}/P^{N} .

[c] This reported potential is an estimate due to instability of MoFeP below −550 mV.

[d] These potentials have not been assigned to specific redox couples of the clusters in MoFeP, and the number of reducing equivalents is not consistently reported. In this review, we tentatively assign these potentials to FeMoco, unless otherwise noted. However, it is possible that these potentials could also be assigned to reduction of the P-cluster beyond the P^{N} state.

[e] These potentials were measured by reduction of oxidized MoFeP. Oxidants used include indigo disulfonate, methylene blue, thionine, and 2,6-dichlorophenolindophenol.

[f] The MoFeP sample used in these experiments contained only 22–27 Fe atoms per molecule of MoFeP, indicating incomplete cluster formation or oxidative cluster degradation.

[g] It is possible that this potential corresponds to the P^{2+}/P^{N} redox couple of the P-cluster.

[h] This study used a nitrogenase complex with reported stoichiometry of 1:1:1 for FeP:MoFeP:Shethna II.

[i] *E1* refers to the semiquinone/hydroquinone couple of FMN and *E2* refers to the oxidized/semiquinone couple of FMN

Table 2.

Nucleotide-dependent changes in physical features of the FeP-MoFeP Complex

Complex (DG)	Buried surface area (Å^2)	γ100s helices angle, ϕ (0° is coplanar)	Center-tocenter distance from P-cluster to [4Fe-4S] (Å)
nf (DG1)	2800	30	23.2
pcp (DG2)	3700	21	17.8
adp (DG3)	1600-2000	26-33	22.6-23.7
alf (DG2)	3400-3600	12-13	17.5-17.6
pcp/adp (DG2)	3600	11	17.9

Adapted with permission from ref 26. Copyright 2005 AAAS.

Table 3.

Reported rates of reduction of FeP_{OX} using various reductants. Rates that were not determined are marked 'ND'.

Reductant of FeP	Reaction conditions	Rate order	Rate constant of reduction of FeP			Reference
			Nucleotide-free FeP^{ox}	$FeP^{ox}(MgATP)_2$	$FeP^{ox}(MgADP)_2$	
DT	[*Kp* $FePo_{ox}$] = 73 μM [DT] = 2-160 mM pH 7.4 23°C	Second order	ND	ND	3.0 ×; 10^6 $M^{-1}s^{-1}$	221
DT	[*Kp* FeP_{ox}] = 72 μM [DT] = up to 500 μM pH 7.4 23°C	Second order	> 10^8 $M^{-1}s^{-1}$ [a]	ND	3.0 × 10^6 $M^{-1}s^{-1}$ [a]	226
NifF	[*Kp* FeP] = 15 pM /*Kp* NifF] = 90 pM pH 7.4 23°C	Second order	ND	ND	> 10^6 $M^{-1}s^{-1}$	165
Ti^{III}	[*Av* FeP] = 15 μM [Ti^{III}] = 0.5, 1.0. or 5.0 mM pH 7.5 30°C	Second order	66 $M^{-1}s^{-1}$ [b]	ND	ND	205
NifF	[*Av* FeP] = 15 μM [NifF] = 0.5 mM pH 7.5 30°C	Second order	>1000 $M^{-1}s^{-1}$ [b]	ND	ND	205
DT	[*Av* FeP] = 40 μM [DT] = 10 mM pH 7.3 25°C	Pseudo first order	152 s^{-1}	1.6 s^{-1}	1.1 s^{-1}	204
NifF	[*Av* FeP] = 40 μM [DT] = 10 mM [NifF] = 300 μM pH 7.3 25°C	Pseudo first order	1188 s^{-1}	1217 s^{-1}	1538 s^{-1}	204

[a] These rate constants were determined assuming that reduction of FeP requires conformational changes.

[b] The methods did not specify if nucleotides were used.

Table 4.

Reported FeP-MoFeP dissociation rate constants measured indirectly by monitoring the reduction of oxidized $FeP_{OX}(MgADP)_2$ in the presence of MoFeP.

Reductant used	Rate constant for dissociation of FeP-Mo-FeP complex (s^{-1})	Reference
DT	10	66
DT	6.4	221
DT	6	246
DT	3.9	204
MV	100	204
NifF	759	204

Table 5.

Dependence of nitrogenase activity and energy utilization on the reductant used. Values that were not reported are marked ‘ND’.

Reductant used	Organism	Molar ratio of FeP:MoFeP	ATP/e^-	Substrate	Specific activity (nmol product formed $min^{-1}.mg^{-1}$ FeP)	Reference
DT	*Azotobacter chroococcum*	2.1	ND	C_2H_2	440	166
NifF	*Azotobacter chroococcum*	2.1	ND	C_2H_2	495	166
DT	*Av*	2.4	ND	C_2H_2	1968	163
NifF and DT	*Av*	2.4	ND	C_2H_2	3195	163
DT	*Av*	0.2	ND	C_2H_2	978	163
NifF and DT	*Av*	0.2	ND	C_2H_2	1981	163
Ti^{III}	*Av*	0.2	1.1	N_2	ND	205
DT	*Av*	0.2	2.3	N_2	ND	205
NifF	*Av*	0.2	1.1	N_2	ND	205
Ti^{III}	*Av*	5.0	1.1	N_2	ND	205
DT	*Av*	5.0	6.4	N_2	ND	205
DT	*Av*	0.9	2.17	C_2H_2	~2250[a]	204
NifF and DT	*Av*	0.9	2.26	C_2H_2	~4000[a]	204
DT	*Av*	19.5	1.89	C_2H_2	~2250[a]	204
NifF and DT	*Av*	19.5	2.74	C_2H_2	~2250[a]	204
DT	*Av*	0.9	1.87	H^+	~3000[a]	204
NifF and DT	*Av*	0.9	1.91	H^+	~5000[a]	204
DT	*Av*	19.5	1.63	H^+	~1500[b]	204
NifF and DT	*Av*	19.5	1.96	H^+	~5000[b]	204
DT	*Av*	0.9	1.85	N_2	~600[a]	204
NifF and DT	*Av*	0.9	1.91	N_2	~1300[a]	204
DT	*Av*	19.5	1.82	N_2	~200[b]	204

Reductant used	Organism	Molar ratio of FeP:MoFeP	ATP/e$^-$	Substrate	Specific activity (nmol product formed min^{-1}.mg^{-1} FeP)	Reference
NifF and DT	*Av*	19.5	1.78	N_2	~600[b]	204

[a] These values are estimates from graphs in the supplemental information of reference 200.

[b] These values are estimates from extrapolation of graphs in the supplemental information of reference 200.